Document P-2832-F

Prepared for
Water and Power Resources Service
U.S. Department of the Interior
Denver, Colorado 80225

Sponsored by
U.S. Department of Transport
Federal Aviation Administration
Systems Research and Development Service
Aviation Weather Branch

LEVEL II

Thunderstorm Turbulence
Hazard Detection

DTIC
SELECTED
AUG 1 7 1981

A

ERT

ENVIRONMENTAL RESEARCH & TECHNOLOGY, INC.
ATLANTA · CHICAGO · CONCORD, MA · FORT COLLINS, CO
HOUSTON · LOS ANGELES · PITTSBURGH · WASHINGTON, DC

AD A103008

DTIC FILE COPY
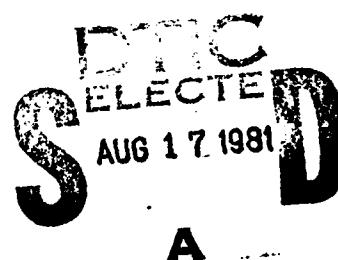
81 8 14 078

ERT-

Document P-2832-F

Prepared for
Water and Power Resources Service
U.S. Department of the Interior
Denver, Colorado 80225

Sponsored by
U.S. Department of Transport
Federal Aviation Administration
Systems Research and Development Service
Aviation Weather Branch

Thunderstorm Turbulence
Hazard Detection

ERT

ENVIRONMENTAL RESEARCH & TECHNOLOGY, INC.
ATLANTA · CHICAGO · CONCORD, MA · FORT COLLINS, CO
HOUSTON · LOS ANGELES · PITTSBURGH · WASHINGTON, DC

MS-230 (3-78)
Bureau of Reclamation

TECHNICAL REPORT STANDARD TITLE PAGE

1. REPORT NO.	2. GOVERNMENT ACCESSION NO. AD-A103 008	3. RECIPIENT'S CATALOG NO.
4. TITLE AND SUBTITLE Thunderstorm Turbulence Hazard Detection		5. REPORT DATE March 1981
		6. PERFORMING ORGANIZATION CODE P-2832-F
7. AUTHOR(S) R.K. Crane		8. PERFORMING ORGANIZATION REPORT NO.
9. PERFORMING ORGANIZATION NAME AND ADDRESS Environmental Research & Technology, Inc. 696 Virginia Road Concord, Massachusetts 01742		10. WORK UNIT NO.
		11. CONTRACT OR GRANT NO. 14-06-D-7673
12. SPONSORING AGENCY NAME AND ADDRESS Water and Power Resources Service U.S. Department of the Interior P.O. Box 25007 Denver Federal Center, Denver, Colorado 80225		13. TYPE OF REPORT AND PERIOD COVERED Final Report January 1978 - June 1980
		14. SPONSORING AGENCY CODE

15. SUPPLEMENTARY NOTES Work performed under interagency agreement
U.S. Department of Transportation   DOT-FA 77WAI-806
Federal Aviation Administration
Systems Research & Development Service, Aviation Weather Branch ARD 410

16. ABSTRACT A technique was developed for the automatic detection of regions
of potentially hazardous turbulence in thunderstorms utilizing data from
conventional or from Doppler weather radars. The technique is based on a
presumed proximity between turbulent patches and significant cells or
clusters of cells. The efficacy of the cell approach to thunderstorm tur-
bulence hazard detection was evaluated using T-28 aircraft penetration
flights. Data were obtained from two National Hail Research Experiment
(NHRE) case studies, 22 June 1976 and 22 July 1976.

Statistical analyses were made of the probability of detection of a tur-
bulent patch within the radius of influence of a significant cell, of the
probability of a false alarm, and of a critical success index which combines
both the probability of detection and the false alarm rate. The results
indicated that the probability of detecting moderate turbulence was in excess
of 90 percent, the false alarm rate was less than 10 percent, and the criti-
cal success index was in excess of 80 percent for aircraft penetrations in
the regions with precipitation detectable by radar. The results for the
entire flight path were a probability of detection in excess of 70 percent,
a false alarm rate less than 10 percent and a critical success index in
excess of 60 percent.

17. KEY WORDS AND DOCUMENT ANALYSIS

a. DESCRIPTORS-- thunderstorm turbulence   cloud dynamics
                 Doppler radar
                 cell tracking
                 storm detection
                 weather radar data processing

b. IDENTIFIERS-- turbulence hazard detection

c. COSATI Field/Group   COWRR:

18. DISTRIBUTION STATEMENT *Available from the National Technical Information Service, Operations Division, Springfield, Virginia 22161.*	19. SECURITY CLASS (THIS REPORT) UNCLASSIFIED	21. NO. OF PAGES
	20. SECURITY CLASS (THIS PAGE) UNCLASSIFIED	22. PRICE

GPO 845-830

TABLE OF CONTENTS

iii

1. INTRODUCTION

1.1 Program Objectives

The timely detection and short range forecast of regions of convective storms which are hazardous to aircraft operations is of vital importance to the safety of flight and the efficient management of the nation's airspace. Weather radars have the capacity to observe the fine structure of severe weather and to localize regions of potential hazard. Crane (1976) postulated that the potentially hazardous regions should coincide with the boundaries of strong updrafts during the growing stage of a convective cell and that these regions could be identified by radar-detected local reflectivity maxima. The objective of this research program was to test the hypothesis that reflectivity or tangential shear cells observed by a Doppler weather radar would be associated with potentially hazardous turbulence.

Specifically, the research program was to:

1) develop and test algorithms for the fine-scale detection of severe weather areas,

2) develop and test algorithms for the tracking and extrapolation of movement of the detected turbulent areas, and

3) develop ways to utilize the detection and tracking algorithms in enroute and terminal air traffic control operations.

Data from both conventional (reflectivity only) and Doppler weather radars were to be used in the research. The algorithms were to be tested using observations from instrumented aircraft obtained during severe weather penetration flights.

1.2 Summary of Results

1.2.1 Significant Findings

The following results were obtained from an analysis of data from

1

15 penetration flights supplied by the South Dakota School of Mines and Technology (SDSMT) and of simultaneous weather radar observations provided by the National Center for Atmospheric Research (NCAR); the data were from two of the National Hail Research Experiment (NHRE) case studies, 22 June 1976 and 22 July 1976.

1) Cell detection algorithms were developed which successfully operated on reflectivity or on Doppler velocity variation (shear) data.

2) Tracking and position extrapolation algorithms were developed which successfully combined reflectivity and shear data obtained at different elevation angles and generated a number of volume cell attributes which were used to evaluate cell significance.

3) A total of 135 encounters with moderate or more intense turbulence were recorded during the 15 penetration flights. Only 89 (67 percent) of the encounters were within storm areas (contoured regions) having reflectivity values greater than 20 dBZ*; 110 (82 percent) were within the 7 dBZ contour areas. Noting that most weather radar systems have insufficient sensitivity to make observations over large areas at levels less than 20 dBZ, the maximum probability of detecting a turbulent patch employing such a radar is less than 67 percent.

4) Significant reflectivity cells were highly correlated with aircraft encounters with turbulence. It was found that 82 percent of the moderate or more intense turbulence encounters were within 6 km (3.2 nm) of a significant reflectivity cell. For encounters within 6 km (3.2 nm) of a region having 20 dBZ or higher reflectivities, the probability of detection was 94 percent.

---

*Radar reflectivity factor expressed in decibels relative to a value of 1 mm^6/m^3.

5) The addition of Doppler information did not appreciably change the detection probability. For turbulence encounters within 6 km (3.2 nm) of a significant tangential shear cell, the two C-band radars averaged a 71 percent detection probability; the two X-band radars averaged a 57 percent detection probability. For encounters within 6 km (3.2 nm) of a region having 20 dBZ or higher reflectivities, the probabilities were increased to 81 and 65 percent respectively.

6) The intensity of turbulence encountered by the aircraft showed little correlation with either cell reflectivity or tangential shear. The observed tangential shear values depended on the relative locations of the radars and the cells.

7) The false alarm rate (probability of cell not being turbulent) depended critically on the assumed radius of influence of the cell and the intensity of turbulence. For moderate or more intense turbulence and a 6-km (3.2 nm) radius of influence, the false alarm rate was 8 percent for the significant reflectivity cells observed by the S-band radar, averaged 9 percent for the C-band Doppler radars, and 6 percent for the X-band Doppler radars.

8) The intensity of encountered turbulence depended on the age of the cell. The most intense turbulent patches were associated with cells which were first detected at or just after the time of aircraft penetration. Turbulent patches encountered outside regions with precipitation targets suitable for radar detection usually developed detectable targets after the aircraft encounter. Successful short range forecast of the probable positions for new cell development will be mandatory for a viable tactical hazard avoidance system.

9)   The spatial organization pattern of new cell develop-
     ment observed in the two Colorado hail storms was
     similar to the pattern consistently observed by Crane
     and Hardy (1981) during a three-year measurement
     program in Kansas. The constancy of the observed
     spacings between developing cell clusters suggests
     that short term forecast procedures can be developed.

1.2.2 Algorithm Development

The research effort described in this report was the Federal
Aviation Administration (FAA) sponsored segment of a larger program of
automated radar cell detection and tracking algorithm development and
application undertaken by Environmental Research & Technology, Inc. (ERT)
for the U.S. Air Force Geophysics Laboratory (AFGL), for the Water and
Power Resources Service (WPRS), and for the FAA. The detection and
tracking algorithms have been described by Crane (1979a). The segment
conducted for AFGL included the basic cell detection algorithm develop-
ment for use with either reflectivity or single Doppler velocity data and
the application of the algorithms to real-time processing using a mini-
computer (Crane, 1979b). The segment performed for WPRS included the
development of tracking algorithms (Gustafson, 1980) and the application
of these algorithms to a climatological analysis of precipitation in
western Kansas for use in evaluating weather modification activities
(Crane and Hardy, 1981).

The segment performed for the FAA was conducted under contract to
WPRS. This report constitutes the final report for the 1978-1981 time
period covered by the contract. Under FAA sponsorship, algorithms were
developed to employ both tangential shear and reflectivity data in the
tracking process. The algorithms were designed to accept data from more
than one radar thus solving the multiple radar networking problem for
cell tracking and hazard detection.

The radial velocity data from a Doppler radar were processed to
emphasize local velocity perturbations. In the analysis performed on
the NHRE data, the magnitude of the tangential shear was employed to
measure the velocity perturbation at the edge of an updraft region and
elsewhere. The cell detection algorithm operated on a scalar data

4

field and any scalar measure of velocity perturbation could have been used; measures such as radial shear, magnitude of the vector shear, or Doppler velocity spread (second moment) were possible. The magnitude of the tangential shear was used in this study because (1) it is optimum for the observation of an azimuthally isotropic mesocyclone, (2) it was employed in the Joint Doppler Operational Project (JDOP, 1979) for severe weather detection, and (3) it was readily calculated for each of the Doppler radars. Although second moment data are often recommended for use in hazard detection, they were not employed in this study because they were not stored on the data tapes for all the Doppler radars.

The cell tracking algorithm generated a number of volume cell attributes that could be used to assay cell significance. For application to hazard detection, a significant cell was a cell presumed to have a turbulent patch within a reasonable radius of influence of the cell. Initially, Crane (1976) viewed the radar cells as isolated building blocks in the development of convective storms. He expected that each cell would be associated with an updraft region and that the observed reflectivity maxima would be horizontally displaced from regions of maximum turbulence occurring at the interface between an updraft and a downdraft by distances the order of half a cell diameter. Experience gained from processing the Kansas data for WPRS revealed a far more complex structure to the convective process. Crane and Hardy (1981) reported at least four different cell types, only one of which should be associated with significant levels of turbulence.

The important results from the Kansas data analysis were (1) that clusters of cells, not the individual cells themselves, were the consistent indicators of the important updraft regions which are potentially hazardous, and (2) that significant cells were cells having a high degree of apparent vertical development. The concept of significance applied to the processing of Kansas data included clustering and, for isolated cells, high reflectivity and moderate vertical development or significant vertical development in the absence of high reflectivity. The resultant entity was called a significant cell and cluster (SC).

The cluster detection concept did not work when initially applied to the NHRE data because of the inherently high false tangential shear cell detection rate produced by Doppler velocity observations at low

signal-to-noise ratios. Unfortunately, the solution to the cluster analysis problem was worked out after the final computer tracking runs were completed and cell clusters could only be used in the analysis of data from the 22 July case study day.

Vertical development and persistence of either reflectivity cells, combined reflectivity and tangential shear cells, or tangential shear cells were used in this study as an indicator of significance. As applied, a cell had to be detected on at least three elevation angles (span a height interval of 3 km (10 kft) or more) in a volume scan sequence (90 seconds or more depending on the radar and raster scan limits) and had to exist for at least two volume scans. It is noted that JDOP also employed vertical development and persistence criteria in the detection of mesocyclones. They employed a 3-km (10 kft) minimum height interval restriction but a longer age requirement, 5 to 15 minutes.

Manual analysis of the spatial locations of the significant cells detected using the NHRE case study data revealed that a significant cell generally occurred as a member of a cluster. However, the number of significant cells exceed the number of clusters because some clusters contained more than one significant cell. The net result was that the false alarm rates reported in this study are higher than they would have been if the analysis could have been performed using clusters to detect turbulent patches.

1.2.3 Analysis

The objective of the research conducted under the sponsorship of the FAA was to evaluate the cell approach to thunderstorm hazard detection. Data from five separate radars, the then conventional NCAR CP-2 S-band radar, the two NCAR C-band Doppler radars, CP-3 and CP-4, and the two NOAA Wave Propagation Laboratory X-band Doppler radars, NOAA-C and NOAA-D, were used independently to generate significant cell tracks whose locations were, in turn, compared with simultaneous aircraft encounters with turbulence (see Section 3.1 for a discussion of the radar systems). The aircraft encounters were used as the turbulent-truth indicators of hazard (see Section 4 for a discussion of aircraft observations).

Detection was claimed where the cell centroid location (at ground

level) was within a specified radius of influence of the encountered patch of turbulence. If the segment of aircraft track enclosed within a circle centered at the cell centroid position and having the specified radius of influence was not turbulent at a specified or higher intensity, a false alarm was recorded for that intensity. The total counts of turbulent patches, detected patches, radar cells within the radius of influence of the aircraft track, and radar cells associated with one or more turbulent patches were used to calculate the probabilities of detection of a turbulent patch or the false alarm rate for a radar cell observation.

The observed detection probabilities for each of the Doppler radars and for the use of three different reflectivity thresholds for the conventional S-band radar are listed in Table 1 for moderate or more intense turbulence and a 6-km (3.2 nm) radius of influence. Table 1 also lists the false alarm rate and a critical success index (see Section 5.3) defined as the number of successes (cells associated with turbulence) divided by the total number of detected cells within the radius of influence of the aircraft track plus the number of turbulent patches not associated with a radar cell (failures). Similar statistics for encounters with severe or extreme turbulence levels are listed in Table 2. These tables also show the changes in the probability of detection and the critical success index that occur by restricting the area included in the analysis of the detection of turbulence to (1) all segments of the penetration flights, (2) those segments within a region enclosed by a 4-km (2.2 nm) buffer zone outside the 7 dBZ contour boundaries, and (3) those segments within 4 km (2.2 nm) of the 20 dBZ contour boundaries.

Variations in the probability of detection, false alarm rate, and critical success index with the radius of influence presumed for each cell are displayed in Figures 1 through 3 respectively. The plotted data are for turbulence encounters within the 20 dBZ contour regions plus buffer zones surrounding the contour which are 2 km (1.1 nm) smaller than the radius of influence. The data are displayed by frequency band; the results were combined for the two C-band Doppler radars and for the two X-band Doppler radars. These results are the best that can be expected for the cell approach to hazard detection because the analysis has been restricted to the areas of the radar displays having precipitation tracers

7

TABLE 1

RESULTS FOR MODERATE OR MORE INTENSE TURBULENCE ($\epsilon^{1/3} \geq 5 \text{ cm}^{2/3} \text{ s}^{-1}$), 6 KM (3.2 nm) RADIUS OF INFLUENCE

Radar	Probability of Detection			False Alarm Rate (%)	Critical Success Index		
	Within 20 dBZ† (%)	Within 7 dBZ† (%)	All (%)		Within 20 dBZ† (%)	Within 7 dBZ† (%)	All (%)
Reflectivity:							
S-Band							
CP-2	94	93	82	8	85	85	72
>40 dBZ	69	69	60	0	59	58	49
>50 dBZ	50	49	43	0	31	31	26
Doppler:							
C-Band							
CP-3*	91	91	91	5	88	88	88
CP-4	76	75	63	9	76	75	65
X-Band							
NOAA-C	67	66	62	7	68	68	65
NOAA-D	62	61	51	3	55	54	44
Clusters							
Persistent*			63	14			29
All, CP-2*			87	7			70

*22 July 1976 only

†includes a 4 km buffer zone outside the contoured region

8

TABLE 2

RESULTS FOR SEVERE OR EXTREME TURBULENCE ($\epsilon^{1/3} > 12$ cm$^{2/3}$ s^{-1}),
6 KM (3.2 nm) RADIUS OF INFLUENCE

Radar	Probability of Detection			False Alarm Rate (%)	Critical Success Index		
	Within 20 dBZ† (%)	Within 7 dBZ† (%)	All (%)		Within 20 dBZ† (%)	Within 7 dBZ† (%)	All (%)
Reflectivity:							
S-Band							
CP-2	92	92	85	83	17	17	17
40 dBZ	100	92	85	81	19	19	19
50 dBZ	55	50	46	82	16	15	15
Doppler:							
C-Band							
CP-3*	100	100	100	89	11	11	11
CP-4	100	100	80	88	12	12	12
X-Band							
NOAA-C	100	100	90	82	18	18	18
NOAA-D	80	67	57	78	22	21	21
Clusters							
Persistent*			50	71			22
All, CP-2*			100	67			33

*22 July 1976 only

†includes a 4 km buffer zone outside the contoured region

9

Figure 1   Probability of detection (POD) of turbulent patches within regions
with reflectivity values in excess of 20 dBZ plus a 4 km surrounding
buffer zone; T-28 aircraft at 6 km height and 90 m/s airspeed
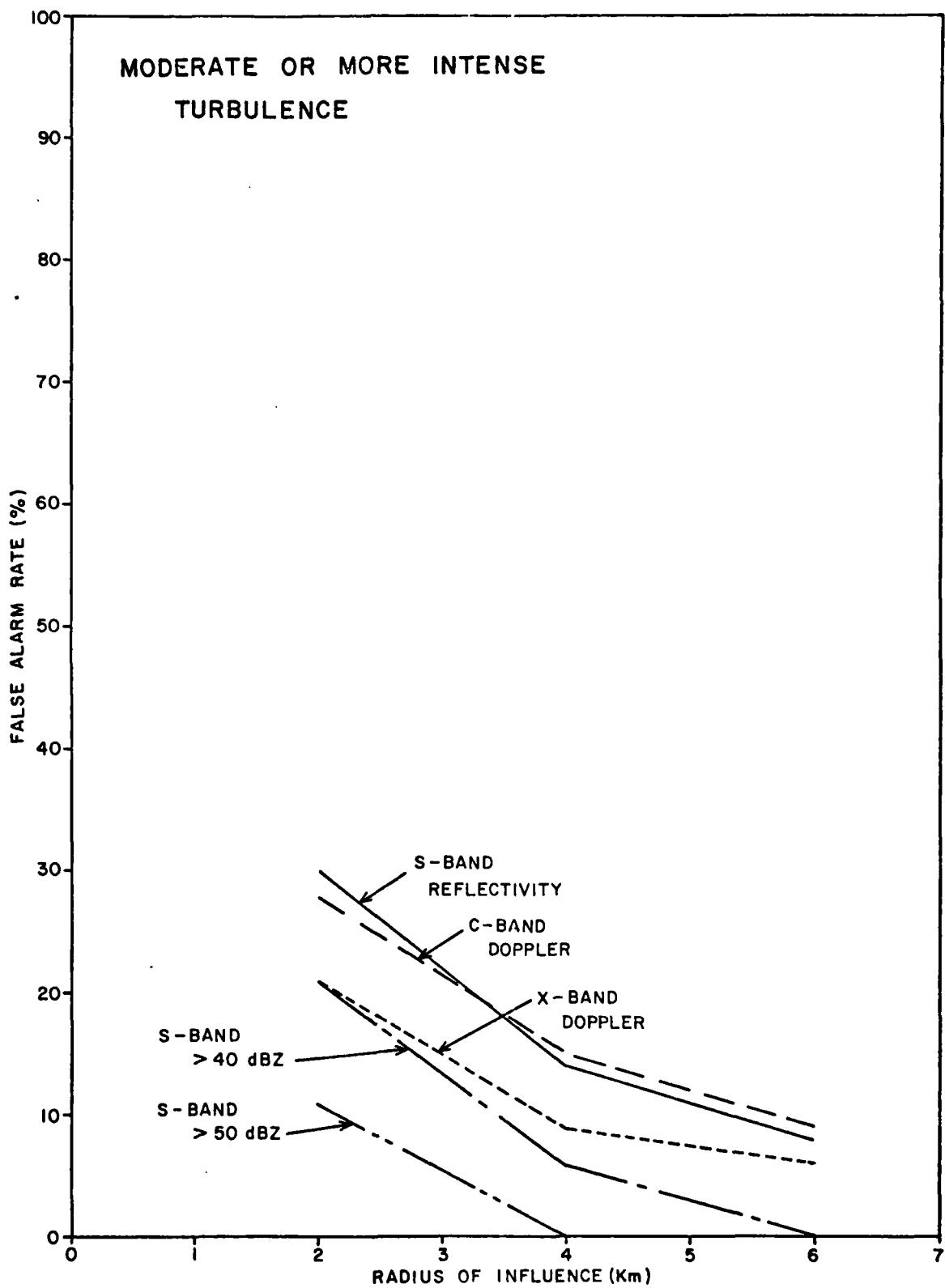
Figure 2   Probability of a false turbulent patch detection (FAR); T-28
aircraft at 6 km height and 90 m/s airspeed

11
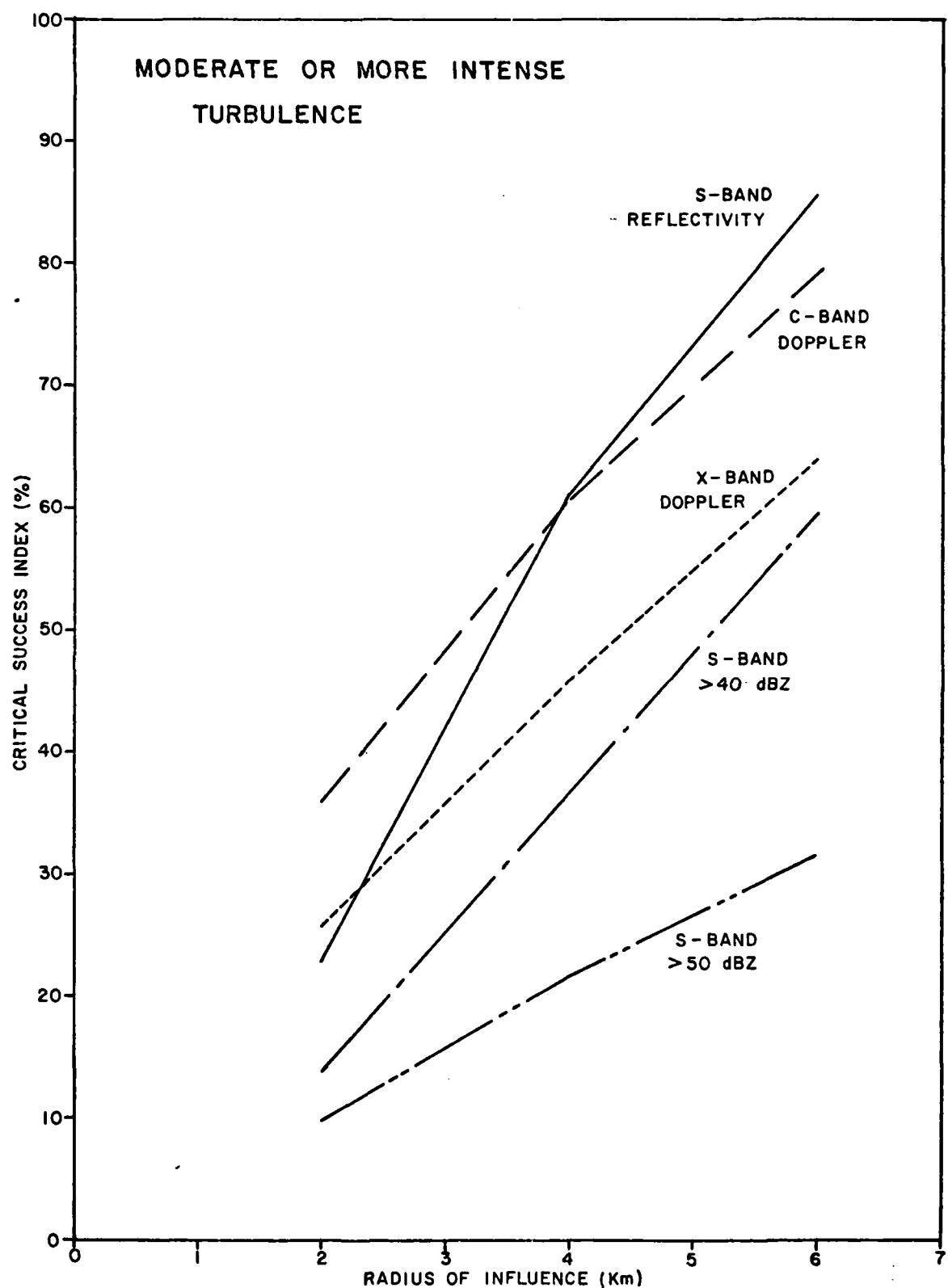
Figure 3 Critical success index (CSI) for the detection of turbulent patches within regions with reflectivity values in excess of 20 dBZ plus a 4 km surrounding buffer zone; T-28 aircraft at 6 km height and 90 m/s airspeed

observable by radar. They show that the radius of influence of the cells was in excess of 4 km (2.2 nm). By a 6-km (3.2 nm) radius, the rate of increase in detection probability and of decrease in false alarm rate had slowed perceptibly. The use of too large a radius of influence is not recommended because of the increase in false alarm rate and attendent decrease in the critical success index expected for aircraft flights through the weaker, widespread areas of a storm surrounding the intense updraft regions. Such regions were not adequately probed in this study because the primary reason for the aircraft penetration flights was the study of hail development in the most active regions of the storm.

The critical success index (CSI) was used as a convenient way to combine the two parameters of interest, probability of detection and false alarm rate. High CSI values can only be achieved when the detection probability is high and the false alarm rate is low. Referring to Table 2, it is noted that although the probability of the detection of severe turbulence was high, as much as 100 percent in some instances, the CSI values were uniformly low due to the high numbers of false alarms. For aviation safety, the probability of detection is the most important factor. A viable hazard detection system must also have a low false alarm rate to be acceptable to the aviation industry. A combined index such as the CSI was used in this study to provide a single measure of both factors.

The CSI values for reflectivity data alone were not significantly different from the CSI values obtained for the C-band Doppler data using the magnitude of the tangential shear to measure velocity perturbations (Figure 3). The CSI values declined significantly when only high reflectivity (>40 or 50 dBZ) cells were used for the detection of turbulence. This result is consistent with the earlier analysis of Burnham and Lee (1969) but differs from the results presented by Barclay (1968, 1974) which suggested that severe turbulence occurs only within 5.4 nm (10 km) of reflectivities 50 dBZ or higher. The results from the two NHRE case studies show that more than 28 percent of the encounters with moderate turbulence occurred outside the 10 km (5.4 nm) buffer zone surrounding a 50 dBZ contour. Two encounters with severe or more intense turbulence occurred outside the 10 km (5.4 nm) buffer zone surrounding a 50 dBZ contour (15 percent of the encounters with severe or more intense turbulence). Burnham and Lee observed that lower reflectivities could be

13

associated with severe turbulence and recommended that storms with maximum reflectivities in excess of 40 dBZ should be avoided and that penetrations should not be made within 20 nm (37 km) of the core of such a storm.

Lee (1977) recognized the lack of correlation between the reflectivity values along an aircraft track and the levels of turbulence encountered by the aircraft. He investigated the use of several measures of velocity perturbations for the detection of turbulence and found that Doppler spread was the most promising. He reported a 95 percent probability of detection of moderate or more intense turbulence for velocity perturbations within 2 km (1.1 nm) of the turbulent patches but did not present results for higher turbulent intensities or other measures of velocity perturbations. The C-band data presented in Figure 1 show a similarly high probability of detection for tangential shear at a radius of influence of 6 km (3.2 nm). At 2 km (1.1 nm), the probability of detection of severe turbulence was only 50 percent but, if a threshold of severe turbulence was selected, the probability of detection was 100 percent. In the latter case, the false alarm rate was also high resulting in a critical success index of less than 10 percent.

The X-band radar observations produced lower CSI values than did the C-band observations. The X-band data were affected by attenuation and the signal-to-noise ratios for observations near the aircraft track were lower than for the other radars if, in fact, a signal could be detected. The net results were lower probabilities of detection (see Figure 1) and lower CSI values than for the C-band observations. The data presented in Figures 1-3 included encounters both within the 4-km (2.2 nm) buffer zone and within the 20 dBZ contour region as measured at S-band. Therefore, the loss of detectability due to the effects of attenuation has not been corrected in the X-band (or the C-band) data.

Lee (1977) employed Doppler spread (spectrum breadth) data in his analysis of thunderstorm hazard detection. Spectrum breadth was chosen because of the expectation that the turbulent velocity fluctuations will be isotropic on a scale commensurate with the radar range, beamwidth product (cross range dimension) at the measurement location while the larger scale shear would be anisotropic. He deprecated the use of radial (Doppler) velocity shear because of the expectation that anisotropy would cause the magnitude of the shear to vary with viewing direction and significantly reduce the correlation between the intensity of the turbulence and the magnitude of the shear.

14

Lee reported poor correlations between turbulent intensities and the magnitudes of reflectivity, reflectivity gradient, first or second spatial derivatives of the radial velocity (shear and gradient of shear), or Doppler spread. He reported high probabilities of detection when he used occurrences of Doppler spread above a preset threshold to indicate moderate or more intense turbulence. The plots that he presented (Figures 4.1 to 4.3 of Lee, 1977) also showed relatively good agreement between the magnitude of the vector shear and the turbulent intensity but no statistical comparison was presented.

In this study we found that the occurrence of a velocity perturbation as indicated by a tangential shear cell was a good indicator of moderate turbulence. We also found that the magnitudes of the tangential shear values were not correlated either with simultaneous observations from the other Doppler radars or with the intensity of turbulence, a result indicative of anisotropy on the scale of the separation between adjacent radar beam positions at a given range during an azimuth scan. Anisotropy on this scale should also affect detection using Doppler spread, a result suggestive of one of the underlying causes of the lack of correlation between the intensity of turbulence and Doppler spread noted by Lee.

Neither the reflectivity values nor tangential shear values were good indicators of the intensity of turbulence. The presence of a reflectivity or tangential shear cell (perturbation) was a good indicator of moderate turbulence but, as the intensity of the turbulence increased above the moderate level, the critical success index decreased due to the lack of correlation between the magnitudes of the intensity of the turbulence and the cell parameters. For application to the detection of moderate turbulence, this lack of correlation is not important. For the detection of severe intensity turbulence in a widespread region of less severe weather, the lack of correlation may be important. In the latter case, additional information such as cell age or growth rate may have to be employed to provide a higher critical sucess index for hazard detection.

The penetration flights were into regions of rapid development and strong updrafts, regions that should be turbulent, regions normally avoided by commercial aircraft. Exploration of these highly turbulent regions could bias the results toward lower false alarm rates and higher critical

15

success indicies than would be expected for flight paths through the regions near the storms that could be safely traversed by general or commercial aviation aircraft. This bias is unavoidable when data from hail studies are used for the evaluation of turbulence detection schemes. In an attempt to minimize the bias, the entire flight path, both within the storm and while maneuvering before and after each penetration, was used in the statistical analysis. A full evaluation of the hazard detection algorithms will require flights in and around a wide range of storm types through regions that are expected to be free of turbulence as well as regions that are expected to be turbulent.

1.2.4 Air Traffic Control Applications

The ultimate goal of this research program is an automated thunderstorm hazard detection and short range forecast system for use by enroute and terminal area air traffic controllers. The cells (and clusters) are entities which can be readily identified and displayed to a controller along with aircraft position data. Track velocities are maintained for each cell and cluster and may be used to extrapolate cell positions to forecast the locations of potentially hazardous regions. The potentially hazardous regions may be displayed as circles of cell radius of influence (6 km (3.2 nm), say) about the forecast cell position. The radius for potential hazard may also be expanded to allow for forecast uncertainties.

The forecast position of the potentially hazardous region must be available for display to the controller. The controller is interested in the probable locations of turbulence along the flight path some 5 to 20 minutes ahead of an aircraft encounter, not in turbulence that has been experienced by the aircraft. A short range forecast is mandatory because of the delays inherent in collecting the radar data, processing the data, transmitting the data to a center and finally displaying the data to a controller.

It is not sufficient to display only potentially hazardous regions within a 20 dBZ contour or forecast by a translation of the hazardous regions along the cell trajectories. Cell lifetimes are relatively short. Crane and Hardy (1981) found that the average cell lifetime was less than 13 minutes and the lifetimes of the significant cells was roughly a factor of two longer. A significant fraction of the observed cells will not be present after 20 minutes from initial detection or,

16

using a minimum of two volume scan sequences to estimate a cell velocity,
10 minutes after display with an observed velocity for extrapolation.
More importantly, the intensity of the turbulence tends to decrease with
age and a forecast of probable locations for new cell development is
required to provide hazard warning at or before the time a cell (or
turbulent patch) is detectable by radar.

Moderate-to-severe turbulence was observed in clear regions (reflec-
tivities less than 7 dBZ) within 15 km (8.1 nm) of the 7 dBZ contoured
region boundaries on one of the days (22 June 1976). Severe turbulence
patches existed out to more than 15 km (8.1 nm) from the closest 40 dBZ
boundary, to 19 km (10.3 nm) from the closest 50 dBZ contour boundary,
and to 20 km (10.8 nm) from the closest multicell storm core with a peak
reflectivity above 40 dBZ. The severe turbulence in clear regions,
regions outside the surveillance capability of Doppler weather radars,
were outside the buffer region employed by the aviation turbulence
advisory service operated in Australia in 1974 (Barclay, 1974) but within
the region to be avoided as specified by FAA Advisory Circular 00-24A
(FAA, 1978) and recommended by Burnham and Lee (1969). Doppler or conven-
tional weather radar observations cannot be used directly to reduce the
size of the region to be avoided; but forecasts based on cell and cluster
location and movement information should be useful in significantly reduc-
ing the size of the area to be avoided.

Analyses of an extensive set of significant cell and cluster (SC)
data from Kansas and of limited data sets from Colorado, Oklahoma, and
Virginia have revealed the existence of a preferred spacing between SC's.
Forecasts based on the preferred spacing concept together with informa-
tion on the organization and motion of the regions of severe convection
(detected SC's) should be developed to reduce the size of the region to
be avoided, an important goal of hazard detection and forecast systems
especially for terminal area operations. What is evident is that new
cell development location forecasts are required to solve the hazard
detection problem.

Ultimately, a completely objective forecast system will be required
to generate automatically timely hazard warnings for display to a con-
troller. Practically, this goal will not be reached in the foreseeable
future. Our current knowledge of the mesoscale dynamics of storm systems

17

is imperfect and complete automation at this time will produce more problems than solutions. The cell detection and tracking algorithms developed during this research program and the allied programs for WPRS and AFGL provide the essential information required for display to a meteorologist for manual analysis and forecast. Automated forecast products should be displayed to the meteorologist for interpretation prior to display to a controller. These products should also be recorded for post mission analysis and forecast verification. With experience, the gradual automation of the entire system should be possible.

1.3 Organization of Report

This report summarizes the results of the 1978-1981 research program conducted for the Federal Aviation Administration under contract to the Water and Power Resources Service of the Department of Interior. Section 2 reviews the background of the thunderstorm hazard detection problem and the application of the cell association hypothesis for the solution to the problem. Section 3 presents the analysis of the radar observations, Section 4 describes the aircraft penetration data and Section 5 provides a detailed statistical analysis of the validity of the cell, turbulence association hypothesis. Recommendations for further research are presented in Section 6.

2. BACKGROUND

2.1 Thunderstorm Hazards

Thunderstorms have long been known to be potentially hazardous to aircraft operations. Several types of hazards exist. Hail encounters can present major difficulties. As an example, the Southern Airways DC-9 crash on April 4, 1977 was attributed to the ingestion of massive amounts of water and hail during a penetration of an area of severe weather (AWST, 1978). Turbulence and low level wind shear encounters also present safety hazards. Brunstein (1971) reported 58 air carrier accidents during the 1965-1969 time period attributed to turbulence produced by convective activity. Fujita (1978) documented a number of recent air carrier accidents attributed to low level wind shear induced by cold outflow from convective showers. The microburst outflows affect aircraft while landing or taking off and therefore are important to the terminal area controller.

Occurrences of hail or heavy rain are readily associated with local increases in reflectivity, i.e. reflectivity cells, observable by weather radar. The association between turbulence in convective storms and radar observables is more tenuous, especially if only conventional radar data (reflectivity) are available. An association between a microburst detectable by direct observations only near the ground and either reflectivity or Doppler radar observations at heights well above the ground is even more tenuous.

2.2 The Cell Approach to Hazard Detection

Crane (1976) argued that the cloud-to-small mesoscale structure of the reflectivity field (1-10 km scale size) should provide adequate clues for the detection of thunderstorm hazards due to hail, to heavy rain, or to convective turbulence. The argument was based on the physics of cloud scale motions within the active regions of convection. During the early stage of the development of a convective cell, an updraft driven by the increased buoyancy produced by the release of the latent heat of condensation transports moisture aloft which, when condensed and converted to ice, is detectable by radar as a local reflectivity maxima. The stages

of development of an isolated cell are depicted schematically in Figures
4a-d. The initial stage, presented in Figure 4a, depicts the updraft air
flow and the initial echo region which is detected as a three-dimensional
reflectivity (volume) cell. Turbulence is expected to occur in the
localized region of higher shear at the edge of the updraft. In this
picture, precipitation tracers are not available in the region of turbu-
lence for observation by a Doppler radar and hazard detection is possible
only by the presumed proximity between the updraft edge and the volume
(reflectivity) cell. The turbulence patch is depicted as a cross-hatched
region along the aircraft track. In this and following figures, the
cross-hatched region represents moderate turbulence; a solid black region
represents severe levels of turbulence (see Figure 5 and Section 4).

As the cell develops, more precipitation particles are deposited by
the updraft which settle and produce a localized downdraft by evaporative
cooling and atmospheric drag. The downdraft concentrates the return flow
from the updraft and produces a higher shear and more turbulence at the
updraft, downdraft boundary (see Figure 4b). In this case, precipitation
tracers are available within the turbulent patch and the velocity pertur-
bations produced by the updraft, downdraft combination are detectable by
Doppler radar. The cell detection algorithms developed by Crane (1979a)
define either reflectivity cells which enclose the area within 3 dB of a
local reflectivity maxima or tangential shear cells which enclose the
region within 1.5 m/s/km (0.9 kts/1000') of a local maxima in the magnitude
of the tangential shear. Using these criteria, a displacement must be
expected between the centroid locations of the reflectivity cell and the
tangential shear cell at the updraft, downdraft interface associated with
the cell. This displacement is depicted in Figure 4b by an offset between
the volume cell and the turbulent patch. The volume cell is a three-
dimensional assemblage of associated reflectivity (and/or tangential
shear) cells detected at successive azimuth scans in a volume scan (tilt)
sequence.

The downdraft may accelerate and produce a microburst when it and
the accompanying rain shaft strike the ground (Figure 4c). In this case,
a volume cell, a middle level turbulent patch, and a microburst (ground
level) are all in close proximity and lie within the radius of influence
of the volume cell. Successive observations of newly developing volume

20

SINGLE CELL — INITIAL STAGE

VOLUME CELL

TURBULENCE

AIRCRAFT

AIR
FLOW
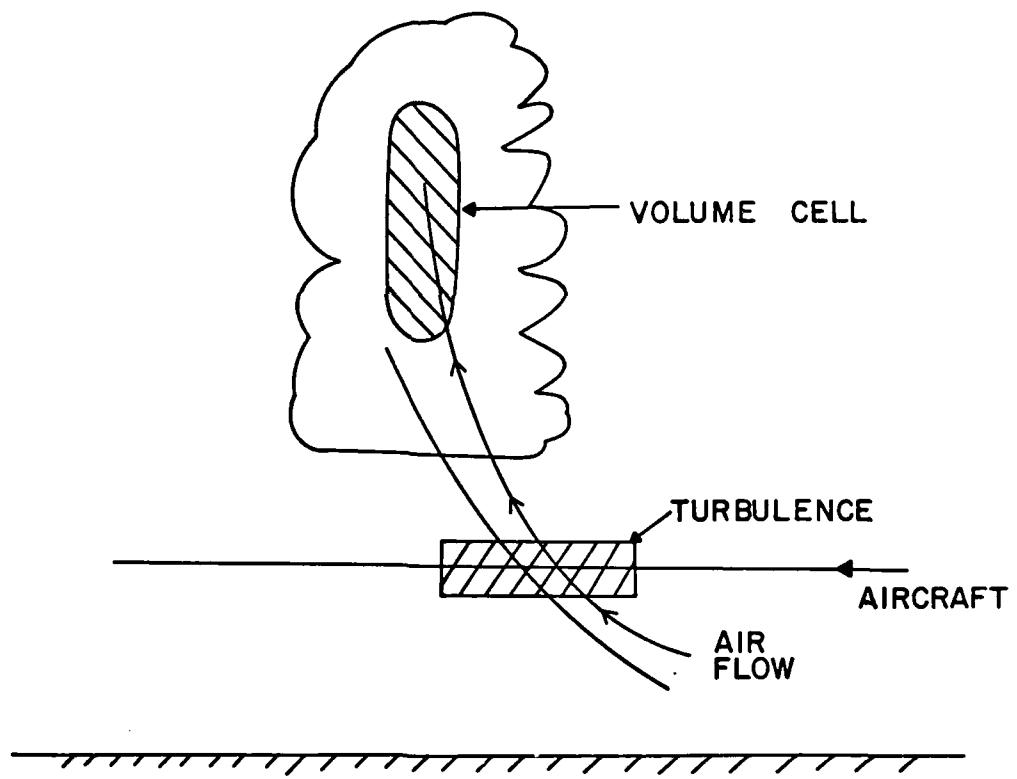
Figure 4a   Stages in the development of an isolated convective cell

SINGLE CELL—SECOND STAGE
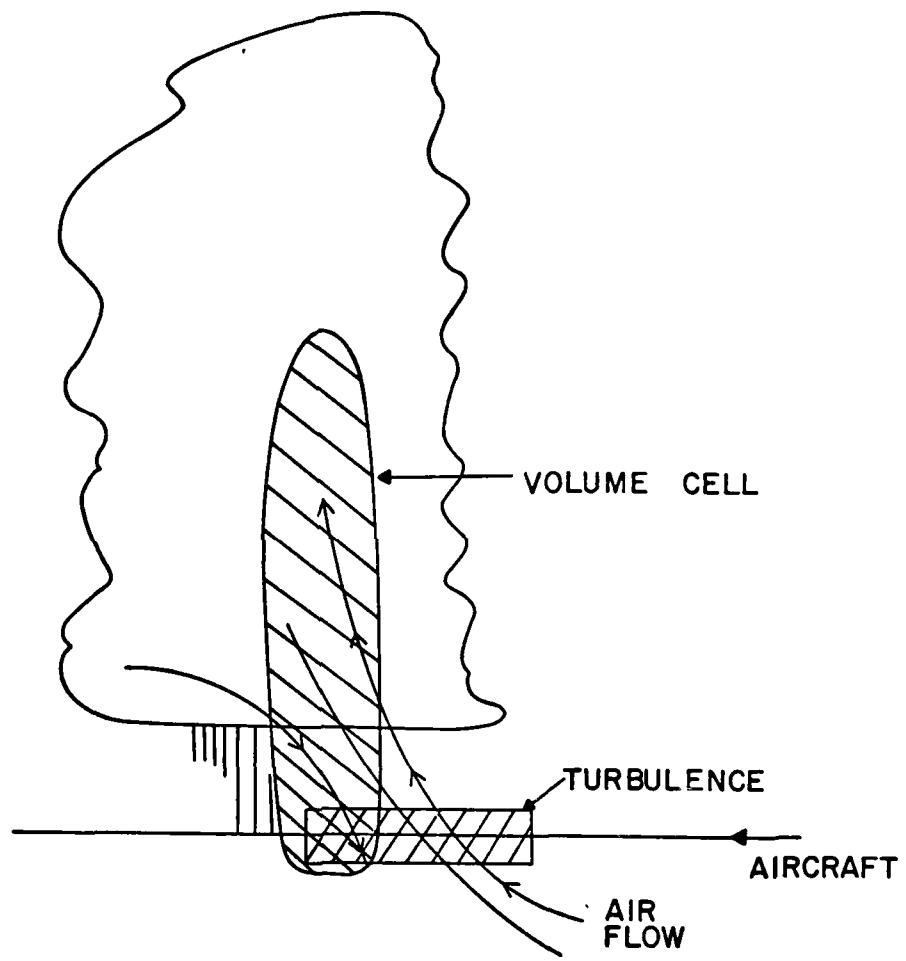
Figure 4b   Stages in the development of an isolated convective cell

SINGLE CELL—RAIN OR GROUND
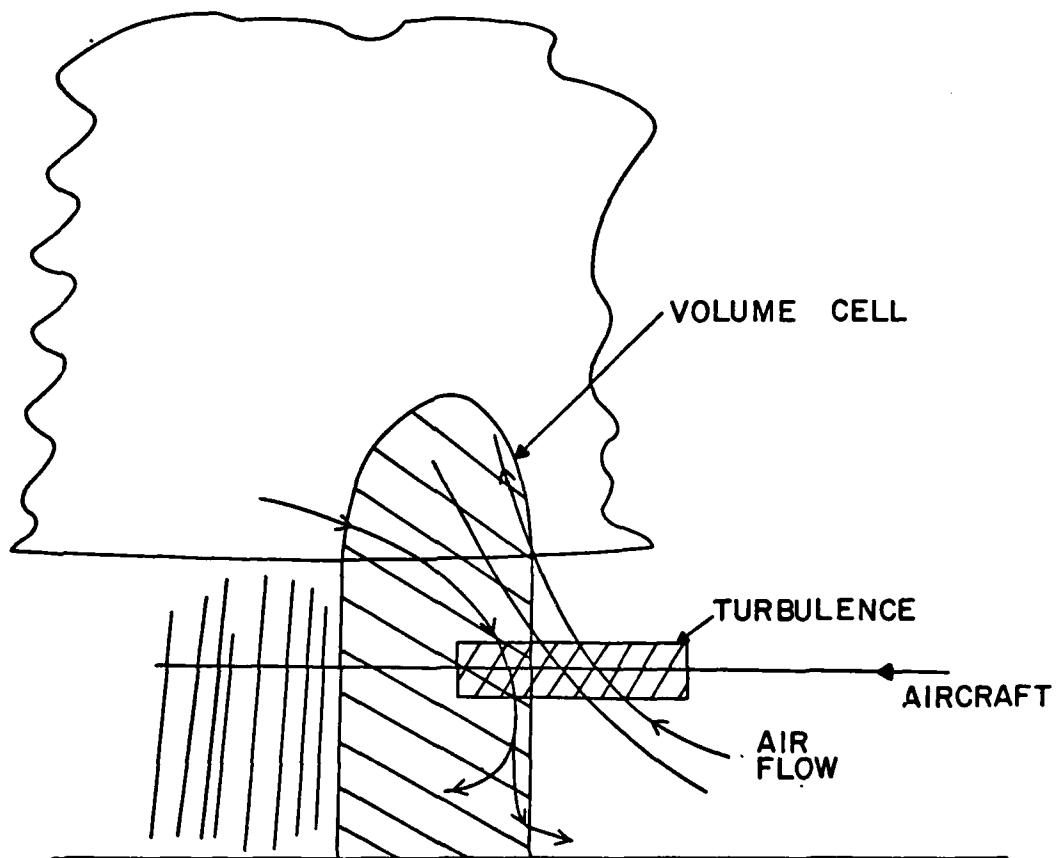
Figure 4c   Stages in the development of an isolated convective cell

VOLUME CELL

0°C

TURBULENCE

AIRCRAFT

AIR
FLOW
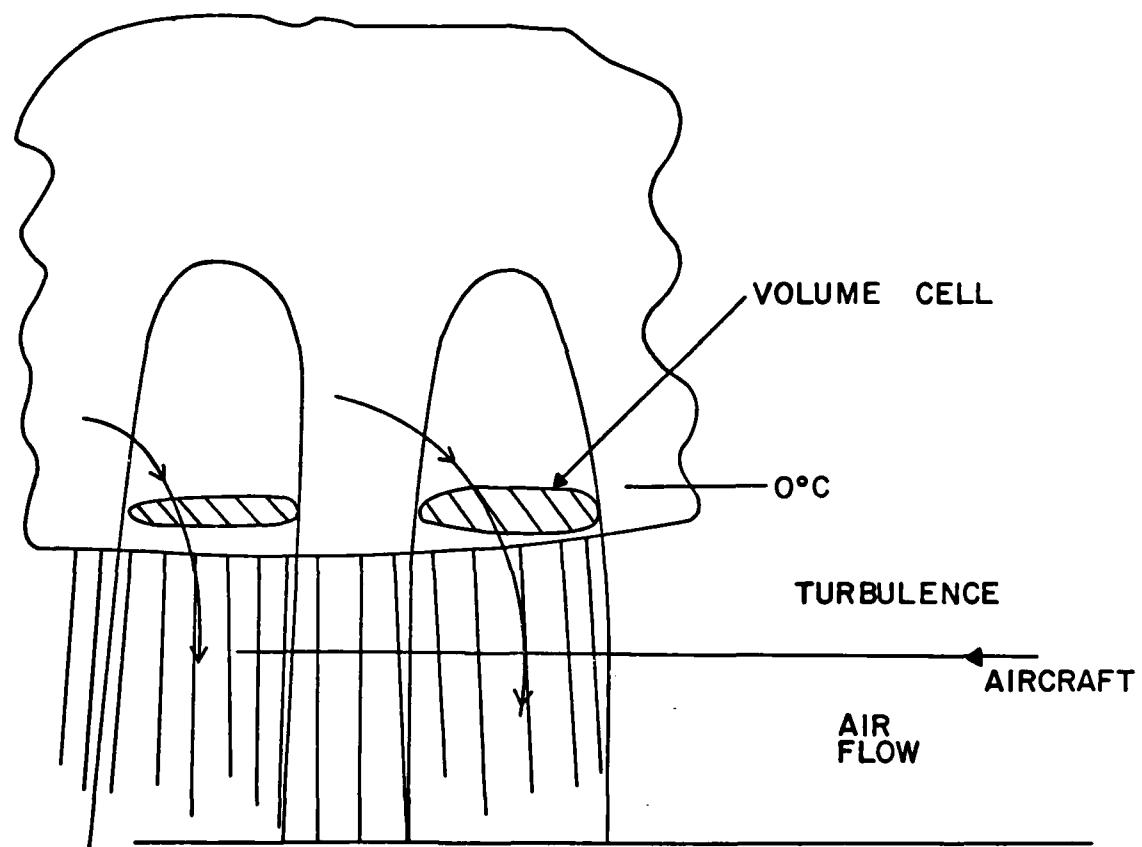
Figure 4d   Stages in the development of an isolated convective cell

cells associated with isolated updraft regions show initial cell development aloft, followed by a rise in cell height, then a sinking of the cell (Crane and Hardy, 1981). The sink rate approximates the expected fall velocity of a pulse of precipitation. From the first few observations of a cell, the time at which the rain pulse strikes the ground may be calculated and used to locate possible microbursts. Not every cell will produce a microburst, however, because mixing may occur between the downdraft and the environmental wind both above and near the surface; this mixing will reduce the magnitude and velocity of the outflow.

Finally, the updraft weakens, the remaining precipitation debris settles, clumping into smaller cells and producing reflectivity maxima (volume cells) in a horizontally inhomogeneous bright band by aggregation and melting. In this case, depicted in Figure 4d, one or more volume cells may be detected but no turbulence is expected. The volume cells appear in a cluster which is not associated with turbulence.

This physical model as initially proposed by Crane predicted a high degree of association between reflectivity cells, hail in the cores of the reflectivity cells, turbulence at middle levels, heavy rain on the ground, and low level wind shear produced by microbursts. It was the basis for the turbulence hazard detection hypothesis that initiated this research program. Concomitant research for WPRS revealed that in one of the Kansas 1978 aircraft case studies the mode of cell development switched from isolated cells as depicted in Figure 4 to the multi-cell structure depicted in Figure 5 (see Section 4.4, Crane and Hardy, 1981). In this case, the updraft continued to strengthen and cells formed in a cluster. At the time of cluster development, the aircraft crews noted a shift to more vigorous development and a stronger updraft. The updraft region coincided with a weaker reflectivity region surrounded by four volume cells. The higher cell depicted schematically in the overhang region in Figure 5 appeared with a high initial reflectivity value, greater than 40 dBZ. As illustrated in Figure 5, the cluster of cells is to be associated with stronger, perhaps extreme, turbulence. If hail is present, the volume cells in the cluster will coincide with the individual hail shafts if the radar system has sufficient resolution to separate the shafts.

The multi-volume-cell cluster surrounding a strong, and persistent

MULTIPLE CELL – (CLUSTER)
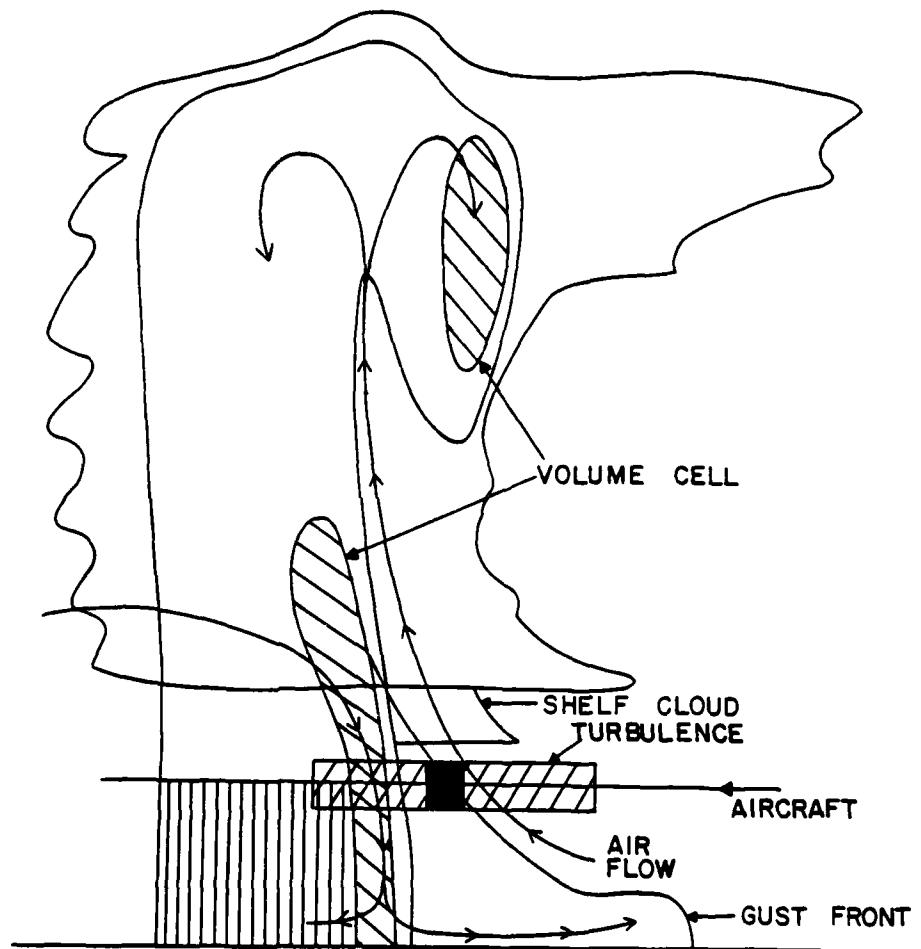
Figure 5   Volume cells in a cluster

updraft can be identified with individual weak echo regions in multi-cell storms or with a supercell (Browning and Foote, 1976). In the detailed Kansas case study, the cluster was an element of a multi-cell storm with separations between isolated significant cells and the observed cluster of the order of 10 km; the average spacings between isolated significant cells and clusters (SC's) during the most active period of the entire storm was 11.7 km. The model to be evaluated therefore evolved into a consideration of significant cells and clusters.

2.3 The Use of Doppler Radar Data

Historically, attempts have been made to identify thunderstorm turbulence hazards on the basis of reflectivity or Doppler data field features that could be matched on a point-by-point basis with turbulence encounters during aircraft penetrations. In these analyses, features, such as the maximum reflectivity value or reflectivity gradient value encountered by an aircraft when its track was superimposed upon the reflectivity field measured at the height of aircraft penetration, were used for comparison with the spatially coincident aircraft observations of turbulence. Lee (1977) produced similar point-by-point comparisons with features of the radial velocity (Doppler velocity) field and with the Doppler spectrum width field after finding little correlation between the point-by-point reflectivity features and aircraft turbulence. He found a significant number of coincidences between Doppler spread values in excess of a threshold value of 4 m/s and moderate or more intense turbulence. Using occurrences of Doppler spread values in excess of 4 m/s as predictors of moderate or stronger turbulence, he obtained a 93 percent probability of detection. If he used Doppler velocity spread values observed within 2 km of the aircraft track, he increased the probability of detection to 95 percent.

In contrast to point-by-point matching, the cell detection model anticipates coincidence between the cell and turbulence only within a radius of influence of the cell. The coincidence is expected over a wide range of heights, from ground level (microbursts) to the upper levels of the troposphere; the detection or delineation of regions of potential hazard therefore apply to all heights within the troposphere. In proposing the cell detection hypothesis, Crane (1976) contended that,

by relaxing the coincidence requirement, conventional weather radar data would be as useful as Doppler radar data for the detection of thunderstorm turbulence. He further anticipated that Doppler radars could not be used directly for the estimation of the intensity of turbulence because of anisotropy on the scale of the radar resolution volume. Lee (1977) confirmed this expectation by observing a lack of correlation between the magnitudes of the Doppler spread and the derived gust velocity values.

Crane (Figure A1, 1976) summarized turbulent velocity measurements made by Sinclair (1974), measurements reproduced in Figure 6, which show that the vertical velocity variance produced by thunderstorm turbulence is anisotropic at scales larger than about 200 m (departure from the $\kappa^{-5/3}$ line at scale sizes larger than 200 m is indicative of anisotropy, see Monin and Yaglom, 1967). Doppler spectral broadening is produced by turbulence induced velocity fluctuations on scales commensurate with the maximum dimension of the radar resolution volume. For radar observations with maximum resolution volume dimensions in excess of 500 m (at ranges in excess of 30 km for a 1° beamwidth radar) the Doppler spread is produced by anisotropic turbulence. When the turbulence is anisotropic, the observed Doppler spread values no longer depend on the intensity of the turbulence in the isotropic region (the region of each spectrum at scales marked "range for maximum aircraft response" and smaller scales) which can be specified by an eddy dissipation rate, ε, but depend on the departure from isotropy produced by the three-dimensional cloud scale updraft, downdraft motion and larger scale vertical and horizontal shear. The result is an observed Doppler velocity variance which depends on the azimuthal location of the radar relative to the turbulent patch but does not depend on ε.

The magnitude of the velocity fluctuations (perturbations) increase as the scale size increases up to scales of the order of 5 km (cloud scale); as shown in Figure 6, for larger scales, the vertical velocity (and corresponding horizontal velocity) variance does not continue to increase. Observations in the 1 to 10 km size range are optimum for the observation of velocity perturbations induced by turbulence. Gate-to-gate (radial) shear or beam-to-beam (tangential) shear may be readily observed on this scale producing larger perturbation signatures than can be expected from Doppler spread observations. Tangential shear appeared to
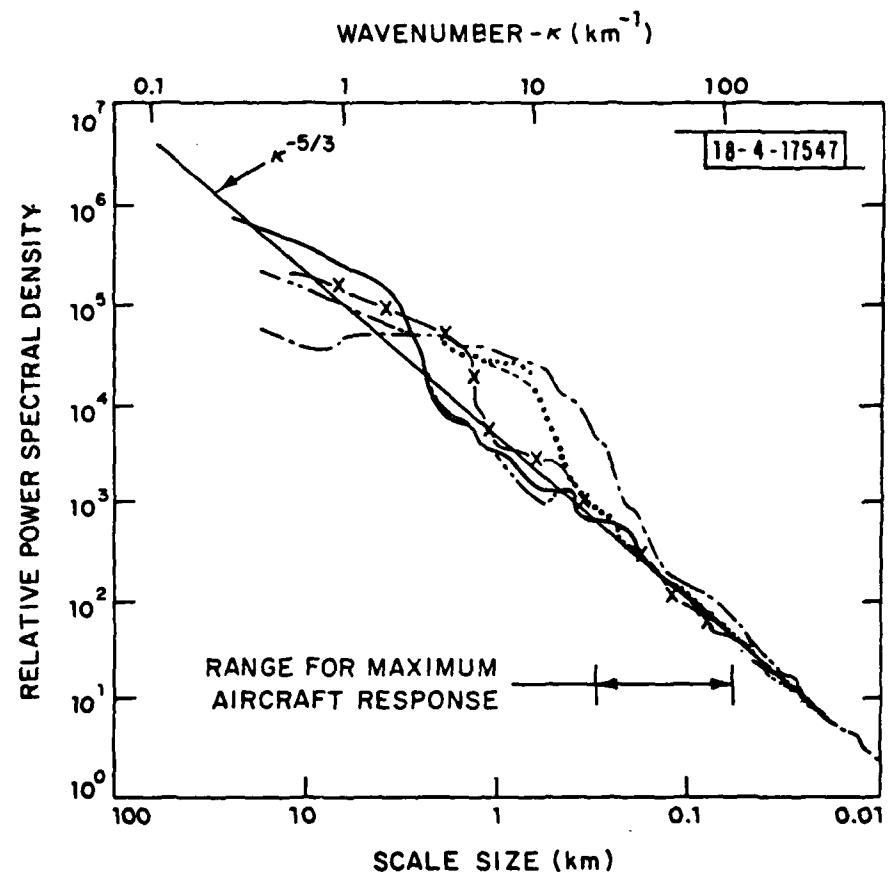
Figure 6   Power spectra of vertical velocity fluctuations obtained
within thunderstorms (adapted from Sinclair, 1974)

be optimum for the observation of the cloud scale velocity perturbations because of the success reported by Burgess (1975) and by Brown and Lemon (1976) in using tangential shear for the detection of tornadoes and meso-cyclones. They found significant correlations between tangential shear peaks (mesocyclones or tornadic vortex signatures) greater than 5 m/s/km and occurrences of tornadoes, wind, and hail. Using mesocyclone and tornado vortex signatures to detect severe weather or tornadoes, the JDOP report (1979) indicates a probability of detection of 70 percent, a false alarm rate of 24 percent and a critical sucess index of 60 percent for the 1977-1978 seasons.

The justification for the use of tangential shear for severe weather analysis is based on the idealized Rankin vortex model (Figure 7) for the flow within a tornado or mesocyclone (Donaldson, 1970). The idealized vortex is azimuthally symmetric and observation should not depend on the location of the vortex relative to the radar. The strong updrafts experienced in multi-volume-cell clusters however show a tendency to block the flow at middle levels of the troposphere producing flow patterns similar to the one illustrated in Figure 8. In this case, the tangential shear is anisotropic and the observed magnitude will depend on the direc-tion to the radar relative to the direction of the middle level flow. It is noted from the magnitude of the tangential shear plots that more than one tangential shear cell may be associated with a vortex or blocking updraft.

In a recent review of the use of single Doppler weather radars (Wilson et al., 1980), the use of radial shear was demonstrated for the detection of shear lines. Either radial shear or tangential shear may be employed to detect localized or linear velocity perturbation features. Radial shear observations cannot be used for the detection of idealized Rankin vortices but idealized azimuthally symmetric vortices do not exist and real vorticies should produce measurable radial shears. Similarly, idealized horizontal shear regions along constant radius arcs cannot be detected using tangential shear observations but, again, they do not occur in nature. The use of either one or the other or the magnitude of the vector sum of the two shears depends on which measure of velocity field perturbation is least susceptible to measurement uncertainties. Crane (1977) investigated the use of radial and tangential shear in the analysis of weak convective activity in New England and found that

SIMPLE VORTEX (RANKIN)

VORTEX IN QUIET AIR

RADAR

RADIAL VELOCITY

MAGNITUDE TANGENTIAL SHEAR
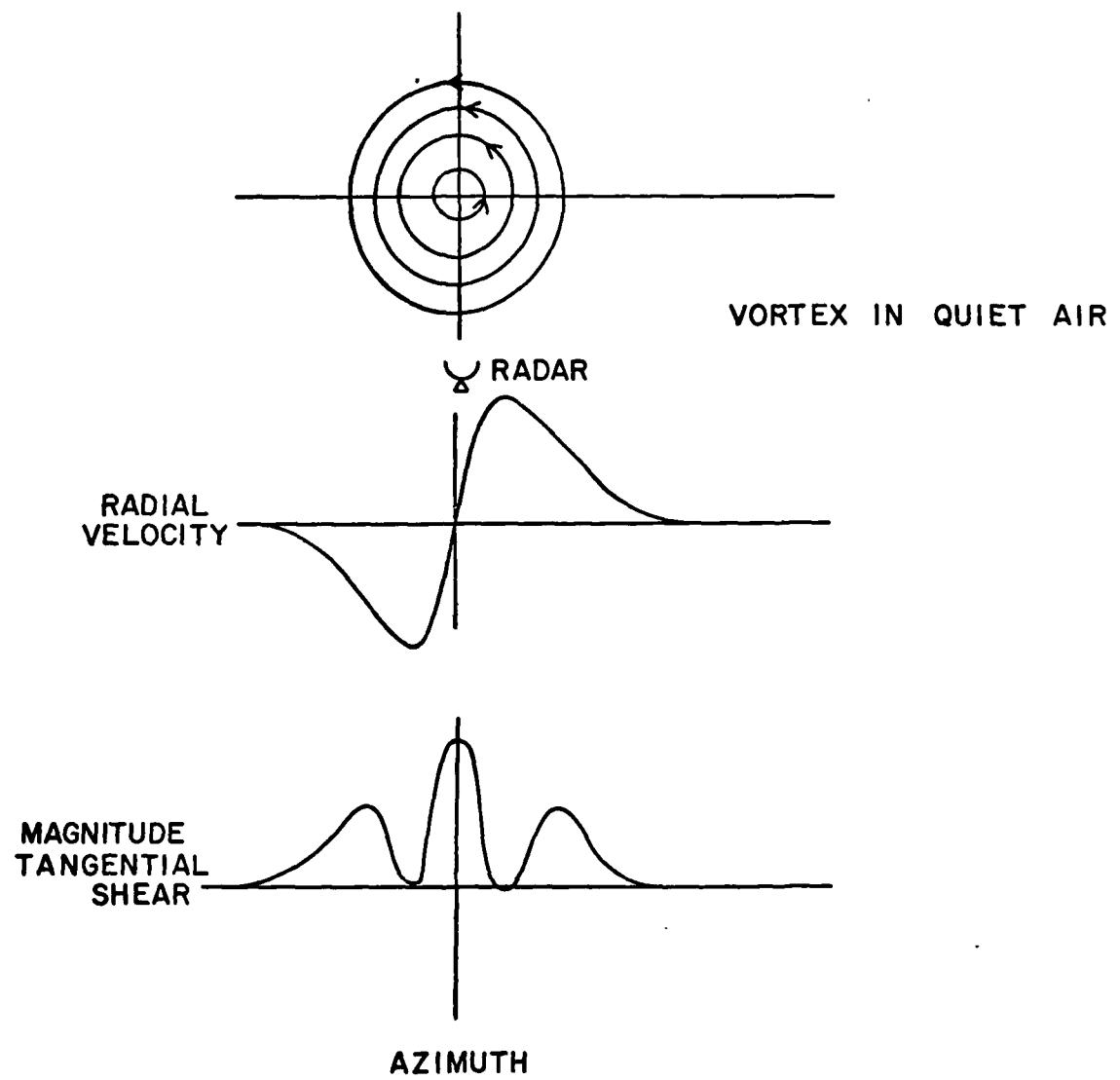
AZIMUTH

Figure 7   Mid-level flow pattern for an idealized azimuthally
            symmetric vortex

LIFTING   WITH   SUPPRESSED   ENTRAINMENT

STREAM   LINES

↑ DIRECTION   OF   LOW
LEVEL   FLOW

⟋ DIRECTION   OF
AMBIENT   FLOW   AT
HEIGHT

𝖸 RADAR

RADIAL
VELOCITY

MAGNITUDE
TANGENTIAL
SHEAR

AZIMUTH
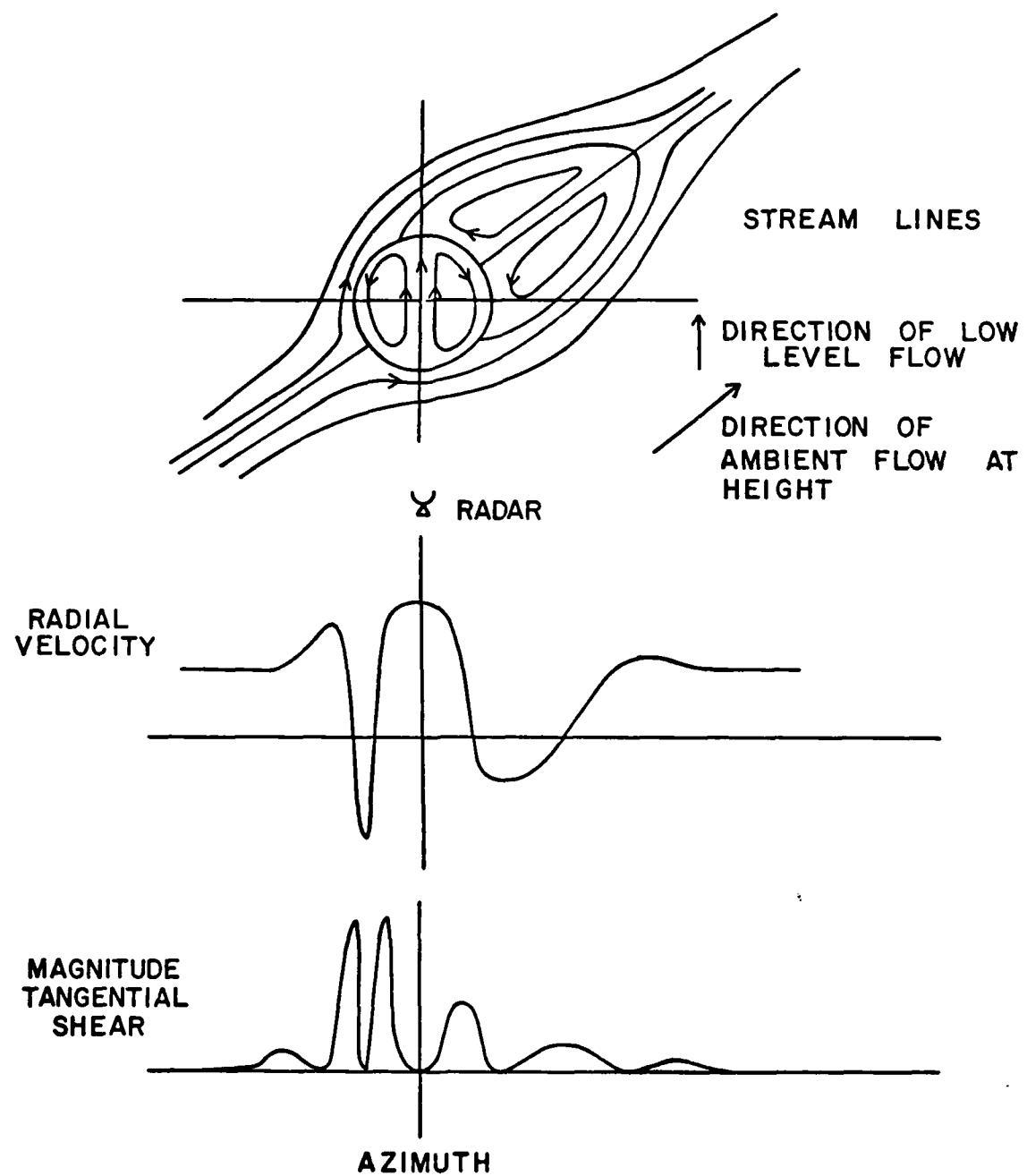
Figure 8   Mid-level flow pattern for a blocking updraft (Reynolds
Number of 40)

tangential shear perturbations (cells) were less affected by the statistical variations in velocity measurements than were radial shear cells and recommended the use of tangential shear.

3. RADAR OBSERVATIONS

3.1 Significant Cells and Clusters

The cell detection and tracking algorithms developed by Crane (1979a) provided the significant cell output used for comparison to aircraft encounters with turbulence in the evaluation of the cell approach to hazard detection. In brief, the radar data were (1) read from magnetic tapes, (2) calibrated, (3) averaged to roughly a 1.5 km range interval, (4) contoured to establish the regions of data to be processed through the cell detection program, and (5) processed through cell detection; the cells were then tracked (associated from one azimuth scan to the next to generate volume cells for each raster scan sequence). Data from the Doppler radars were used to prepare reflectivity and tangential shear maps for each azimuth scan and both data fields were processed independently by the cell detection program. The output from cell detection consisted of an interleaved array of reflectivity and tangential shear attributes. The output from tracking the reflectivity and tangential shear cells included volume cell centroid location, track velocity, and the average values of reflectivity and tangential shear.

3.1.1 Conventional Radar Data

The radar data employed for analysis were acquired in two different formats and processed using two different computer systems. Data from the conventional CP-2 S-band radar were acquired in the packed DADS 7-track radar data format* after being reformatted to 9-track tape. Table 3 contains a listing of the characteristics of the radars which have provided data for processing through the cell detection and tracking programs. The CP-2 data were read and processed by an early version of the cell detection program which operated on an IBM 370/158 computer. The program provided contour line data (vectors) and reflectivity cell attributes. The contour lines were plotted as shown in Figure 9 together with the cell centroid locations. Cell attributes were recorded on magnetic tape and stored for later use. The attributes included reflectivity, area, centroid location, time, and elevation angle (height).

---

*supplied by R. Rinehart, NCAR

TABLE 3

RADAR CHARACTERISTICS

PARAMETER	RADAR DESIGNATION					
	CP-2	CP-3	CP-4	NOAA-C	NOAA-D
Frequency Band	S-Band	C-Band	C-Band	X-Band	X-Band
Wavelength	10.7 cm	5.45 cm	5.45 cm	3.22 cm	3.22 cm
Beamwidth	1.0°	1.2°	1.2°	0.8°	0.8°
Pulse Length	0.9 μsec	1.0 μsec	1.0 μsec	0.7 μsec	0.7 μsec
Averaged Range Interval	1.2 km	1.6 km	1.6 km	1.5 km	1.4 km
No Samples	64*	32*	32*	64*	64*
Type	Conventional	Doppler	Doppler	Doppler	Doppler
Unambiguous Velocity	-	13.6 m/s*	13.6 m/s*	21.8 m/s*	17.5 m/s*

*varied during experiment, value shown for 22 June 1976
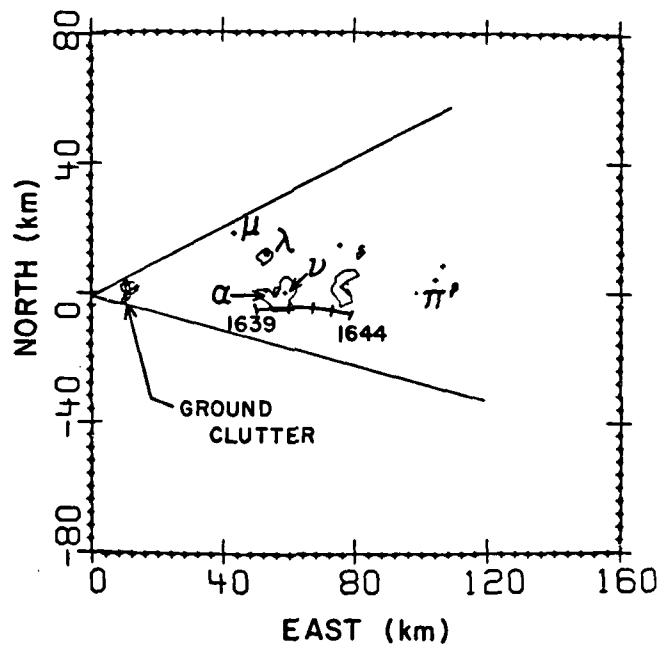
Figure 9   Computer generated contour and cell location plot. Data
are for 0.6° elevation angle, 1640:50 MDT on 22 July 1976.
The contours enclose reflectivity values ≥40 dBZ.

36

Figure 9 presents observations obtained on the lowest elevation angle azimuth scan of a raster scan sequence on 22 July 1976. Contour data were prepared at two thresholds, 17 and 40 dBZ. Only the 40 dBZ contours are displayed. The + symbols mark the centroid locations of reflectivity cells detected at the same elevation angle. The Greek symbols designate the persistent clusters (Section 3.2.1). No editing has been performed on the data and both ground clutter (ring at about 10 km) and precipitation targets are displayed. The track for aircraft penetration Number 2 and the Greek symbols were manually superimposed on the figure. Figures 10a and b present an enlarged view of the area around the aircraft track at the height and time of penetration. The constant altitude contour plot (Figure 10a) was provided by NCAR. The cell locations and intensities displayed in Figure 10b were manually obtained from each of the azimuth scans in the raster scan sequence for cell detections within 1 km in height of the 6 km height constant altitude plot.

The cell detection program operated on all the input data corresponding to reflectivity levels greater than the lowest threshold (17 dBZ). The cells enclosed areas with reflectivity values within 3 dB of a local maxima. Only areas which did not simultaneously enclose any higher level reflectivity cells were used to define a cell. Crane and Hardy (1981) found that cells defined in this manner were relatively small with an average area of 5 km^2. The cells with reflectivities greater than 50 dBZ displayed in Figure 10b correspond to the centers of the 50 dBZ contours displayed in Figure 10a. The locations of the other cells in Figure 10b cannot be readily compared to the contours in 10a because of the differences in the contouring intervals used for display and for cell detection. Of interest is the apparent clustering of cells within the two 45 dBZ contours labeled α and ν. The significant cell and cluster association hypothesis would designate the region of aircraft track between 1640 and 1641 MDT as having a high probability of encountering severe turbulence.

3.1.2 Doppler Radar Data

Doppler data from the NCAR CP-3 and CP-4 radars and the NOAA Wave Propagation Laboratory NOAA-C and NOAA-D radars were supplied* in the

*supplied by F.I. Harris, NCAR
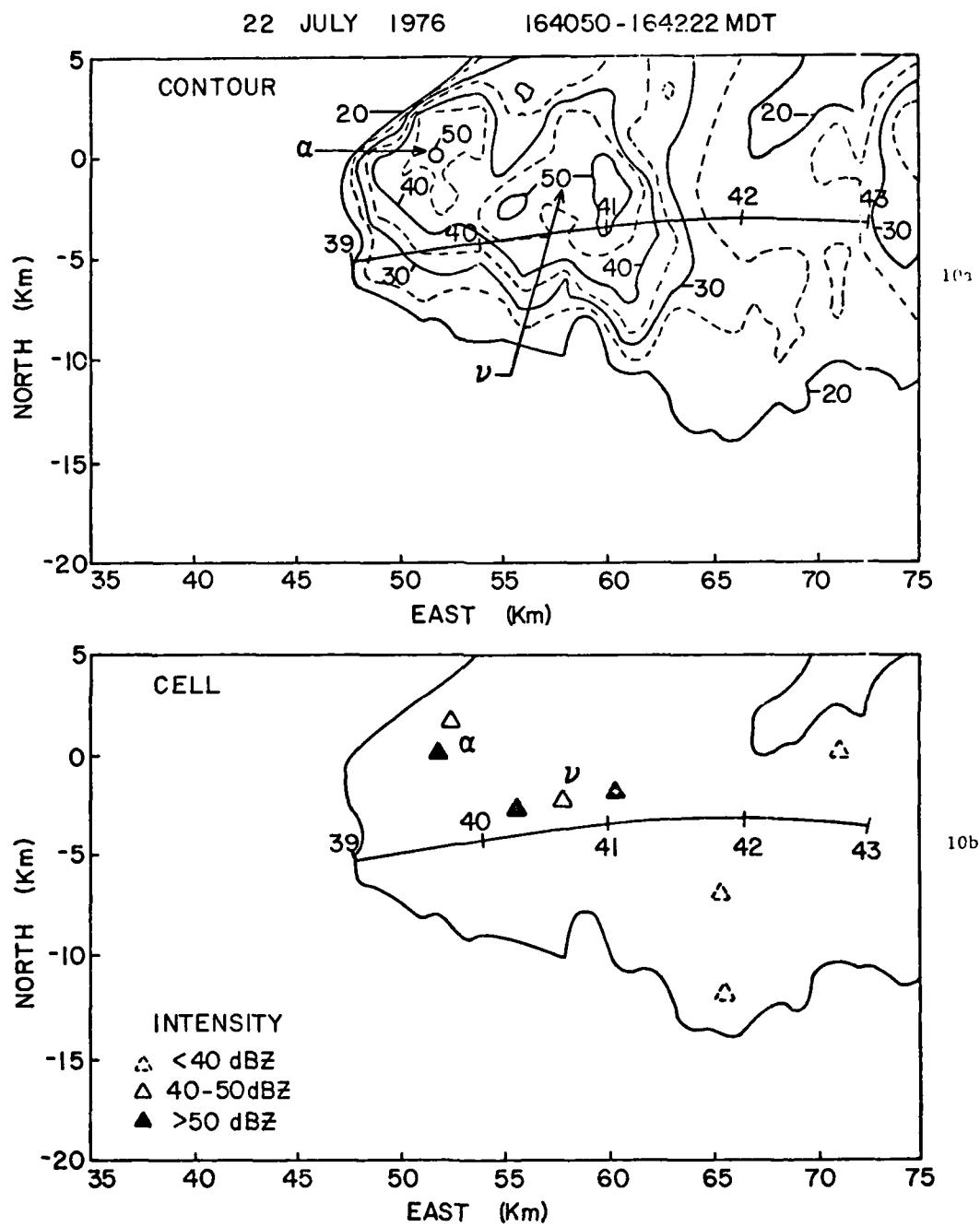
Figure 10   Detailed contour and cell locations at an altitude of 6 km
            (msl) for 1640 MDT, 22 July 1976. Distances are measured
            relative to the location of the CP-2 radar (Grover, Colorado).

expanded FOFRAW data format then used as a universal format for NHRE data storage (see Table 3 for radar characteristics). These data were read and processed on the CYBER-74 computer at the Denver Federal Center by a modified version of the cell detection program developed for WPRS (see Gustafson, 1980 for a description of the basic WPRS version of the cell detection program). The basic program was revised to accept the FOFRAW data, perform the required calibration analysis, resolve automatically velocity ambiguities (Crane, 1978), calculate and average tangential shear estimates, and generate tangential shear cells by operating on the magnitude of the tangential shear field with the same cell detection subroutine as used for reflectivity analysis.

Both reflectivity and tangential shear cells were generated for regions having reflectivity values in excess of the lowest processing threshold (17 dBZ). The attributes recorded for each cell type were identical: reflectivity, magnitude of the tangential shear, area, centroid location, time, and elevation angle. Contour lines were generated at two reflectivity levels, 17 and 40 dBZ and recorded on magnetic tape for future display but none was plotted.

The cell detection algorithm operated on quantized scalar data fields. Cells are regions enclosed within areas corresponding to recorded observations which fall three quantization steps below the highest enclosed value. For reflectivity data processing, the quantization step was 1 dB and the cells enclosed regions within 3 dB of the cell maximum. For tangential shear, the data were quantized in 1/2 m/s/km shear intervals and cells enclosed regions within 1.5 m/s/km of the largest magnitude shear. Attributes were calculated using data from the radar resolution elements included within a cell boundary. The average reflectivity value was calculated from the reflectivities at the range, azimuth locations within a tangential shear cell; conversely, the average magnitude of the tangential shear was calculated from the tangential shear values enclosed within a reflectivity cell.

3.1.3 Volume Cell Tracking

A statistical, best match association process was used in the automated, computer tracking of volume cells (Crane, 1979a). A Lagrangian tracking procedure was employed which shifted the location of a cell* from

---

*volume cell refers to the 3-dimensional entity being tracked; a cell refers to the output of the cell detection program obtained at a fixed elevation angle on a single azimuth scan.

its position at the time of detection to the position it would have had at the reference time for each volume scan. The volume cells were initially given the average velocity of all the cells being tracked during the prior volume scan and the velocity of an individual volume cell was adjusted from its initial value as tracking proceeded. A starting average track velocity was estimated from radiosonde data for each of the case study days although the precise starting value was not critical to the successful operation of the tracking program.

When Doppler radar data were available, the tracking program operated first on the reflectivity cells from an azimuth scan, then on the tangential shear cells for the same azimuth scan. Data of either type were handled in the same way although cell associations with a volume cell were tallied by type. A number of additional attributes were calculated for each volume scan (tilt sequence) including volume cell translation velocity, height, and the identities of the contour and cluster in which it was imbedded.

Clusters were defined on the basis of volume cell similarity and proximity. The best match association procedure tallied all the cells (reflectivity or tangential shear) and all the volume cells that could be matched with each other on a volume scan. The best cell, volume cell pairings were used for tracking and the list of possible matches was used to identify the elements of a cluster. The maximum cell, volume cell separation allowed in a cluster at the reference time was 4.5 km. A cluster with a number of volume cells could span a larger region since a cell could provide the bridge between two volume cells and a volume cell could bridge two cells spreading the domain of a cluster over a number of volume cells.

Clusters defined in this manner are generally small in horizonal extent. The maximum cluster size observed in the CP-2 (reflectivity only) data from the 22 July 1976 case study was 18 km (area of 82 km^2); the average maximum dimension of a best fit ellipsoid spanning a cluster was 5.8±.3 km (average area 13±1 km^2). The association logic was sensitive, however, to false cell detections which were common in the tangential shear data at low signal-to-noise ratios. As an example, cluster observations at 1640 MDT on 22 July 1976 are presented in Figure 11. The Doppler radars were operated with a five-minute volume (tilt)
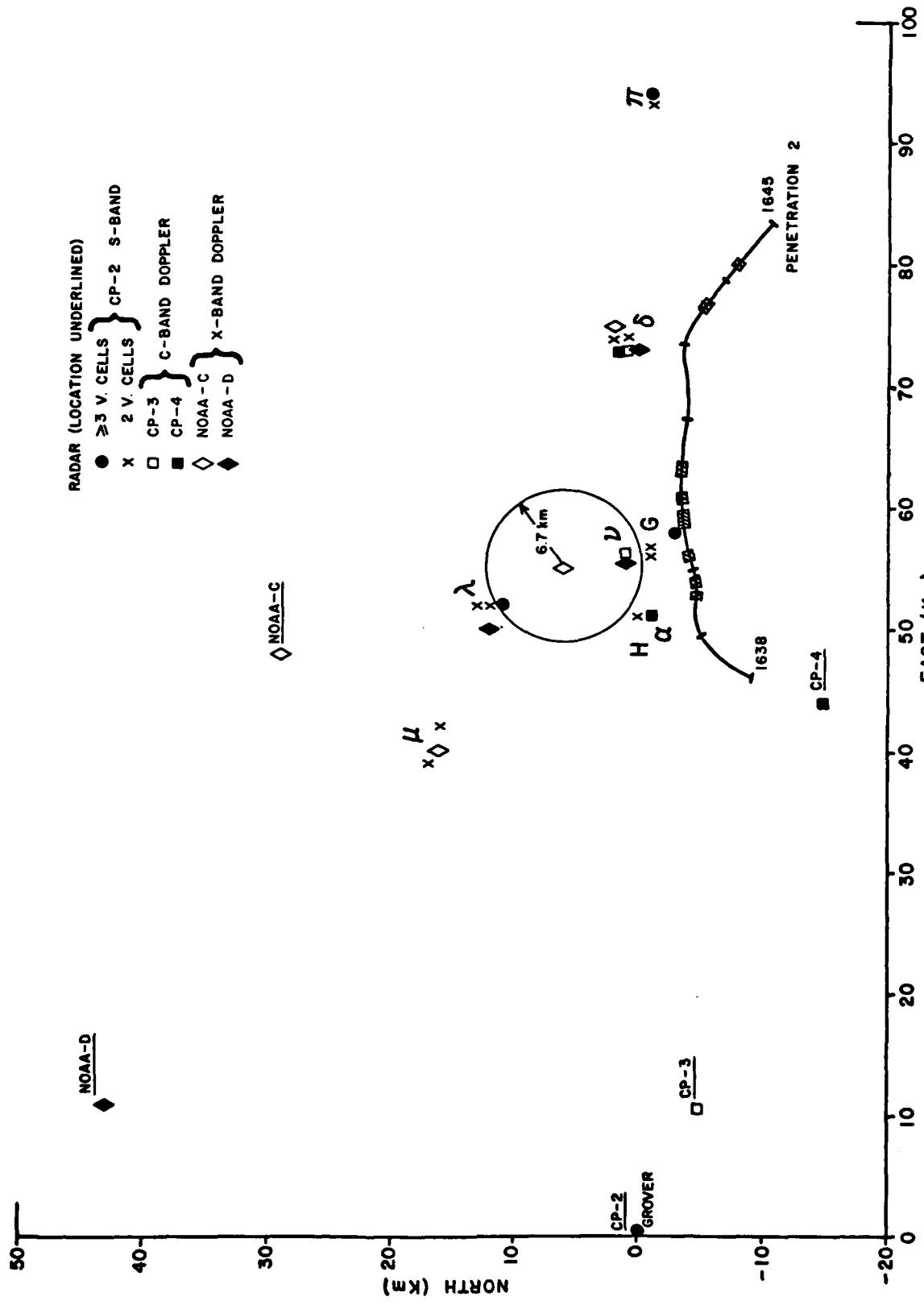
Figure 11 Cluster locations, by radar, for observations between 1637-1642 MDT, 22 July 1976

41

scan sequence. The data from the conventional, CP-2 radar were combined in a composite volume scan spanning the same five-minute time interval. Because of the sequence of elevation angles employed by the CP-2 radar during a five-minute interval, the version of the tracking program used for analysis reported the data as if from seven volume scans, not the expected composite volume scan nor the two to three volume scans actually made during the interval. Unfortunately, all seven reported scans were labeled with the same identification number making separation difficult. As a result, all the data are plotted with an additional code to identify the number of volume cells in a cluster. The Doppler data all correspond to single volume scans and the existence of three or more volume cells in a cluster.

The clusters labeled α and ν in Figure 11, correspond to the major cellular impulses H and G depicted by Wade and Foote (1978) and by Heymsfield et al. (1980) for storm III. The cellular impulses correspond to the clusters automatically separated by the tracking algorithm for all but the NOAA-C radar. The low reflectivity region between cluster λ to the North and the combined α,ν region of higher reflectivity (see Figures 9 and 10a and also Jameson and Heymsfield, 1980) was populated by low reflectivity tangential shear cells which bridged the gap between the separate clusters. These false cells are in evidence in Figure 12. In this figure, only the significant cells were plotted.

For this study, a significant cell consisted of three or more cells (reflectivity or tangential shear) associated with a volume cell during the five-minute composite volume scan. With the exception of cell detections by the NOAA-C radar, the cells appear as a number of tightly grouped clumps corresponding to the clusters in Figure 11. As before, multiple cells are depicted at each significant cell location due to the increased number of apparent volume scans in a composite volume scan interval for the CP-2 radar. The wider area of false alarms contributed to the large area cluster depicted in Figure 11 for the NOAA-C radar. Since the centroid location for the cluster was computed using reflectivity weighted volume cell positions, the cluster is positioned between the three high reflectivity clusters corresponding to α, ν and λ. The area associated with this cluster was 139 km^2, more than 10 times the average observed using CP-2.

42
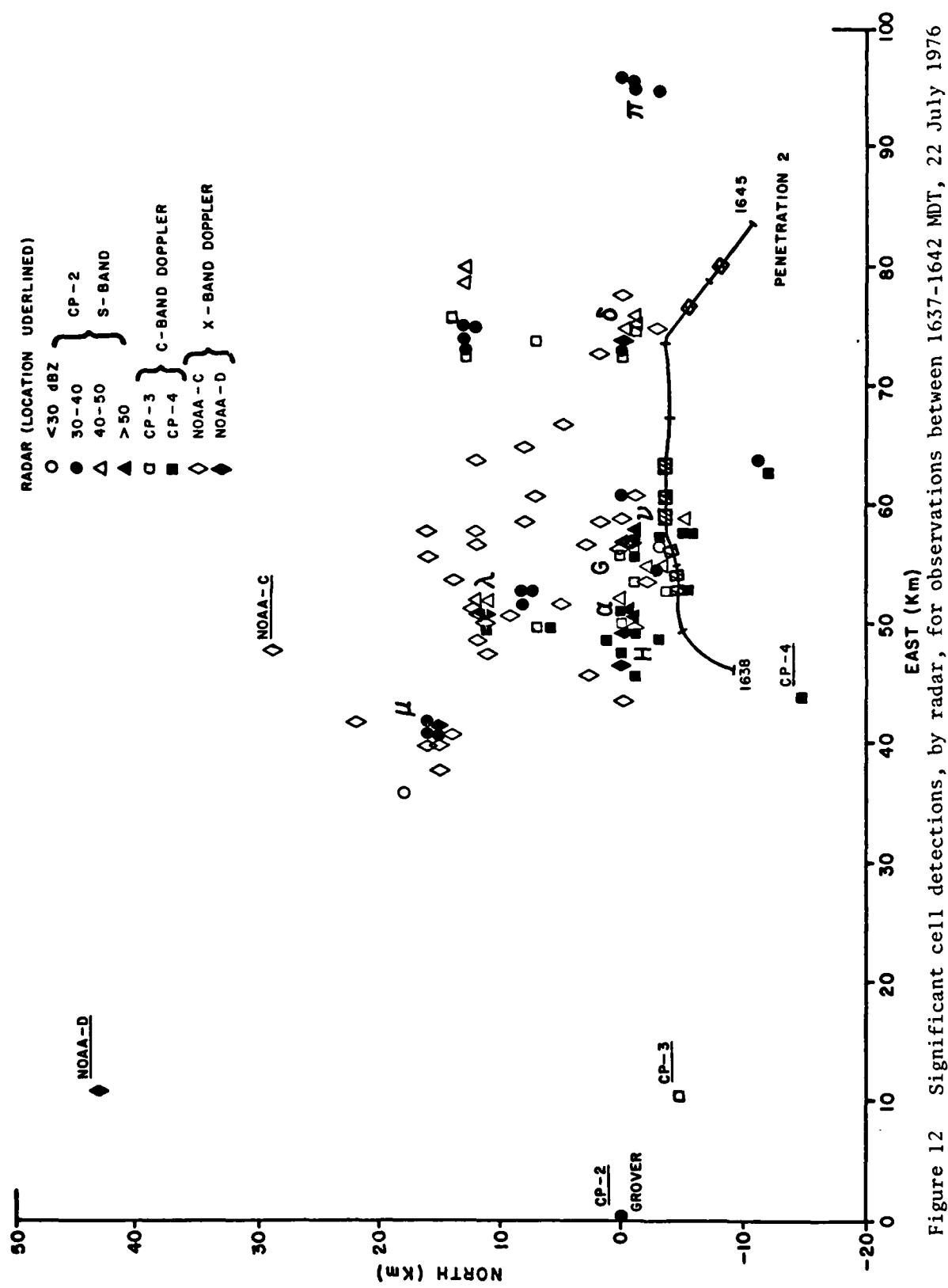
Figure 12   Significant cell detections, by radar, for observations between 1637-1642 MDT, 22 July 1976

43

Fictitiously large and improperly positioned clusters were also
detected by each of the Doppler radars on 22 June 1976 and both the
NOAA-C and CP-3 radars occasionally produced large clusters for the 22
July case study. Because of the large clusters (high false alarm rates
for tangential shear cells) and, more importantly, because the computer
tape containing the cell detection output for the CP-2 data for the
aircraft penetration time periods on 22 June 1976 was lost, the cluster
data were only partially analyzed for the evaluation of hazard detection.
Because the significant cell data were readily available and reliably
positioned, the principal statistical analyses were performed using only
the significant cell data. The increase in false cell detections near
the aircraft track will bias the statistics towards higher false alarm
rates than would be expected for the cluster data alone. Because the
aircraft penetration flights were generally through the higher reflec-
tivity regions of the storm, the effect of the bias on the evaluation of
the utility of the Doppler radar should be small. The cluster and
significant cell results listed in Tables 1 and 2 are not significantly
different.

3.2 The NHRE Case Studies

Radar data were supplied by NCAR and aircraft data were supplied by
South Dakota School of Mines and Technology (SDSMT) for two of the
National Hail Research Experiment (NHRE) case study days, 22 June 1976
and 22 July 1976. An analysis of the former day was published by Harris
et al. (1978); analyses of the latter by Wade and Foote (1978), Kelley
et al. (1978), Heymsfield et al. (1978), Foote et al. (1978), Jameson
and Heymsfield (1980), and Heymsfield et al. (1980).

The two case studies correspond to the occurrence of multicell hail
storms optimumly positioned for triple Doppler radar analyses of the
three-dimensional wind fields. Four Doppler radars were employed. Their
characteristics have been summarized by Harris et al. (1978) and by Wade
and Foote (1978). The important radar characteristics are listed in
Table 3. Their locations are depicted in Figures 11 and 12. Extensive
manual (computer aided) editing was required to prepare the data for
multiple Doppler radar analysis. Because of the large manpower commit-
ment required for multiple Doppler analysis, only a limited number of

44

volume scans were prepared for each of the case studies. Although the automated processing programs employed in this research did not require editing, the data to be processed for the case studies were prepared in the universal format by NCAR, and consequently only these data to be edited were available for further analysis. As a result, only 6 to 11 volume scans (depending on the radar) or less than 55 min of data were available for the 22 June case study and 2 to 4 volume scans (less than 20 minutes) for the 22 July case study. The scans were spaced by intervals as large as 15 to 20 minutes negating their utility for automated tracking.

Continuous, rapid volume scan (1.5 minutes per scan) data were available for the CP-2 radar. Because of the missing computer output tape, only data from 22 July could be automatically processed but, because of the elevation angle sequence employed by the radar, the resultant volume cells could not be tracked automatically from one volume scan to the next. The tracking program (and, for CP-2 and 22 June, the plotted data) did provide significant volume cell data which could be readily compared to the aircraft observations. Figure 12 provides a sample of such a comparison.

Triple-Doppler generated velocity fields were available for two of the volume scans for 22 June (Harris et al., 1978) and for four volume scans for 22 July (Kelly et al., 1978). A detailed cell and storm development analysis was also available for the latter storm (Wade and Foote, 1978; Foote et al., 1978). The latter storm is considered in more detail in this report because of the wealth of material for comparison.

Superficially, both case study days were similar. A number of cells - major (peak) cellular impulses (PCI) - were observed which developed on the upwind flank of the storm, moved through the storm, and decayed on the downwind side. This type of storm behavior was observed in Kansas (Crane and Hardy, 1981) and has been documented many times (Renick, 1971; Marwitz, 1972). However, the 22 July storm revealed an abrupt change in its mode of development part way through the period of analysis (Foote, et al., 1978). Cluster data for the 22 July storm provided an additional means for observing the change. The lack of sufficient data on a scale larger than that provided by the limited surveillance volumes imposed by the rapid raster scan observations make a detailed analysis impossible, however.

3.2.1 Storm Structure, 22 July 1976

Wade and Foote (1978) described the morphological development of
Storm III on 22 July in terms of a succession of major convective
impulses which developed over the 1500-1725 MDT time period and moved
toward the south. They observed the impulses in the CP-2 reflectivity
data near storm top (11 km) and tracked the peak reflectivity impulses
using 5 dBZ contour maps at a constant, 7 km, altitude. The volume
cells and clusters of volume cells that formed during the same time
period can also be used to observe and record storm development and to
compare storm descriptors. Differences are to be expected between the
two methods for depicting storm structure. Persistent clusters should
be indicative of active regions of convection accompanied by a sustained
updraft and associated transient updraft, downdraft couplets and volume
cells. Each reflectivity peak used by Wade and Foote should correspond
to a single volume cell in a cluster which moves through the cluster as
both the volume cells and cluster evolve.

CP-2 data from 1539 to 1722 MDT were processed through the cell
detection and tracking programs. The resultant cluster detections were
plotted for four successive 25-minute time intervals (identified as I to
IV) in Figures 13a-d. The persistent clusters apparent in the data
were labeled by Greek letters α to τ. Where appropriate, the peak
reflectivity convective impulse (PCI) identity provided by Wade and
Foote (1978) was included as well. Cluster α (PCI D at 1540 MDT) was
tracked from one volume scan to the next and its average velocity was
used to adjust for cluster motion. The average velocity for cluster α
during its observation period, 1539-1652 MDT, was 12°/4.4 m/s, which was
almost identical to the average storm velocity, 10°/4.3 m/s, reported by
Wade and Foote for storm III for the 1500 to 1630 time period. This
velocity was used for the Lagrangian adjustment of the cluster positions
in each of the four plots, Figures 13a-d.

The data for tracking period I (Figure 13a) show tightly grouped
cluster locations each corresponding to a separate persistent cluster.
Transient clusters seen only on one or two volume scans were not identi-
fied as persistent. The remnants of Storm I and clusters from Storm II
(cluster δ plus transient clusters perhaps representing the decaying

46
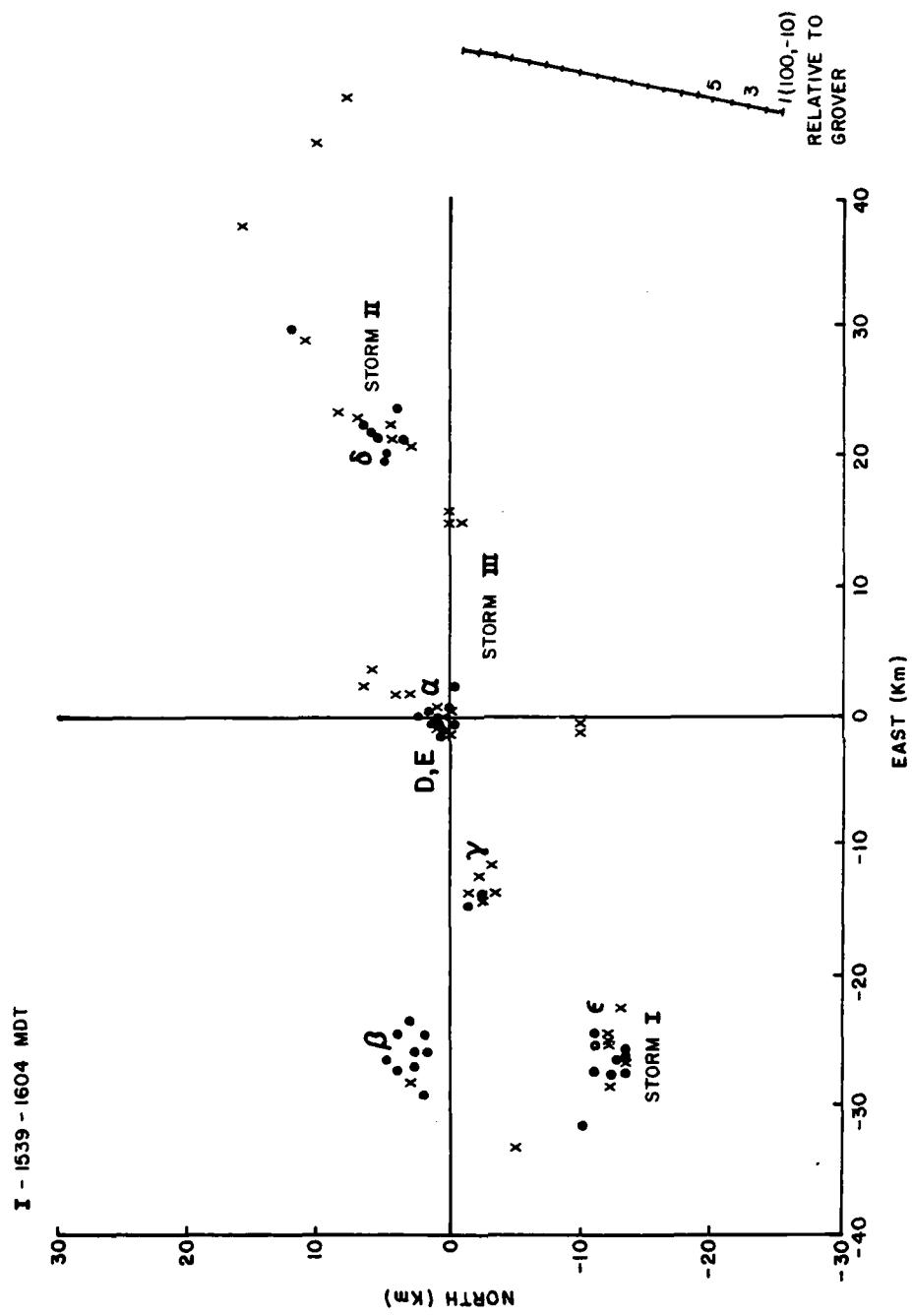
Figure 13a Locations of clusters relative to cluster α for four successive 25-minute time periods on 22 July 1976. Geographical location relative to Grover, Colorado (CP-2) can be obtained from the plotted locations of the (100,-10) coordinate for each of the 5, 5-minute periods in a time interval. The plotted symbols are identified in Figure 11.
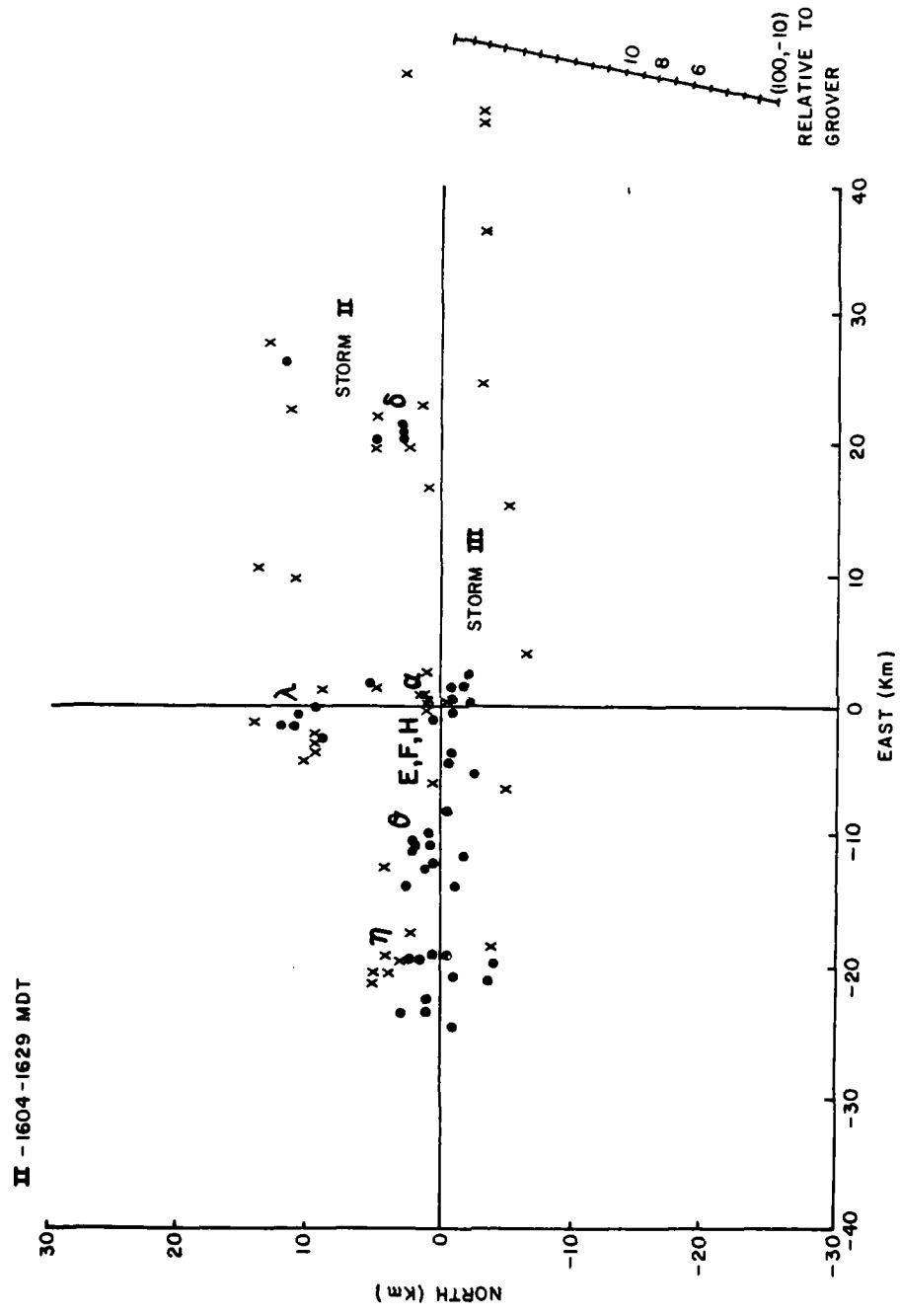
Figure 13b Locations of clusters relative to cluster α for four successive 25-minute time periods on 22 July 1976. Geographical location relative to Grover, Colorado (CP-2) can be obtained from the plotted locations of the (100,-10) coordinate for each of the 5, 5-minute periods in a time interval. The plotted symbols are identified in Figure 11.

48
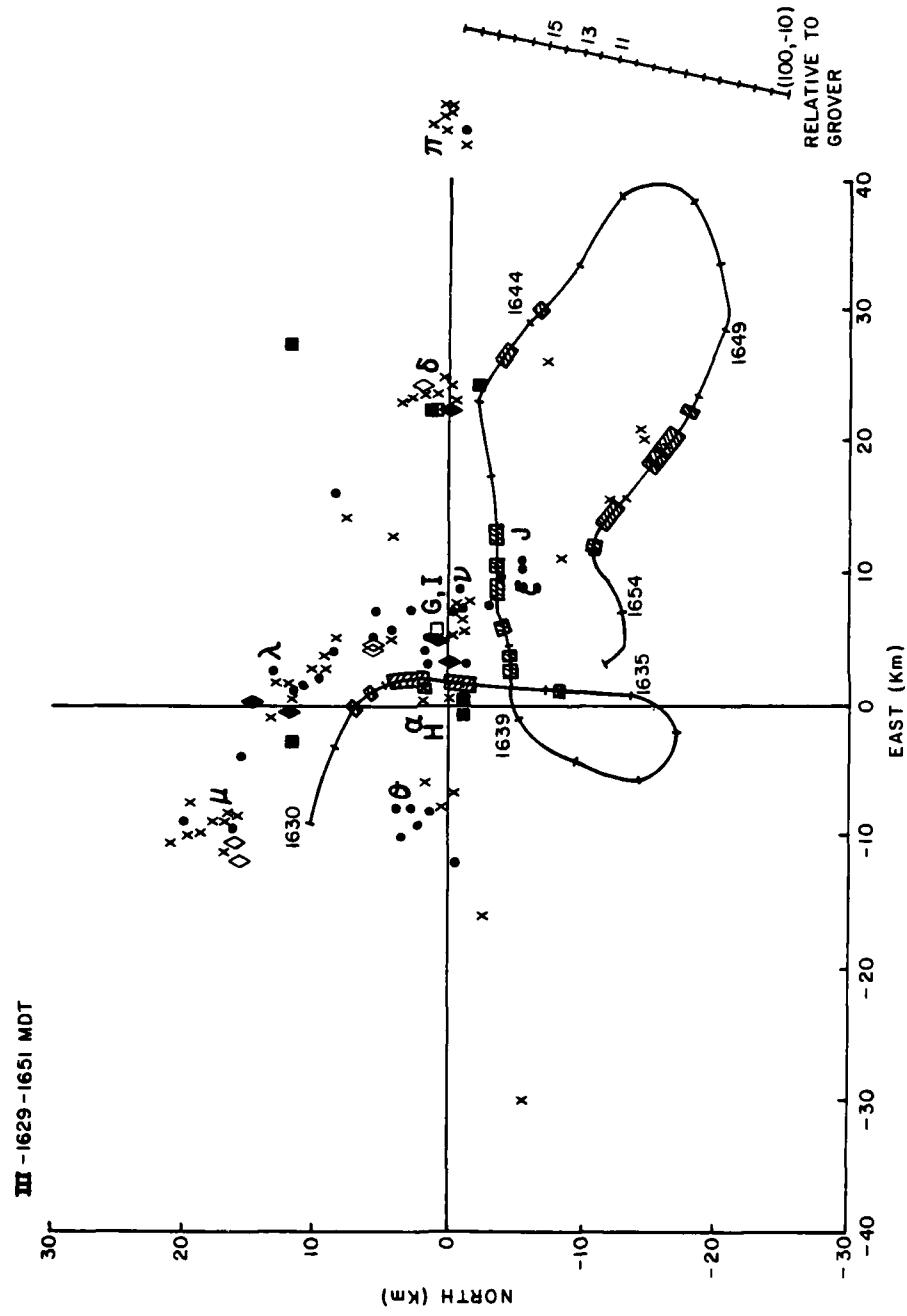
Figure 13c   Locations of clusters relative to cluster α for four successive 25-minute time periods on 22 July 1976. Geographical location relative to Grover, Colorado (CP-2) can be obtained from the plotted locations of the (100,-10) coordinate for each of the 5, 5-minute periods in a time interval. The plotted symbols are identified in Figure 11.
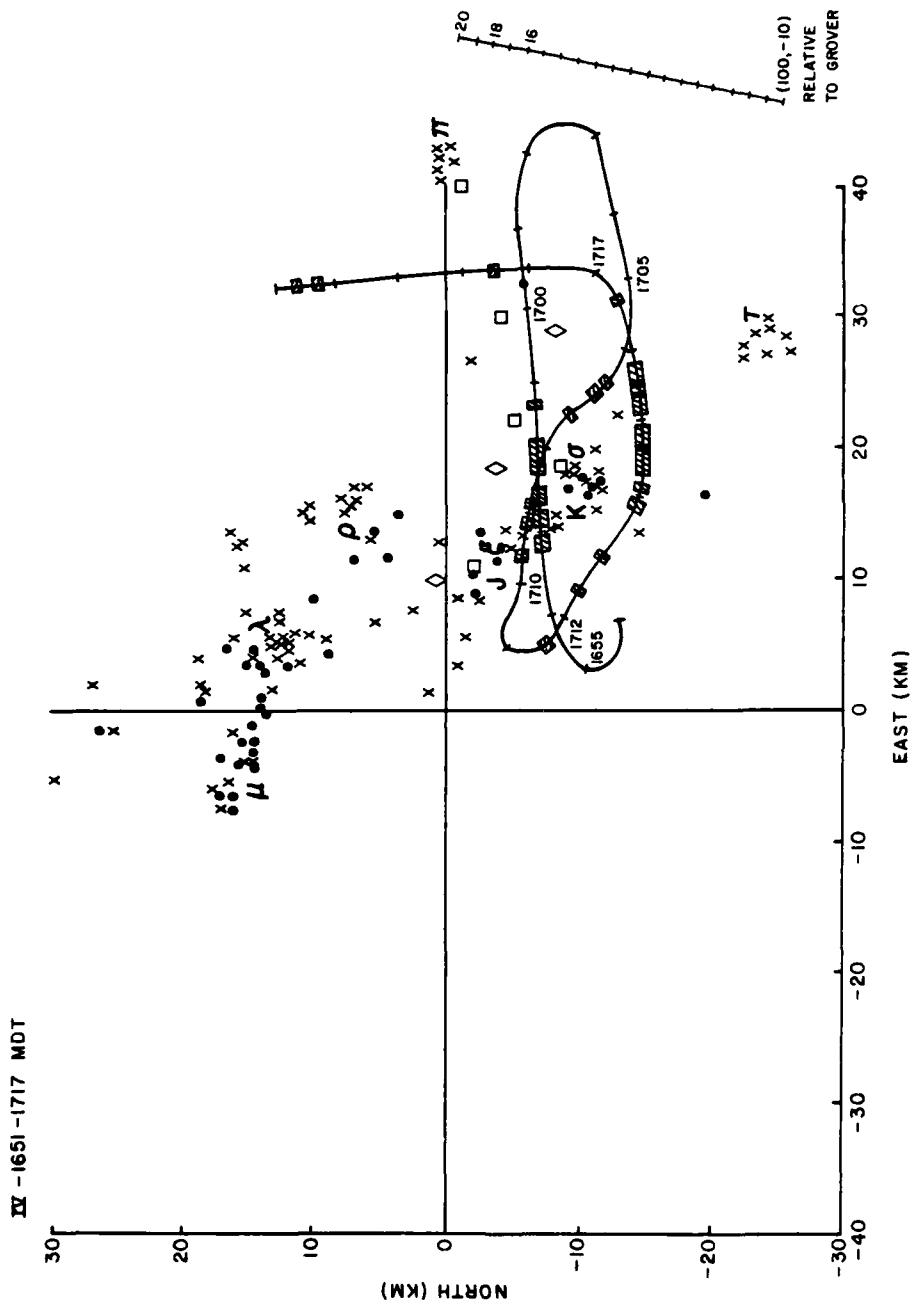
Figure 13d Locations of clusters relative to cluster α for four successive 25-minute time periods on 22 July 1976. Geographical location relative to Grover, Colorado (CP-2) can be obtained from the plotted locations of the (100,-10) coordinate for each of the 5, 5-minute periods in a time interval. The plotted symbols are identified in Figure 11.

state of an earlier persistent cluster) are also displayed. Two of the major convective impulses, D and E, passed through cluster α during this time interval. The volume cells associated with each impulse moved apparently toward the north and east through the cluster finally producing the clusters reported at locations about 5 km from the origin. The cluster pair at 6 km initially appeared at that position and was transient.

Each of the clusters displayed a relatively small spread of its constituent parts, a result indicative of little variation in the track velocities from one cluster to the next. An apparent increase in the spread of a cluster is usually indicative of the demise of one cluster and the formation of a new cluster. Cluster β^I and η^{II} (the superscript designates the time period) were adjacent to each other (compare Figures 13a and b) but the transition from one to the next was made in a discrete step, hence the different labels. The x's in cluster η (two volume cells in a cluster) appeared first separated by about 10 km from the dots ($\cdot$) of cluster β, then the area within cluster η began to fill in. Similarly, cluster Θ formed as a discrete identity separated by about 8 km from Θ and 10 km from η.

New clusters formed as discrete entities along an east-west line just to the north of cluster α is shown by clusters α^I, β^I, η^{II}, Θ^{II} and π^{III} in Figure 14. These clusters were forming on the upwind flank of storms II and III along a broad, 60-km line. During time period II a new cluster formed to the north (downwind) of cluster α. This cluster was separated from α by a region of low reflectivity and its development may be characterized as anomalous rather than normal. New cluster development then shifted to the northwest, southeast line through μ^{III}, ν^{III}, ξ^{III}, σ^{IV} and τ^{IV}. Development along this line was normal with new clusters forming on the upwind flank. Cluster ρ^{IV}, however, developed downwind of δ^{III} along a line parallel to the μ^{III}, τ^{IV} line.

The abrupt shift in the mode of cluster development, from along an east-west line to along the μ^{III}, τ^{IV} line was noted by Foote et al. (1978). It appears to be in response to a larger scale modulation of regions of preferred cell development. Such modulation has been noted by Crane and Hardy (1981). This case differs from the Kansas observations because the pattern presented in Figure 14 was translating relative to the terrain at 12°/4.4 m/s while the patterns observed in Kansas were stationary relative to the terrain.
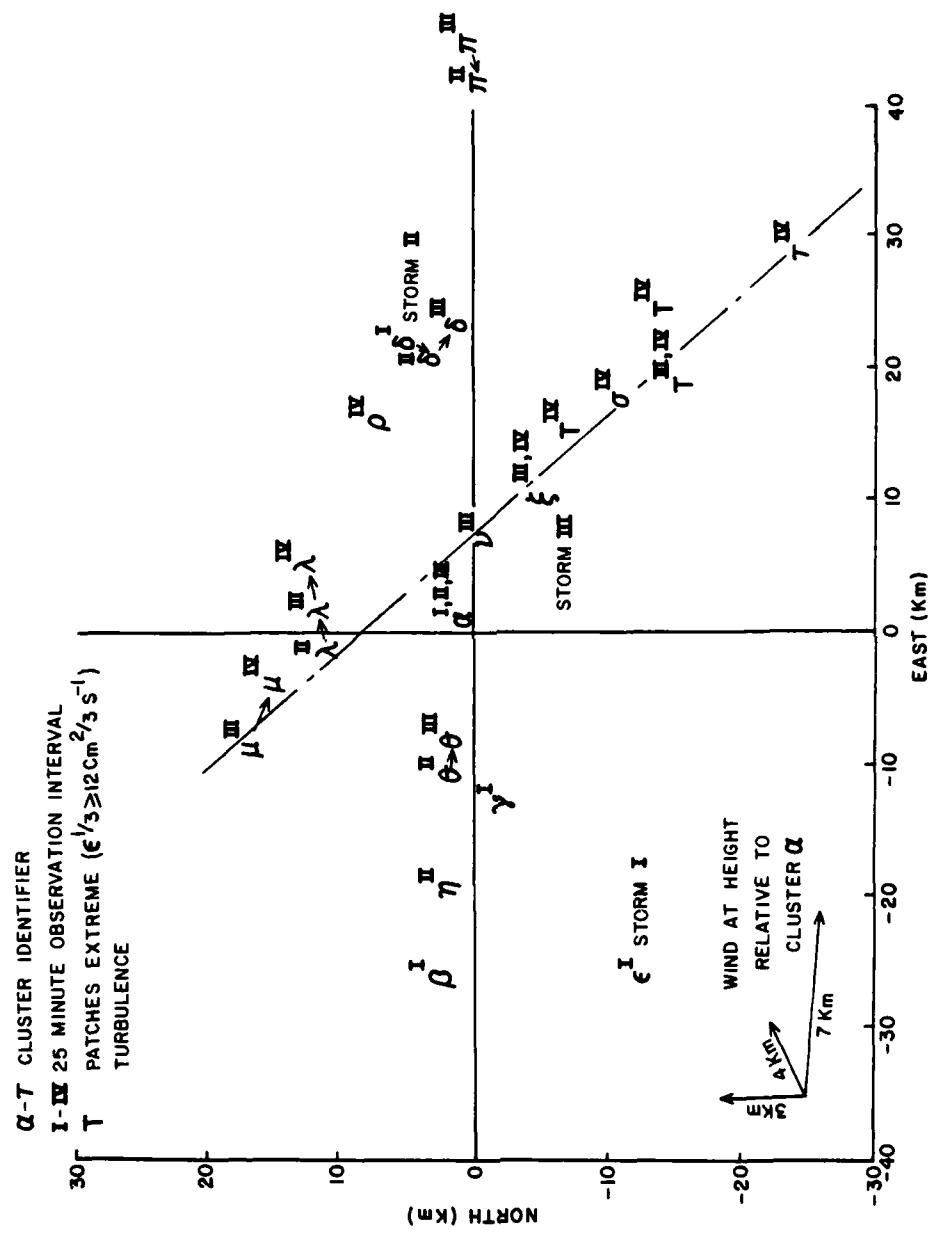
Figure 14   Persistent cluster locations identified by time period (superscript)

These data also showed similarities to the Kansas observations in the average values of the horizontal spacings between clusters. For the 1629-1723 time period (III and IV), the average spacing between SC's (clusters plus isolated significant cells) was 14.8±.5 km, and for the earlier time period (I and II), the average spacing between SC's was 13.4±.8 km. By way of comparison, the average value for the 36 storm elements in the Kansas HIPLEX sample was 14.3±1.0 km, a value essentially identical to the values for the 22 July case study.

The water flux per SC, a value found by Crane and Hardy (1981) to vary little from one convective storm to the next was within 2σ (two standard deviations) of the average value observed in Kansas (after correction for the known difference between the Kansas radar and rain gauge estimates of water flux). The corrected value for Kansas was 0.44 million metric tons per hour per SC (MT/h/SC); the value for time periods III and IV for the 22 July 1976 storm was 1.3±.3 MT/h/SC. Crane and Hardy showed that the relative values of water flux per SC could be used as an indicator of overall storm efficiency. Barring radar calibration differences, the 22 July storm could be judged as being more efficient than the Kansas HIPLEX sample. The Kansas data were for the entire 25 to 150 km annular surveillance region of the Skywater 75 radar but the 22 July data were from the more limited surveillance area of a raster scan imposed by the limited coverage of a dual or triple Doppler radar system. Noting that observations were made of just the most active cells, the data from Colorado should be biased toward higher values.

The NCAR analyses of the 22 July case study included both cell morphology and flow field depictions constructed from the multiple Doppler radar data. The horizontal flow fields at the inflow and mid-levels of storm III at the time of aircraft penetration Number 2, 1640 MDT, are illustrated in Figure 15 (adapted from Kelley et al., 1978). The persistent clusters are identified at both levels. The detailed reflectivity field at mid-level (6 km mol) is shown in Figure 10, the detailed cluster field is presented in Figure 11 and the significant cell locations are depicted in Figure 12. Several features of the flow field are apparent in Figure 15: blocking at low levels by a downdraft in cluster ν, blocking by the updraft in cluster ν at mid-level (6 km mol), and acceleration of the flow between α and ν. In each instance, velocity perturbations are evident which should be detectable by a single Doppler
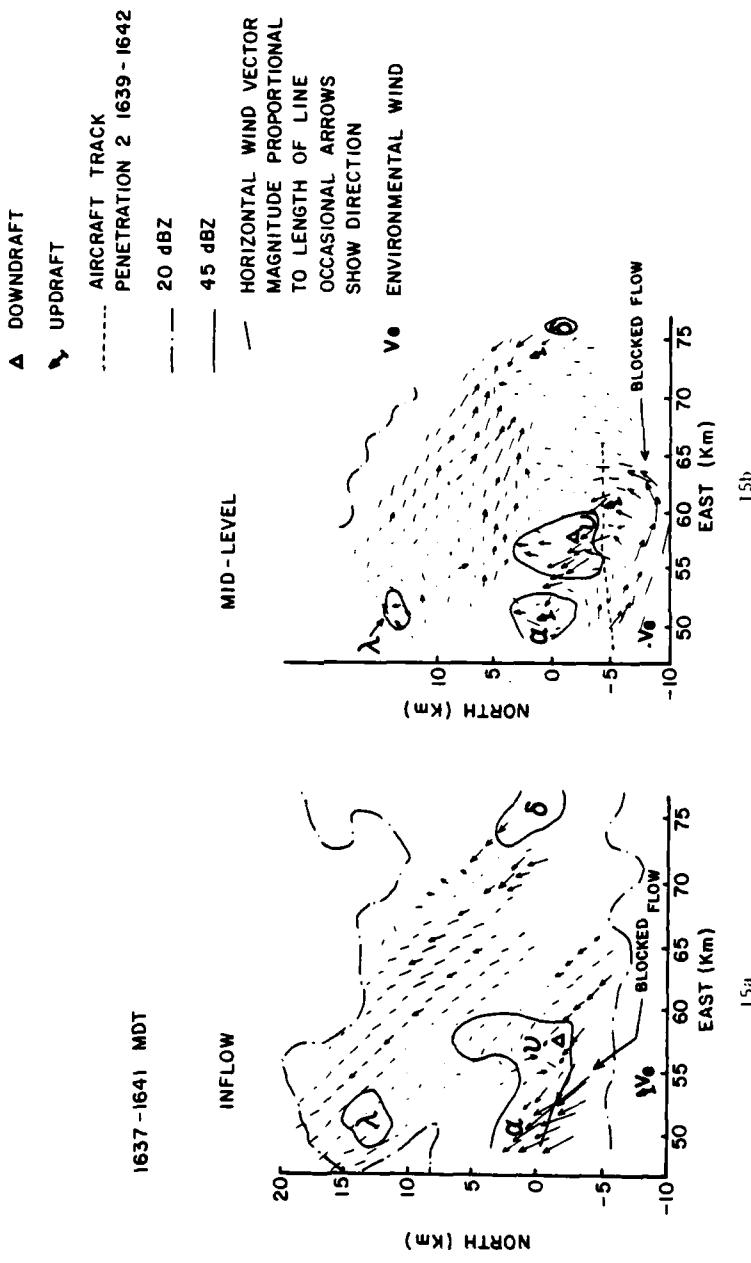
Figure 15   Horizontal flow field at the inflow and mid-level of storm III for the 1637-1641 MDT time period, 22 July 1976 (adapted from Kelley et al., 1978)

54

radar. The mid-level convergence region to the northwest of cluster δ should also be detectable as well as the mid-level perturbations in clusters α, δ, and λ (due to the persistent updrafts in the clusters; clusters α and δ are more than an hour old at the time of Figure 15).

An examination of Figures 12 and 15 reveals that the velocity perturbations are detectable using tangential shear to observe the features. Each of the Doppler radars detected the mid-level perturbations in cluster λ, ν and α. The CP-4 radar apparently could readily sense the low level blocked flow upwind of cluster α. The extended region of velocity perturbations (acceleration) observed by the radar produced a number of closely spaced tangential shear cells which combine to produce a cluster. The clusters observed by the other Doppler radars only depicted the accelerated flow evident higher in the storm and between α and ν (Figure 11). Each of the radars detected δ as a cluster.

The updraft cores were identified and marked by heavy arrows corresponding to the magnitude and direction of the environmental wind at 3.5 km height (inflow) with the magnitude increased by the ratio of the density of the air at 3.5 km to the density at 6.5 km height (mid-level). If the air is lifted without entrainment (see Figure 5) the air in the updraft core should conserve horizontal momentum while being lifted from one height to the other. Using this simple model, the updraft cores could be readily detected by either multiple or single Doppler radar systems. The core locations depicted in Figure 15 correspond to the locations of the mid-level wind vectors having the appropriate magnitude and direction. The analysis presented by Kelley et al. (1978) and by Heymsfield et al. (1980) concentrated on cluster ν (their PCI I) corresponding to the weak echo region produced by the updraft to the south and east of the symbol ν in Figure 15b. They showed a significant updraft extending from the updraft core location on Figure 15b through the region of accelerated flow between α and ν. The aircraft data showed the updraft core (highest value along the aircraft track) to lie just to the west (within 2 km) of the location indicated on Figure 15b. The recent reanalysis of the flow field reported by Heymsfield et al. (1980) indicates that the updraft core (observed from the magnitude and direction of the mid-level flow) should be positioned 1.6 km to the west of

the location indicated in Figure 15b producing even better agreement with the aircraft measurements.

3.2.2 Intercomparison Between Radars

The radars employed for the 22 July case study were operated to provide overlapping surveillance of the region with strong convection enclosing clusters α, ν, λ, δ, ξ and σ. As illustrated in Figure 12, each of the significant cells were observed by more than one radar. A listing of the reflectivity and tangential shear reported for each significant volume cell by radar is given in Appendix A for the volume scans which coincided with the seven aircraft penetration flights. Doppler data were provided by NCAR for four of the seven volume scans and Doppler data were available from all four radars for only two volume scans.

Figure 16 intercompares the S-band (CP-2) and C-band radar data for each of the simultaneously observed volume cells. The reflectivity values used in the analysis were average values for the volume cell as observed by the radar. A comparison between the CP-2 and CP-3 observations show agreement, and one can conclude that there is no calibration differences between the radars. Comparison between CP-2 and CP-4 or between CP-3 and CP-4, as shown in Figure 17, show a decided calibration error for CP-4. The median difference between the CP-4 reflectivity observations and the other two radars was 10 dB.

No correlation was evident between the magnitude of the tangential shear and reflectivity or between the magnitudes of the tangential shear values observed by the two Doppler radars, CP-3 and CP-4. The former result was expected on the basis of the physical models for cell development (Section 2) and on the basis of prior aircraft and radar observations of convective storms. The latter result is due to the anisotropy of the velocity perturbations (turbulence) and to the differences in the observing scale defined by the separation between the positions of the centers of the resolution elements used in the calculation of tangential shear (Section 2). Referring to Appendix A and Figure 15 for observations during penetration 2, the velocity perturbations in clusters α, ν and δ were observable by all four radars. The tangential shear observed by CP-4 for cluster ν ranged from one-half to three times the nearly
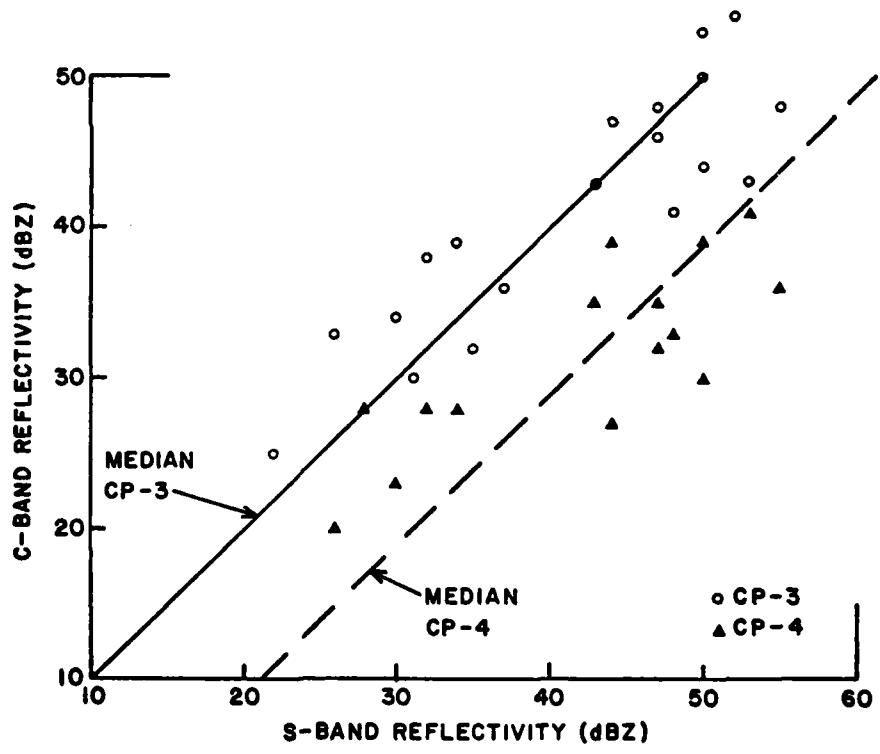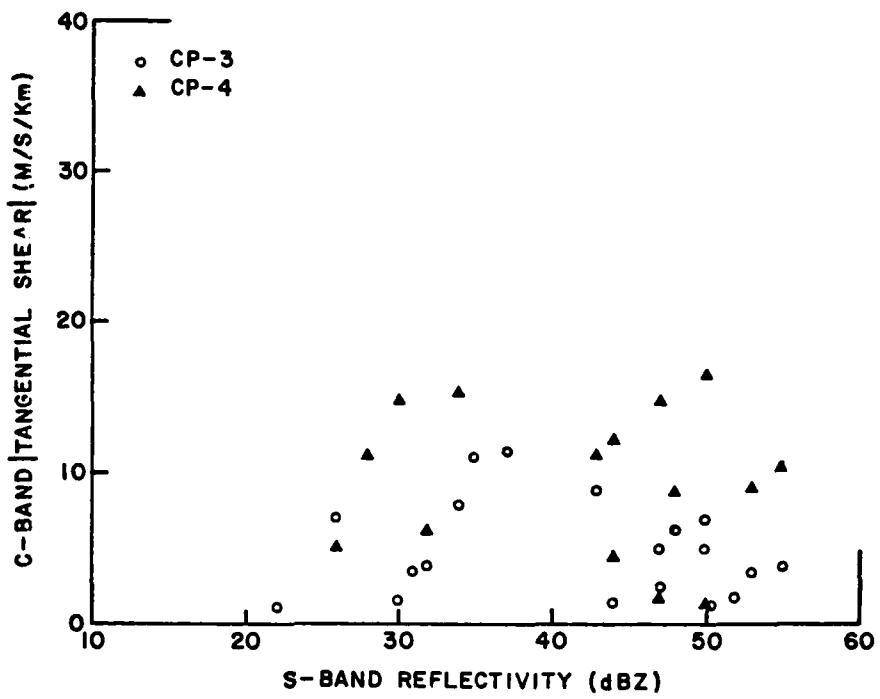
Figure 16   Simultaneously observed reflectivity and tangential shear values, comparison between the C-band and S-band radars, 22 July 1976
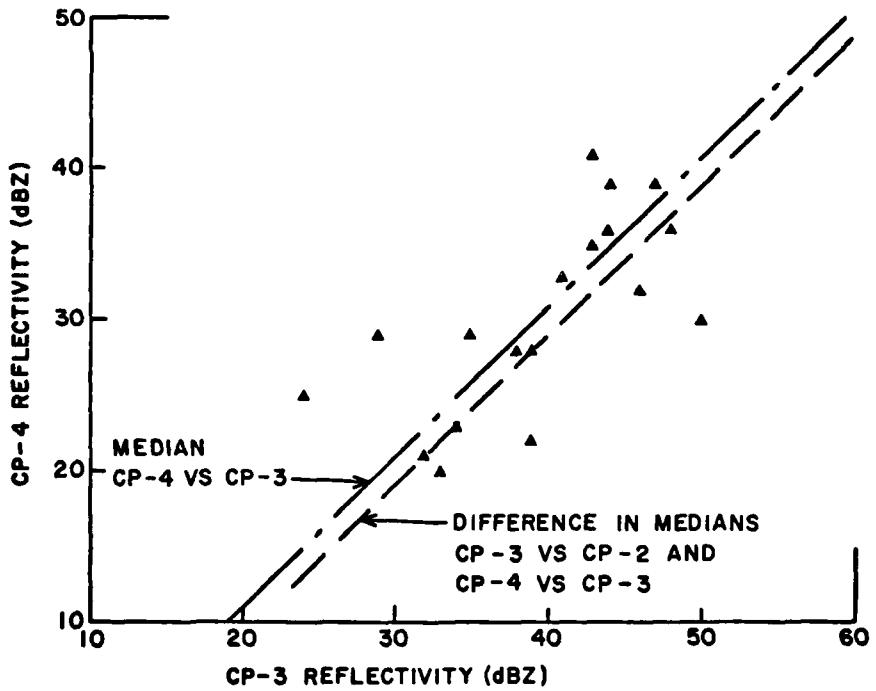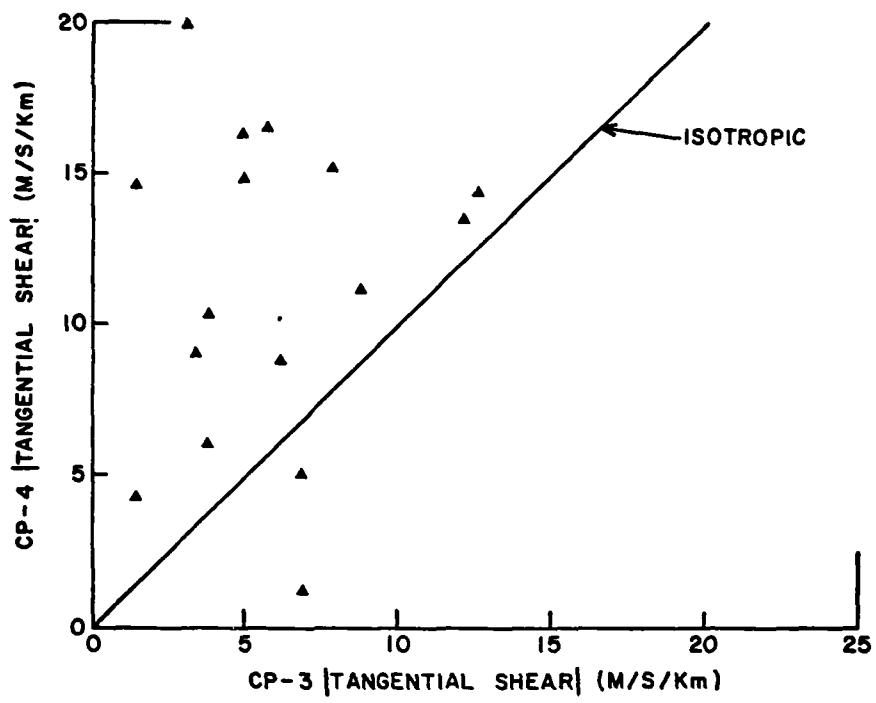
Figure 17   Simultaneously observed reflectivity and tangential shear values, comparison between the two C-band radars, 22 July 1976

58

constant value observed from CP-3. The increased variability evident for CP-4 is most likely due to the differences in range between the volume cells and the radar; CP-4 was about 15 km from cluster ν while CP-3 was about 55 km from the same cluster.

Comparisons between (1) the X-band and S-band radar (Figure 18), (2) the two X-band radars (Figure 19), or between an X-band and a C-band radar (Figure 20) yielded similar results. Again, no consistency was evident between the tangential shear observations of the two radars. An apparent calibration difference was evident but, because of fundamental limitations* in the X-band recording equipment, the difference could be due to the effective saturation of the reported X-band received power observations and the differences in ranges between the radars and the volume cells. Little significance was attributed to the X-band reflectivity data; it was used primarily to set processing thresholds.

The proximity between detections of a volume cell by different radars and the small differences in observed reflectivity between well calibrated radars, less than 5 dB rms, indicate that the cell detection and tracking algorithms are identifying the same features in a storm. The simultaneous observations may be used to intercalibrate the radars. Cell detection data from several radars may be processed simultaneously by the tracking program to provide a single, best estimate output for the network of radars. Refinements are possible to remove differences in the sizes of the resolution elements (differences in the ranges from the radars to a volume cell) and to combine the radial velocity data to detect the positions of updraft cores in a more realistic manner.

---

*private communication with J. Miller of NCAR
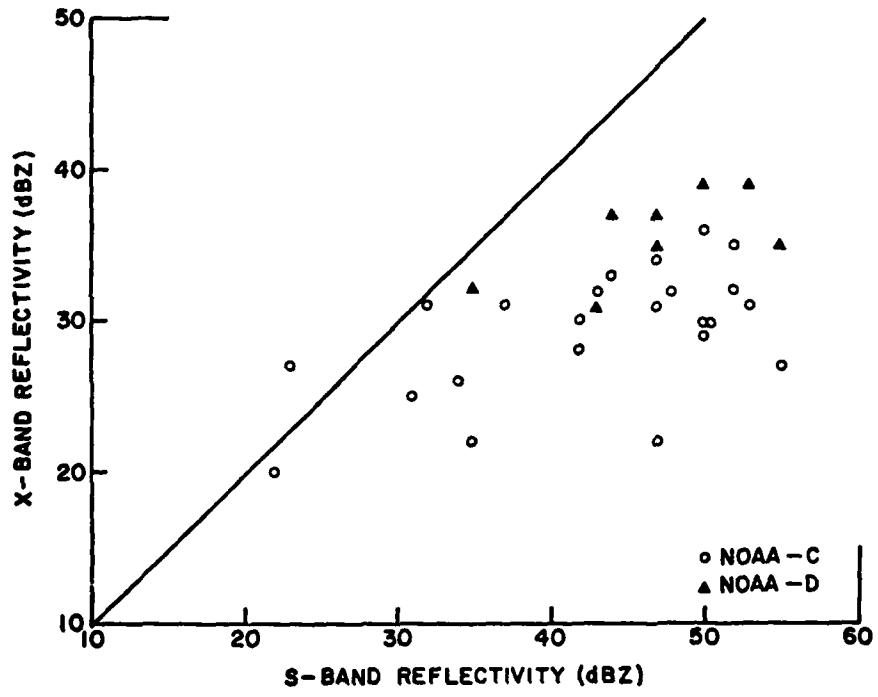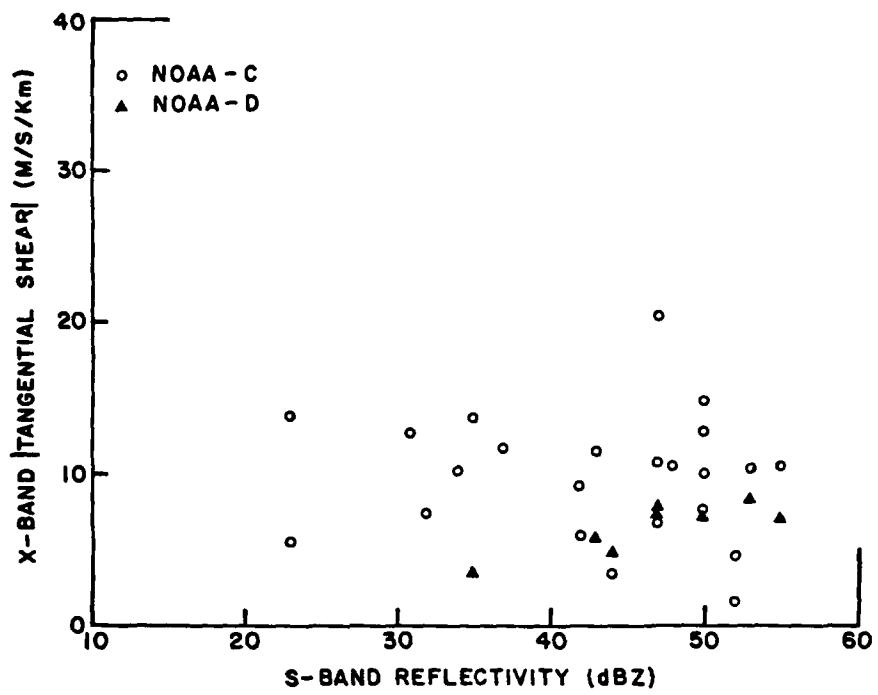
Figure 18   Simultaneously observed reflectivity and tangential shear values, comparison between the X-band and S-band radars, 22 July 1976

60
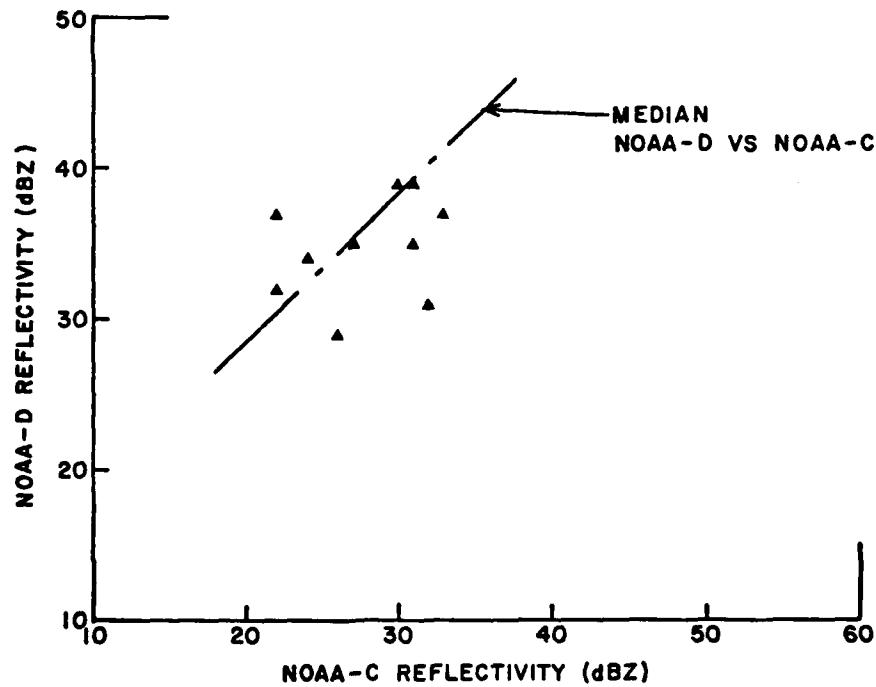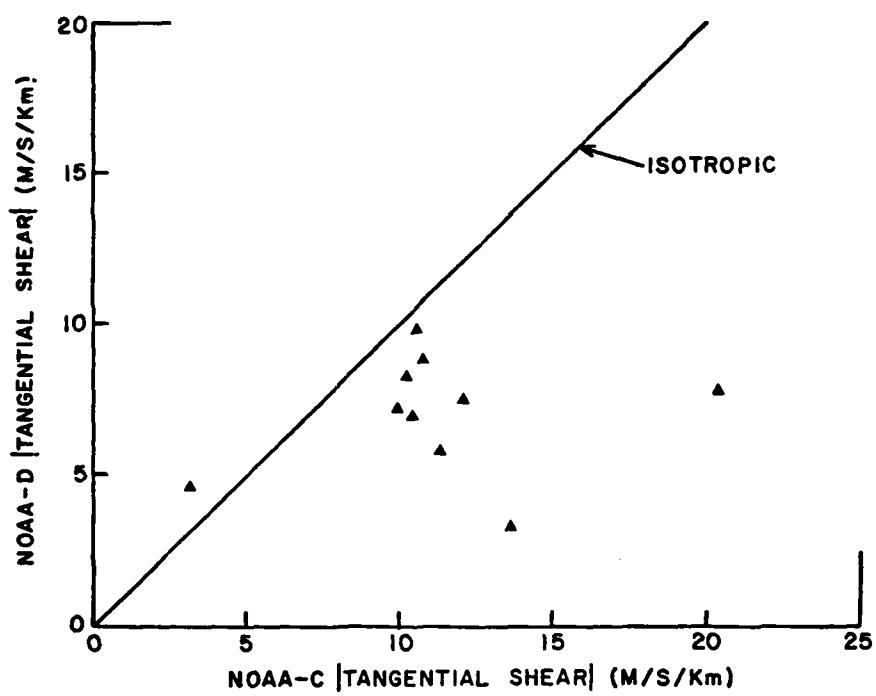
Figure 19   Simultaneously observed reflectivity and tangential shear values,
comparison between the 2 K-band radars, 22 July 1976
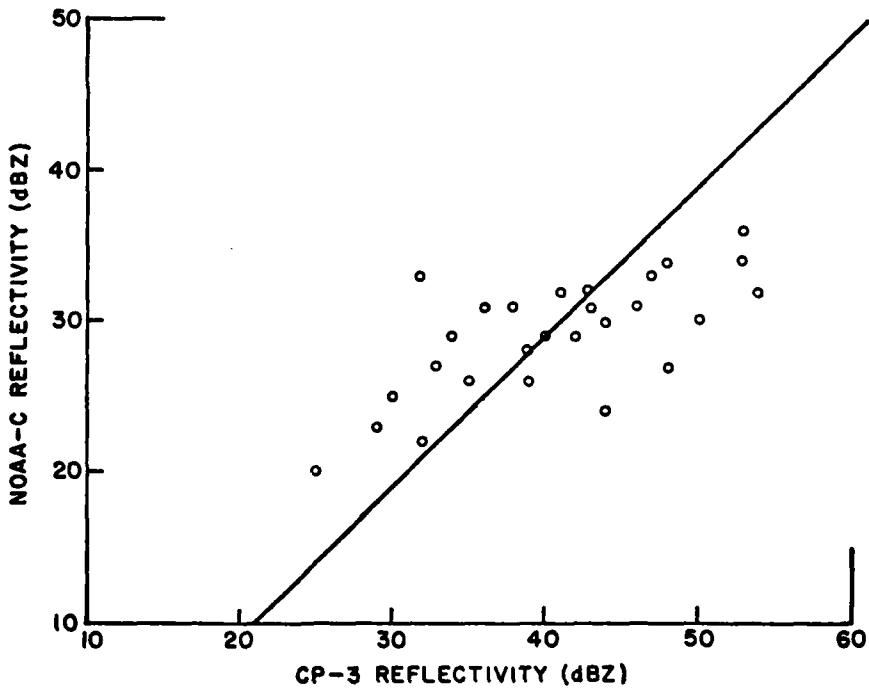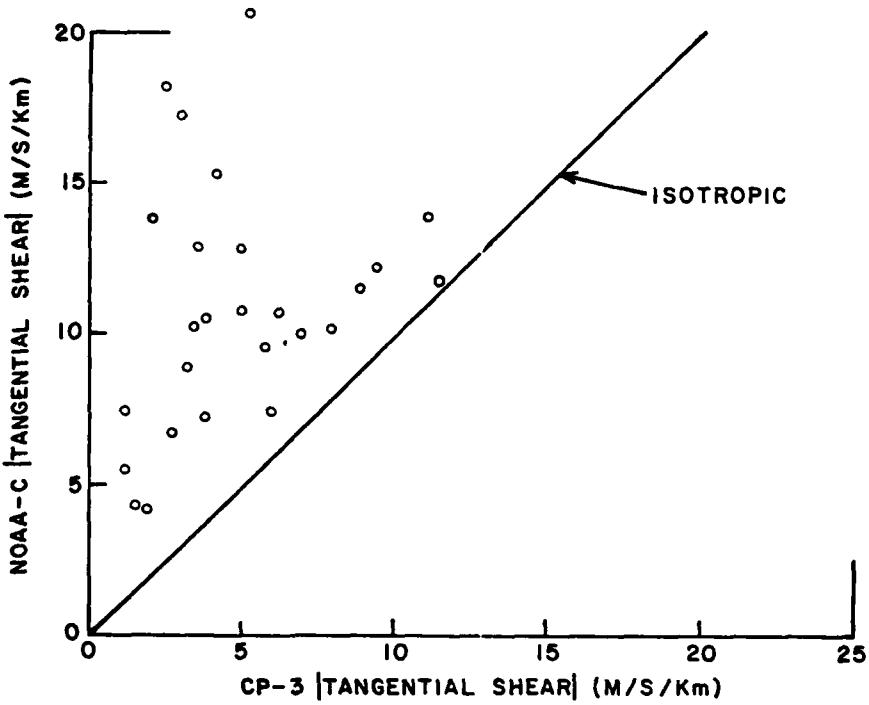
Figure 20   Simultaneously observed reflectivity and tangential shear values, comparison between an X-band and a C-band radar, 22 July 1976

4. AIRCRAFT PENETRATIONS

Aircraft penetration flights were made through the most active
regions of convection within the bounds of multiple Doppler radar cover-
age on each of the case study days. The aircraft employed for the pene-
trations was the armored T-28 operated by the South Dakota School of
MInes and Technology (Sand and Schleuseuer, 1974). The aircraft was
instrumented to record the thermodynamic properties of the air, to
observe liquid water content, hail mass, ice crystal habit and vertical
acceleration, and to calculate turbulence levels and vertical velocity.
For this study, only the vertical velocity, vertical acceleration, and
turbulence levels were of interest. Recorded values for penetration 2
on 22 July 1976 are presented in Figure 21. These data correspond to
the radar observations presented in Figures 9, 10, 11, 12, 13c and 15.

The aircraft track was located in the figures displaying the radar
data on the basis of smoothed position data prepared by NCAR. Several
position determination systems were available such as an M-33 transponder
tracking radar colocated with the CP-2 radar, onboard distance measure-
ment equipment (DME), and the FAA Air Traffic Control transponder network.
The M-33 transponder data were used in this analysis. With smoothing,
the estimated position error is 0.5 km*.

The vertical velocity values displayed in Figure 21 were calculated
from either the aircraft rate of climb or from observed pressure altitude
changes and corrected for the flight characteristics of the aircraft.
The expected measurement uncertainty is less than 5 m/s*. The vertical
acceleration values were instantaneous values measured at the center of
gravity of the aircraft which were sampled once per second. The turbu-
lence levels were calculated from observed true air speed fluctuations
(Sand et al., 1976). The true air speed was obtained from the indicated
air speed which was sampled twice per second. The fluctuations were
spectrally analyzed (16 point FFT) to produce a velocity variance value
in eight different frequency (spatial scale) bands. The variance values
were converted to eddy dissipation rate (ϵ) estimates and averaged to
provide a best estimate value of ϵ consistent with an inertial subrange
spectrum (Monin and Yaglom, 1975). The results were reported as $\epsilon^{1/3}$ in

---

*P. Smith of SDSMT, private communication
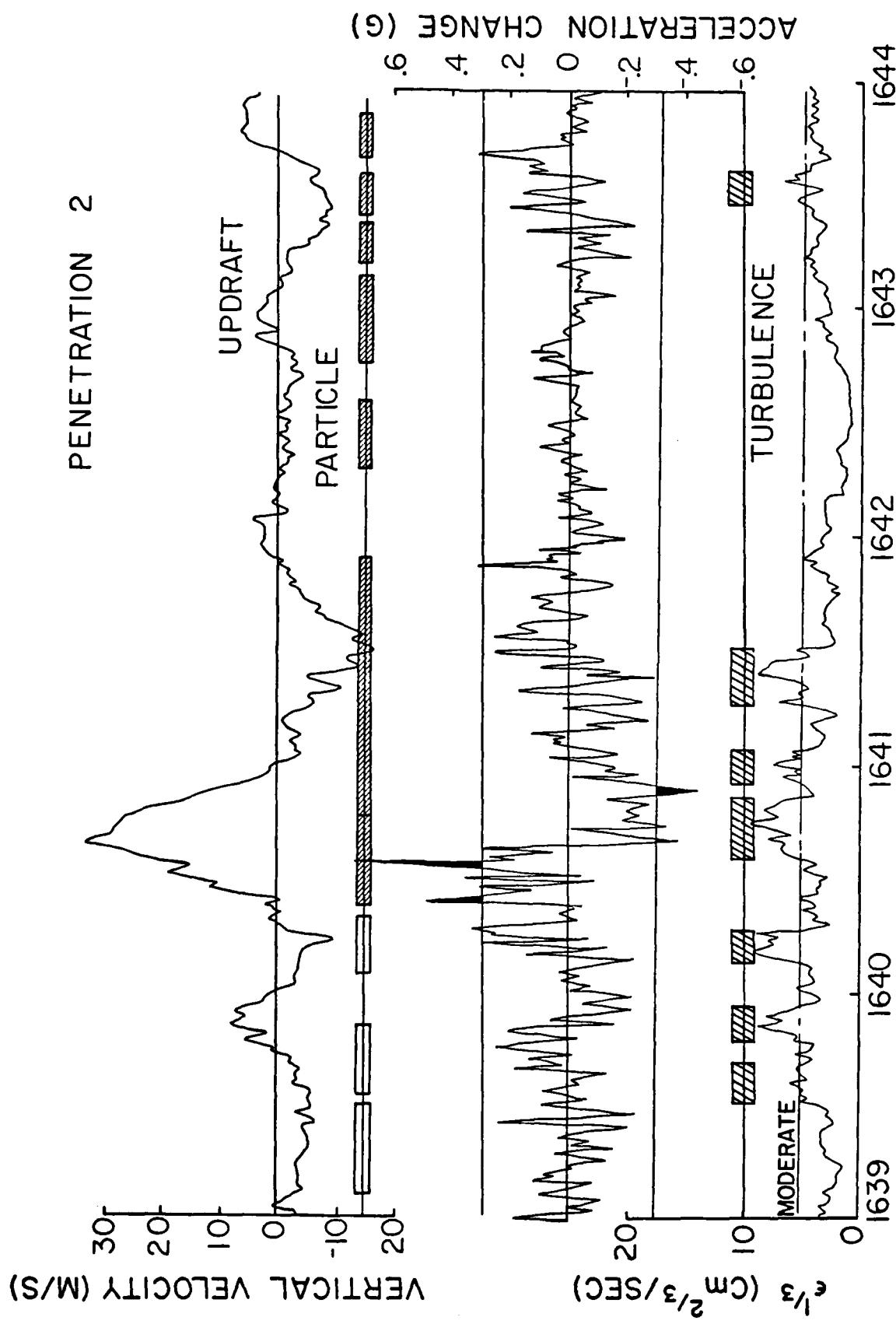
Figure 21 Vertical velocity, vertical acceleration (departure from quiet – IG), and (cúay dissipation rate)1/3 observed during penetration 2, 1639-1644 MDT, 22 July 1976; T-28 aircraft at 6 km height and 90 m/s airspeed

units of $cm^{2/3} s^{-1}$. Based on the spectra presented by Sand et al., the rms uncertainty in $\varepsilon^{1/3}$ is estimated to be 25 percent.

4.1 Turbulence Levels

Two systems have been used to characterize atmospheric turbulence, one based on eddy dissipation rate measurements (MacCready, 1964) and the other employing derived gust velocities (Pratt and Walker, 1954; Lee, 1974). The latter measure of turbulence is proportional to the peak vertical acceleration change encountered in a short time interval (order of a second). The derived gust velocity is the strength of a standardized isolated gust that would have produced the observed vertical acceleration change. The proportionality coefficient depends upon the parameters of the aircraft that relate to the calculation of lift. The derived gust velocity is used to provide an estimate of the level of turbulence that does not depend on the characteristics of the observing aircraft. It may be used to estimate the response (vertical acceleration changes) of other aircraft to the same idealized gust.

Eddy dissipation rate is a measure of the turbulent fluctuations of the air that is independent of the response of a particular aircraft to the turbulence. MacCready (1964) showed that the rms value of vertical acceleration (gust loading) was linearly related to $\varepsilon^{1/3}$ and suggested that $\varepsilon^{1/3}$ be used to characterize turbulence because it does not depend n the characteristics of an aircraft and it can be used to determine the rms gust loading for the aircraft.

Both $\varepsilon^{1/3}$ and the peak acceleration deviations from quiet conditions (1 g) in a short time interval were recorded during the T-28 penetration flights. These data were used to compare the largest $\varepsilon^{1/3}$ values within a 30-second time interval (3 km of flight) and the largest instantaneous acceleration departure from quiet conditions within the same time interval. A one-sided measurement of acceleration was employed rather than the largest instantaneous change used in the estimation of a derived gust velocity because the acceleration observations were made twice per second but displayed only once per second and large exersions were noted as occasionally occurring between the recorded samples. The results of comparing the two observations, peak acceleration and $\varepsilon^{1/3}$, are presented in Figure 22. As predicted by MacCready, a straight line approximation provides a good fit to the observations.
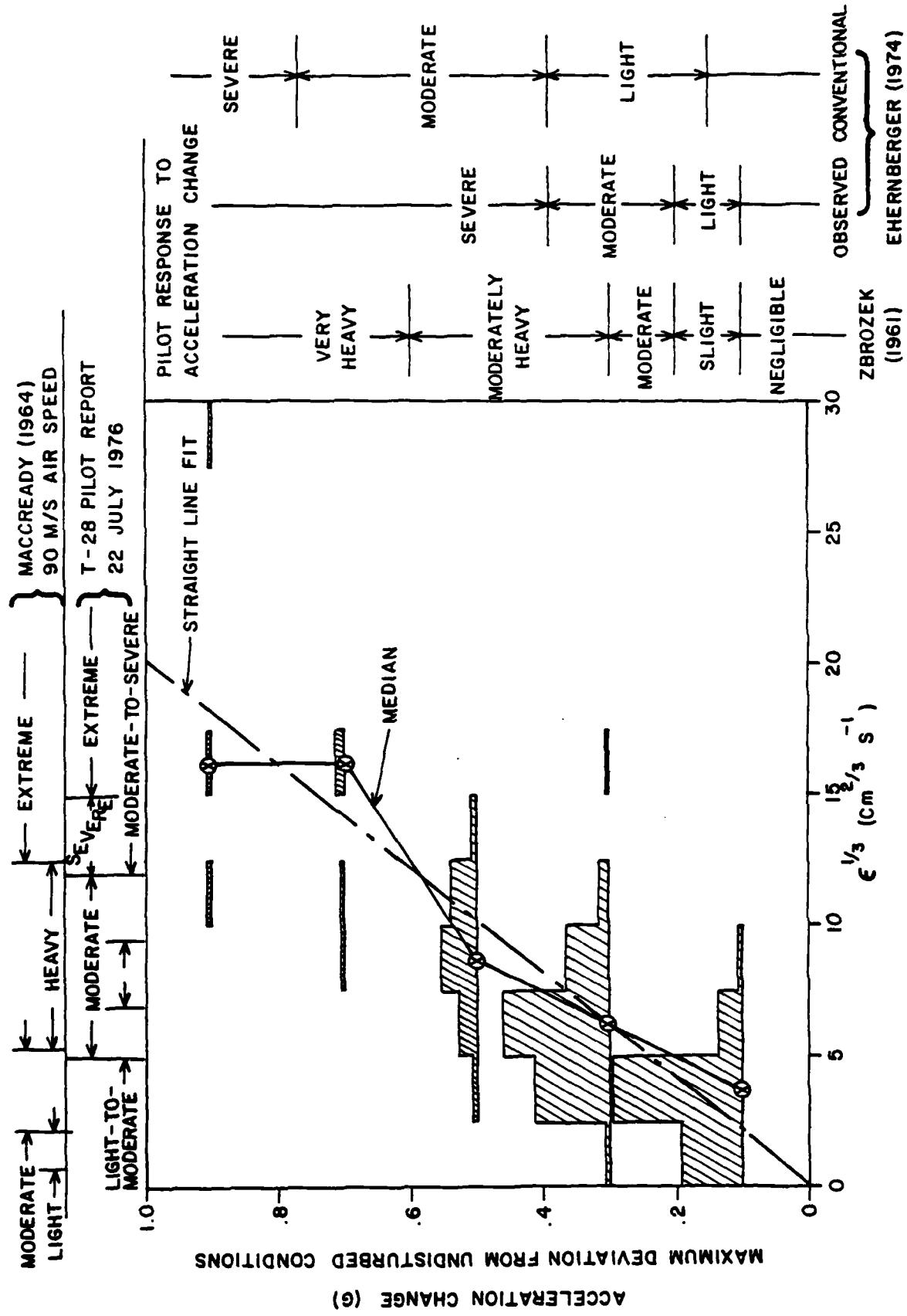
Figure 22   Observed relationship between eddy dissipation rate and peak instantaneous vertical acceleration values, 22 June and 22 July 1976

The eddy dissipation rate is a quantitative measure of the intensity of the turbulence in the atmosphere. The more familiar intensity descriptors, light, moderate, severe, and extreme, are not quantitative but are used to represent the subjective response of a pilot to an encounter with turbulence. A pilot responds to rapid changes in acceleration; the rms gust loading or the peak-to-peak vertical acceleration changes within the time interval of about a second may be used as nearly direct measures of the reaction of a pilot to the turbulence. It is a measure which depends on the response of the aircraft to the turbulence, a response which depends upon aircraft weight, altitude, airspeed, and flight characteristics. The derived gust velocity attempts to compensate for the aircraft parameters which affect its response by providing an estimate of a standardized wind gust that would have produced the measured aircraft response. In particular, the aircraft response (vertical acceleration) is modeled as proportional to airspeed and inversely proportional to aircraft weight (Lee, 1974).

In this study, $\varepsilon^{1/3}$ was chosen as the principal measurement of turbulence. The peak vertical acceleration values were used to provide supporting data about the expected pilot response. Five separate pilot response estimates are displayed in Figure 22. The intensity descriptors recommended by MacCready (1964) on the basis of a study by Zbrozek (1961) are given as well as the descriptors proposed by Zbrozek. The subjective observations reported by Ehernberger (1974) are also presented together with the conventional turbulence level criteria adopted by the U.S. Dept. of Commerce Subcommittee on Aviation Meteorological Services in 1966. The T-28 pilot reports for the 22 July 1976 penetration flights are also included. They are displayed vs $\varepsilon^{1/3}$ because the eddy dissipation rate was used for the primary measurement of turbulence intensity. Reports were not used for the 22 June case studies because the pilot responded only with "good" or "heavy" to characterize the turbulence.

Zbrozek used rms gust loading as his quantitative measure of aircraft response to compare with pilot reaction. Because the peak values used in this study were the largest in each 30-second sample of flight segment used to characterize turbulent intensity levels, the rms vertical acceleration value was estimated as one-half the reported (2 standard deviations) value. Ehernberger employed the peak-to-peak acceleration

67

change measurement to quantify aircraft response. His peak-to-peak
values were reduced by a factor of 1.3 for plotting on Figure 22. The
reduction factor is the median factor relating the observed peak-to-peak
changes in the undersampled acceleration data to the observed peak
deviations from quiet conditions during the 22 July 1976 penetration
flights. The reduction factor is only an approximation since rapid
fluctuations are known to occur between samples.

From Figure 22, it is evident that a wide range of word descriptors
are possible for a given $\varepsilon^{1/3}$ value. Sand et al. (1974), in reporting
T-28 thunderstorm penetrations for the 1972 NHRE field season, adopted
the bounds proposed by MacCready. They used severe rather than heavy to
characterize the region $5 < \varepsilon^{1/3} < 12$ cm$^{2/3}$ s^{-1}. We have adopted the
word descriptors used by the T-28 pilot during the 22 July penetration
flights. The eddy dissipation rate bounds employed were obtained by
comparing the pilot reports to the simultaneously recorded $\varepsilon^{1/3}$ values:
$5 \leq \varepsilon^{1/3} < 12$ is described as moderate, $12 \leq \varepsilon^{1/3} < 15$ is described as
severe, and $\varepsilon^{1/3} \geq 15$ cm$^{2/3}$ s^{-1} is described as extreme. The several
occurrences of $\varepsilon^{1/3}$ greater than 15 cm$^{2/3}$ s^{-1} were accompanied by pilot
reports that the aircraft was barely controllable (Heymsfield et al.,
1978). This condition is best described as extreme, in keeping with the
accepted definition of extreme, rather than by severe or even by moderate
(conventional criterion, see Figure 22).

The severity of the turbulence experienced by an aircraft depends
upon the airspeed, weight, and flight characteristics of the aircraft.
If the derived gust velocity model is employed for the analysis of
severity, aircraft with the same lift parameters will experience
increased severity with increased airspeed and decreased severity with
increased weight in encounters with the same intensity of atmospheric
turbulence (derived gust velocity). Because the weight of many of the
commercial transports is an order of magnitude or more than the weight
of the T-28 but the cruise velocity is only three to four times that of
the T-28, inflight turbulence severity levels should be at least one
intensity class lower than reported for the T-28. Conversely, lighter
general aviation aircraft will find the turbulence to be more severe.

4.2 Penetration Flight Summary

All occurrences of $\varepsilon^{1/3}$ greater than 5 $cm^{2/3}$ s^{-1} were identified and located on radar cell and cluster summary position plots for each of the penetration flights. The flights were subdivided into 15-second segments (approximately 1.5 km of flight) and the largest $\varepsilon^{1/3}$ value for each interval was used to characterize the turbulence within a segment. A tally was kept of all the turbulent segments (patches) and their intensity. Figure 23 presents cumulative distributions of the turbulent patches observed by encounters (1) along the entire flight path, (2) within the 7 dBZ echo region observed by the S-band, CP-2 radar plus a 4-km buffer outside the echo boundary, and (3) within the 20 dBZ echo region plus 4-km buffer.

The plotted locations of the turbulent patches encountered on the second aircraft penetration on 22 July 1976 are depicted in Figures 11 and 12. All the turbulence encounters for the 22 July case study are plotted in Figures 13c and 13d; in these figures, $\varepsilon^{1/3}$ values in excess of 5 $cm^{2/3}$ s^{-1} (moderate) are coded by cross-hatching and values in excess of 12 $cm^{2/3}$ s^{-1} (severe) are indicated by solid bars across the aircraft track. The locations of one (or more) encounters with severe turbulence are also indicated in Figure 14.

The times of the turbulent path encounters were scaled from the computer generated strip chart plots provided by SDSMT. Figure 21 is a reproduction of several of the variables displayed on the computer generated plots. Daily summaries were also provided by SDSMT. Appendix B contains the daily summaries for each case study.
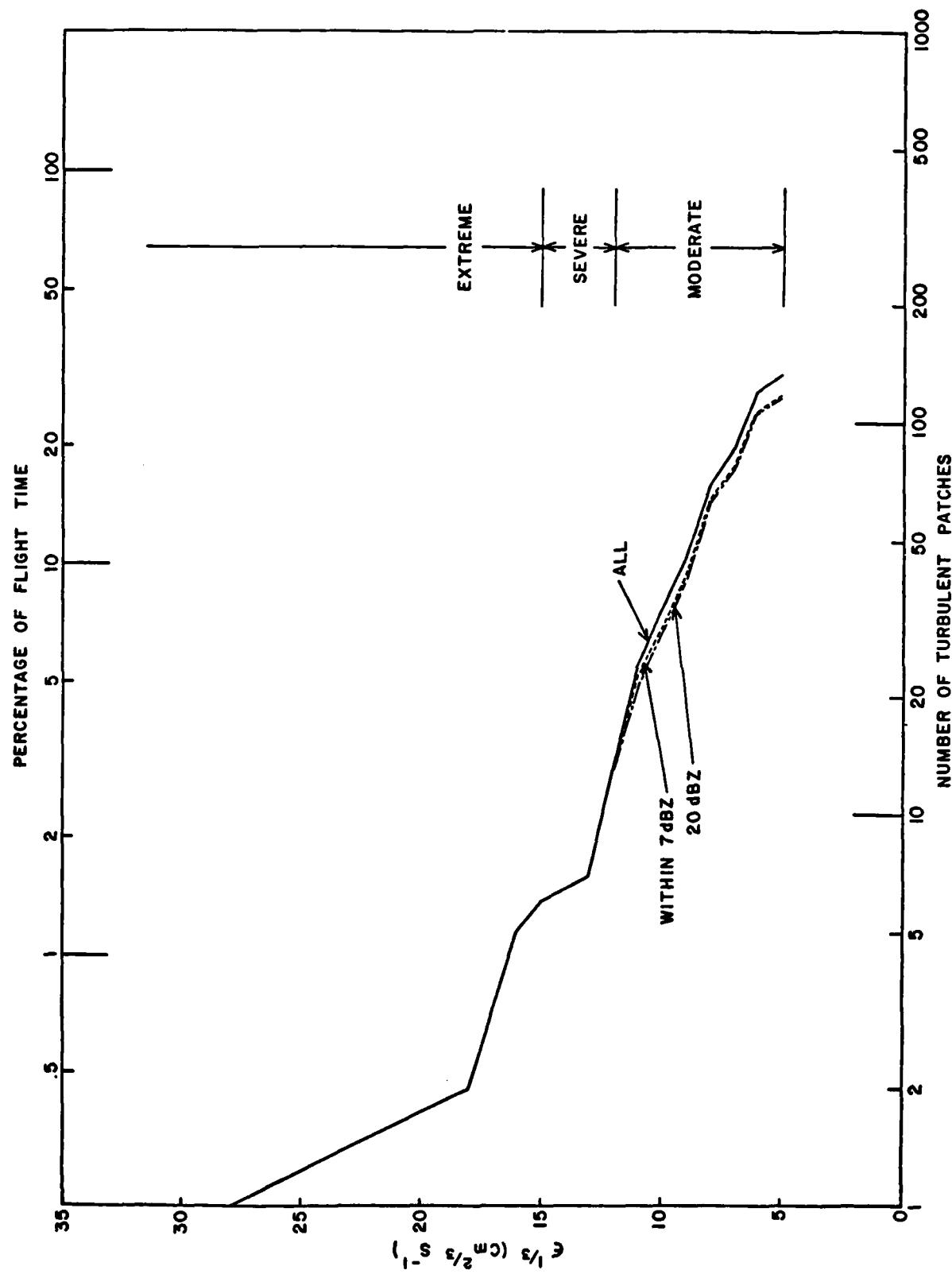
Figure 23 Cumulative distributions of turbulent patches of 1.5 km extent encountered during 660 km of T-28 penetration flights

5. RADAR-AIRCRAFT DATA COMPARISON:
A TEST OF THE HAZARD DETECTION HYPOTHESIS

The cell approach to hazard detection presumed the existence of a turbulent patch within a small radius of influence around a significant cell (or cluster of cells). The underlying physical hypothesis suggests that the radius of influence should approximate half a cell diameter. The statistical analysis of the average cell size for Kansas summer storms reported by Crane and Hardy (1981) indicated that the cells have an exponential size distribution with an average diameter of 2.5 km.

The actual radius of influence to be applied to hazard detection should be larger than half a cell diameter because the statistical uncertainty in the radar reflectivity of a resolution element produces an attendent position uncertainty in the centroid location of a cell. The reflectivity cell encloses all the contiguous radar resolution elements having reflectivity values within 3 dB of the largest value for a cell. If a cell is at a range of 50 km, it will contain four resolution elements on average (1° beamwidth radar system). If a limited number of independent samples are used to calculate the reflectivity value, the statistical uncertainty in the reflectivity values will affect the number of elements included in the cell on any one scan. It was estimated that the cell centroid position uncertainty should increase the radius of influence by about 1 km at a range of 50 km.

Additional uncertainties produced by cell tracking errors and by aircraft tracking errors should increase the radius of influence by about another kilometer. The a priori estimate of the expected radius of influence of a cell was between 2 and 4 km. Inter-radar comparisons of reflectivity and tangential shear locations (see Figure 12 for an example) show tightly clumped significant cells. The clumps of significant cells observed by the different radars can generally be circumscribed by a circle with less than a 1.5 km radius. The statistical positioning uncertainty is therefore less than expected a priori, especially for comparisons between reflectivity and tangential shear cells detected by different radars.

The statistical measures used to test the hazard detection hypothesis were evaluated as functions both of turbulence level and of radius of influence. The cell detection hypothesis presumed the existence of

71

significant turbulence but of an unspecified level. In the statistical analysis, detection is counted if the $\varepsilon^{1/3}$ value was above the threshold level, but a false alarm was tallied if the value was below the threshold. The false alarm rates therefore must increase as the threshold level is increased.

5.1 Probability of Detection

A successful detection of a turbulent patch was counted if one or more significant cells were within the specified radius of influence of the turbulent patch. The probability of detection (POD) was calculated by

$$POD = (X/W) \cdot 100 \qquad (\text{percent}) \qquad (1)$$

where X is the number of detected turbulent patches (successes) and W is the total number of turbulent patches (trials).

The probabilities of detection are plotted versus turbulence intensity threshold ($\varepsilon^{1/3}$) for reflectivity cells detected using the CP-2 radar (Figure 24a), for tangential shear cells detected by the C-band radars (Figure 24b), and for tangential shear cells detected by the X-band radars (Figure 24c). The results are for a 6-km radius of influence. The variation of detection probability with radius of influence for turbulence intensities in excess of 5 $cm^{2/3}$ s^{-1} is displayed in Figure 1. Detailed tabulations of the detection probabilities by radar, radius of influence, and threshold level are included in Appendix C.

Three curves are presented in Figure 24a for the CP-2 radar, one for using all the volume cells, the second for volume cells with an average reflectivity in excess of 40 dBZ and the third for volume cells with an average reflectivity in excess of 50 dBZ. The detection probabilities (POD) increase with increasing threshold level for $5 \leq \varepsilon^{1/3} \leq$ 11 $cm^{2/3}$ s^{-1}. They decrease with increasing average reflectivity values. Figure 1 displays the same dependence on reflectivity and indicates that the larger the radius of influence, the higher the probability of detection.

The data presented in Figure 24 are for all encounters with turbulence; the data presented in Figure 1 are for encounters within regions containing echoes greater than 20 dBZ as observed with the CP-2 radar
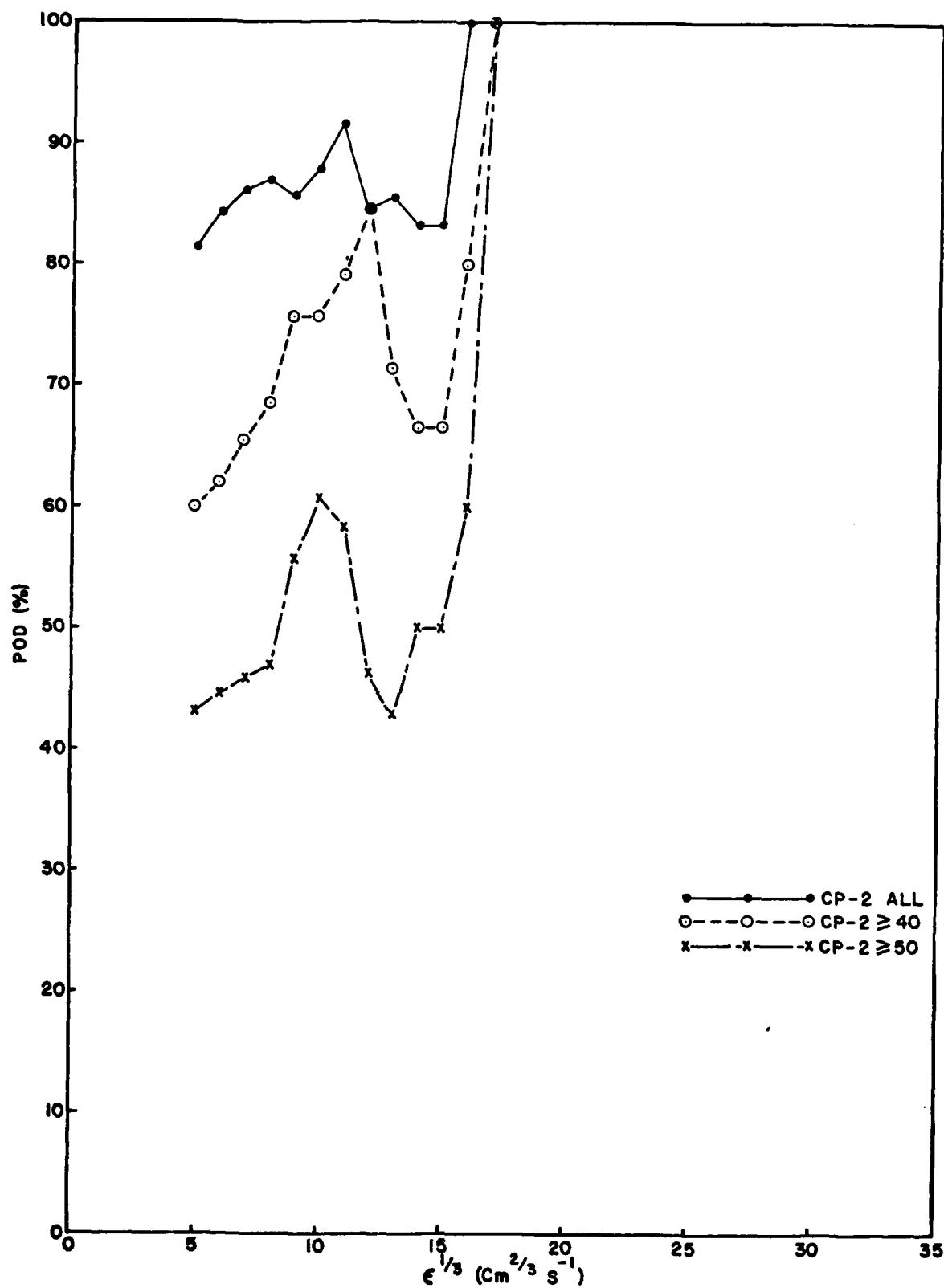
Figure 24a   Probability of detecting a turbulent patch within 6 km of a significant cell
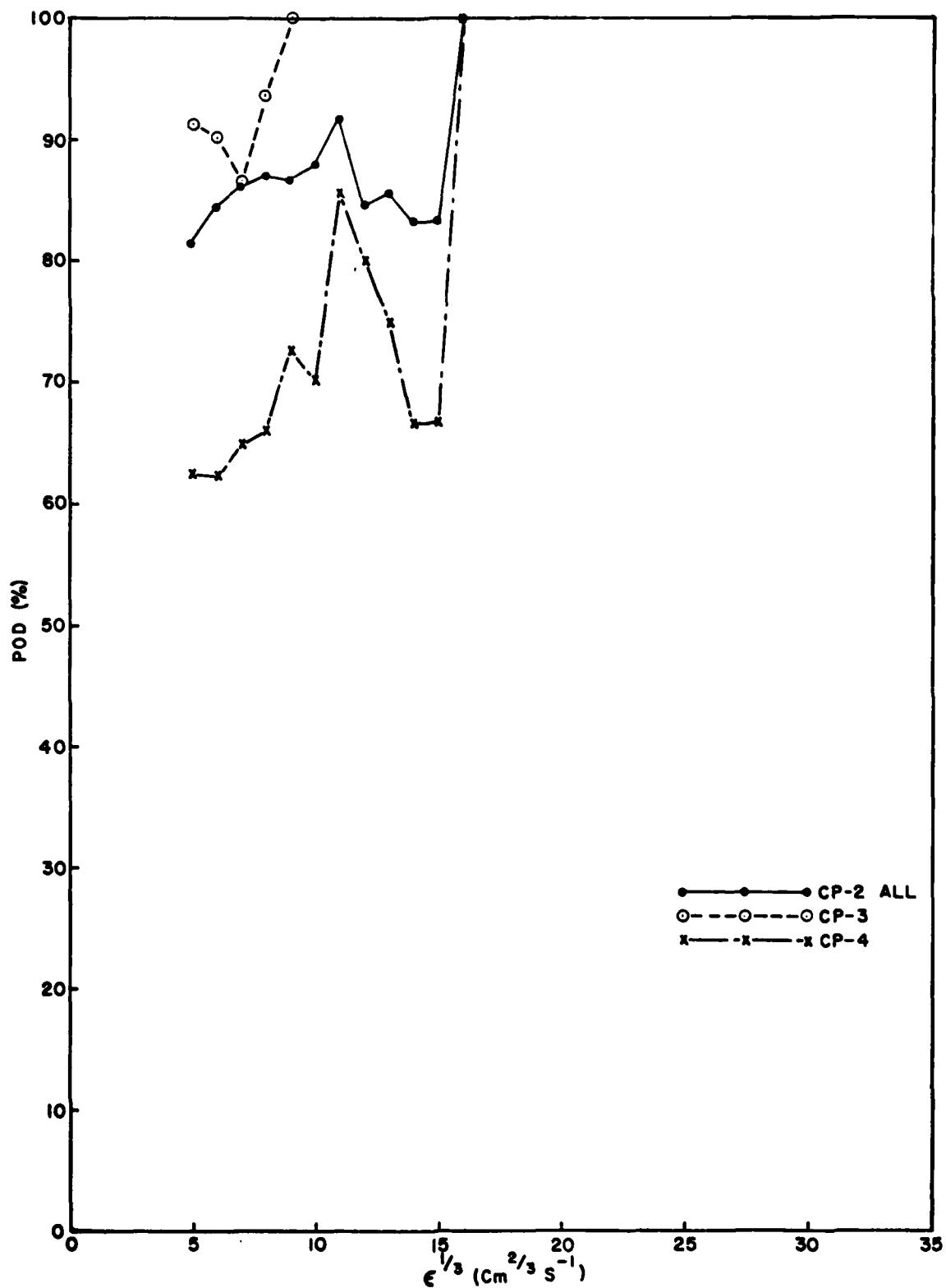
Figure 24b   Probability of detecting a turbulent patch within 6 km of a significant cell

74
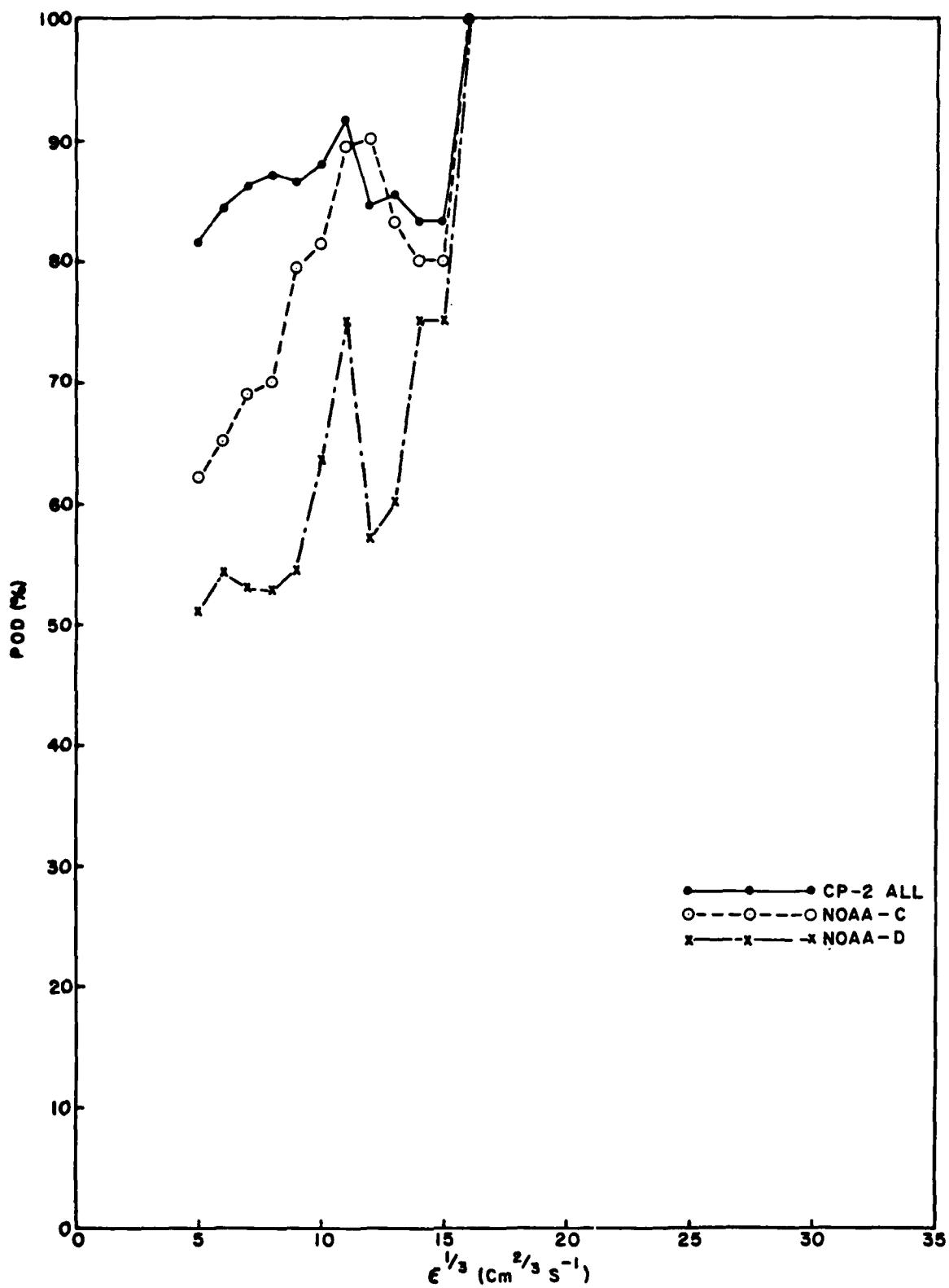
Figure 24c   Probability of detecting a turbulent patch within 6 km of a
significant cell

plus a 4-km buffer zone. Appendix C lists POD values for all encounters, encounters within the 7 dBZ echo region plus buffer zone, and encounters within the 20 dBZ region plus buffer zone. The size of the buffer zone was based on the radius of influence. Assuming that a cell has a radius of between 1 and 2 km, the closest a cell can be to the edge of an echo region is 2 km. The buffer zone is 2 km smaller than the radius of influence and extends the detection region to the maximum possible for cells detected within a region with echoes.

The statistics for turbulent patch detections for the Doppler radars are presented in Figures 24b and 24c. The results for the CP-2 radar using all the observed cells are also presented in these figures for comparison. No significant differences are evident between the results obtained using all the reflectivity derived significant volume cells and the results obtained using the single Doppler C-band radars. CP-3 appeared to have performed better than CP-2 or CP-4, but data for CP-3 were available only from the 22 July case study. The POD values were significantly lower for the 22 June day than for the 22 July day because the aircraft flight included two cloud penetrations (C1 and C2, see Appendix B) on that day which included 22 turbulent patches. Two of the within cloud patches reached an $\varepsilon^{1/3}$ value in excess of 11 $\mathrm{cm}^{2/3} \mathrm{s}^{-1}$.

The X-band Doppler radars displayed lower POD values at the lower $\varepsilon^{1/3}$ threshold levels but produced results equivalent to the other radars at the higher levels. The lower POD values are attributed to attenuation. The aircraft penetration flights tended to be along the upwind flank of the storm which was the other side of the storm from the X-band radars (see Figure 11). The intervening rain apparently reduced the reflectivity values sufficiently to prevent detection at the 17 dBZ reflectivity threshold level employed in the data processing.

5.2 False Alarm Rate

The results of the probability of detection analysis suggest the use of a large radius of influence. A very large radius would defeat the intent of the cell detection approach to localizing the regions of potential hazard and should create a high false alarm rate. False alarms (failures) were defined as aircraft penetrations within the radius of influence of a significant volume cell that were not turbulent at or

above the expected threshold level for $\varepsilon^{1/3}$. The false alarm rate (FAR) was calculated by:

$$FAR = \left(\frac{Y_o - Y}{Y_o}\right) \cdot 100 \qquad (percent) \qquad (2)$$

where Y_o is the total number of significant volume cells within the specified radius of influence of the aircraft track and Y is the number of volume cells within the specified radius of influence of a turbulent patch (success).

The false alarm rates for each of the radars are displayed as a function of threshold level in Figure 25. As expected, the FAR increases with threshold level. However, as shown in Figure 2, the FAR decreased with increasing radius of influence. It is anticipated that the FAR value reaches a minimum then increases as the radius of influence continues to increase.

The aircraft penetration flights were all in regions of new and developing convective cells. If the flights had been through the older regions containing debris cells (see Figure 4d; see also Crane and Hardy, 1981) the false alarm rate could have been higher.

5.3 Critical Success Index

The optimum hazard detection technique would maximize the detection probability and minimize the false alarm rate. Critical success indicies are often used to combine both detection (success) and false alarm (failure) data in a single figure of merit for forecast or detection schemes. A critical success index was adopted for this study which focused on the behavior of the cell approach to hazard detections. It counted cells that were associated (within a radius of influence) with a turbulent patch as a success and a turbulent patch that was not detected as a failure. The resultant critical success index (CSI) is given by:

$$CSI = \left(\frac{Y}{Y_o + W - X}\right) \cdot 100 \qquad (percent) \qquad (3)$$

where the parameters are defined for equations (1) and (2).

The CSI values are plotted as a function of turbulence threshold in Figure 26 and as a function of radius of influence in Figure 3. The results indicate a decrease in the performance of the hazard detection
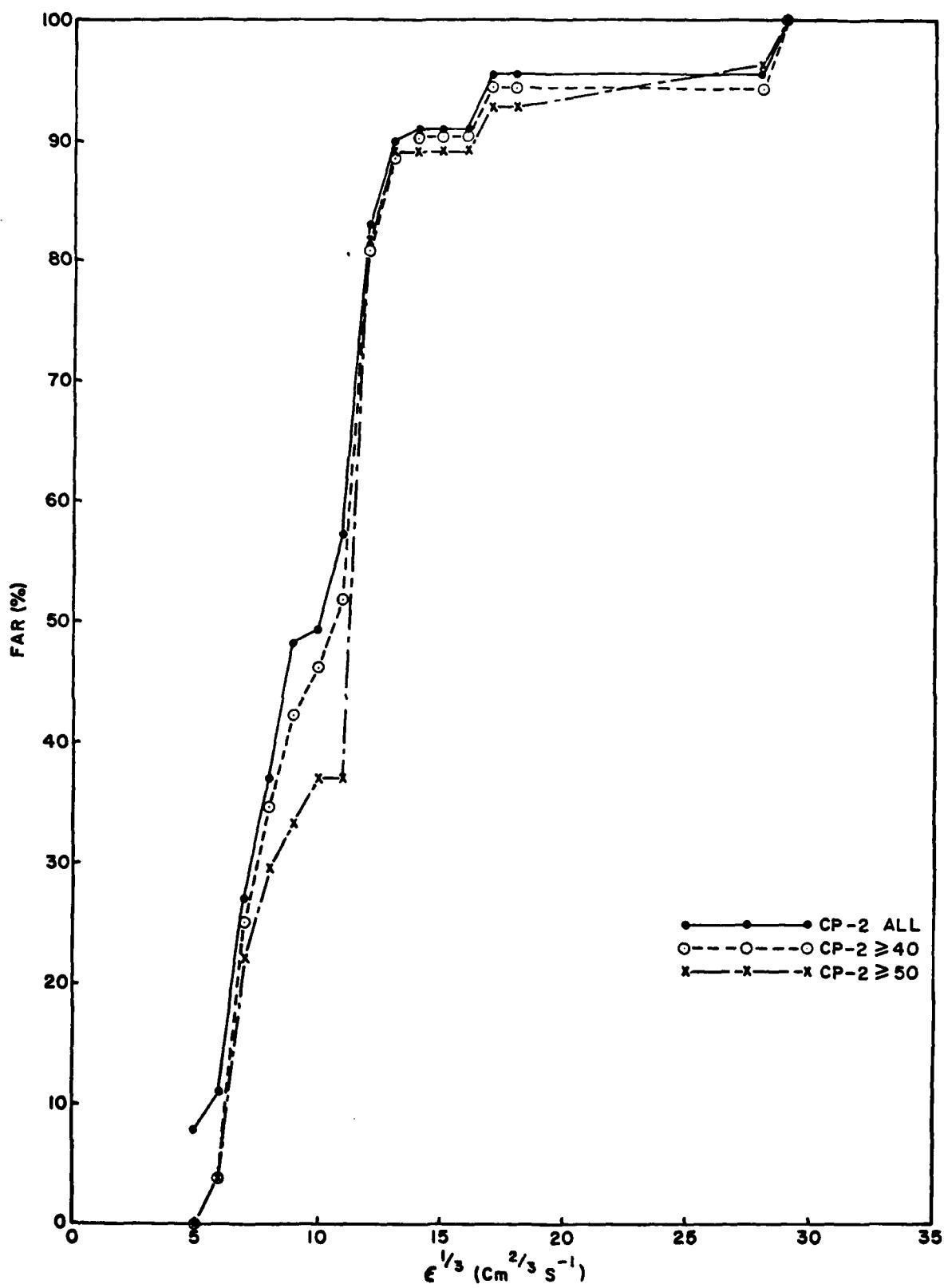
Figure 25a   Probability of a false alarm (no turbulence) along the entire
segment of aircraft track within 6 km of a significant cell
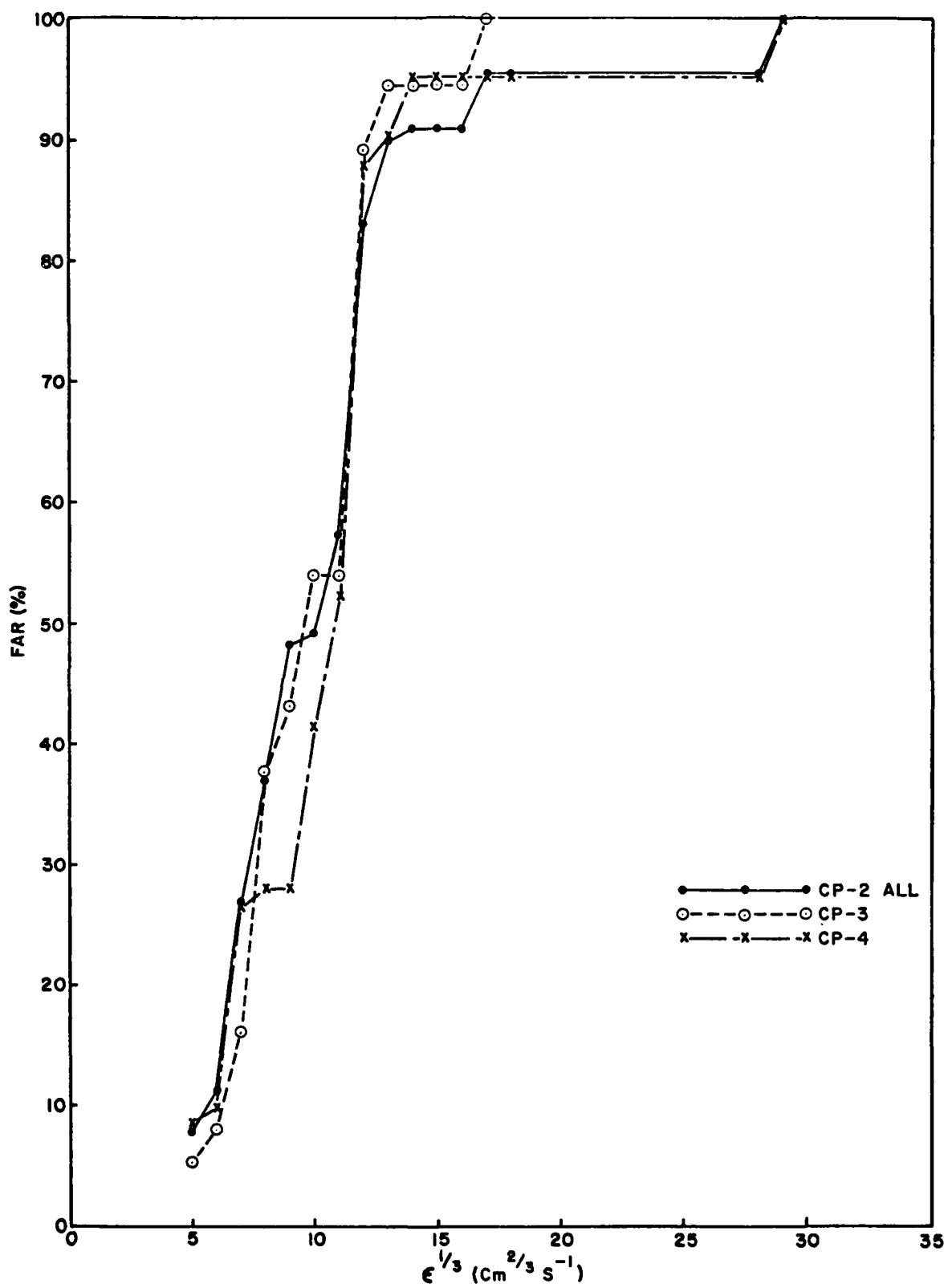
Figure 25b   Probability of a false alarm (no turbulence) along the entire
segment of aircraft track within 6 km of a significant cell
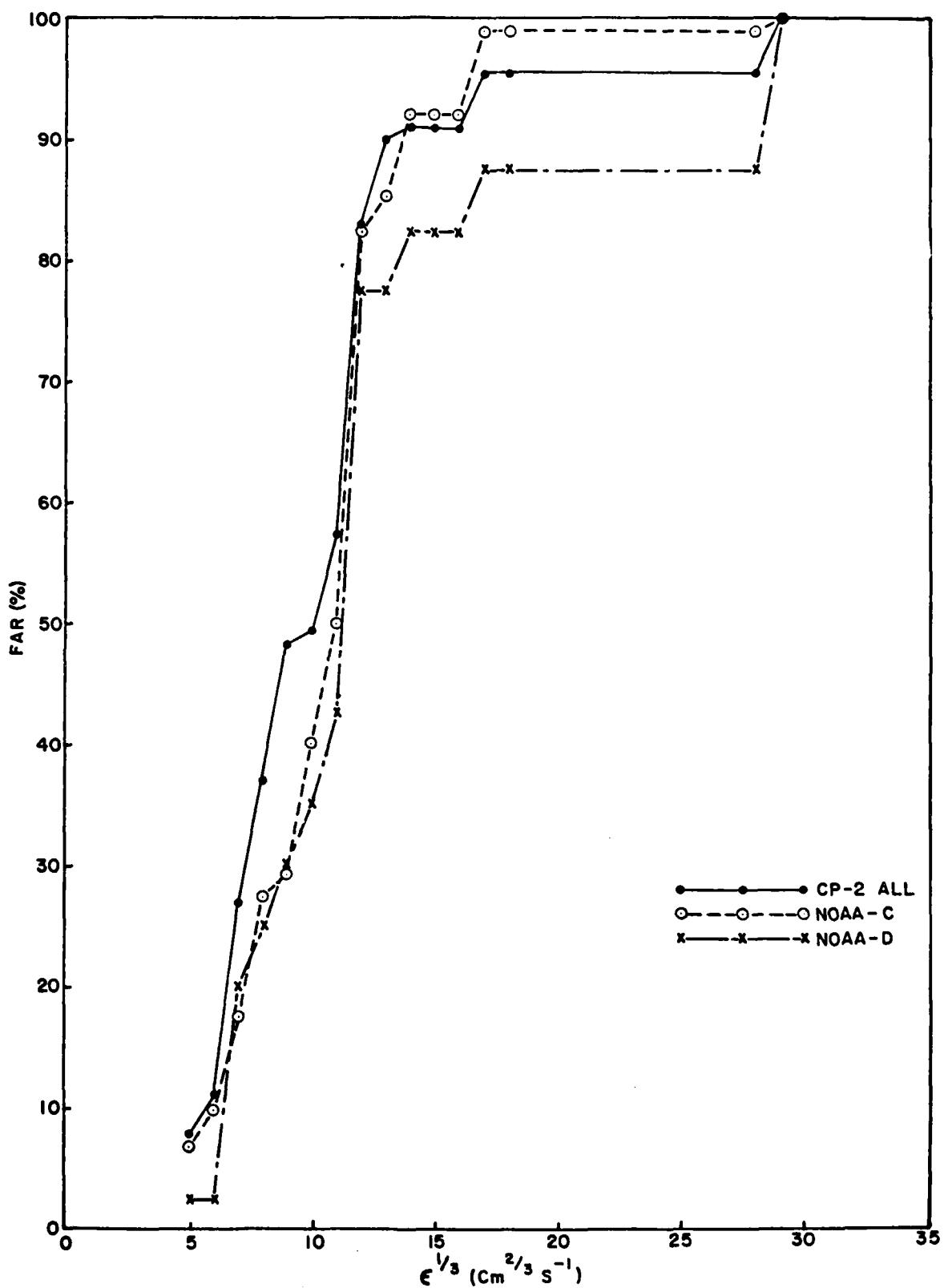
Figure 25c   Probability of a false alarm (no turbulence) along the entire segment of aircraft track within 6 km of a significant cell
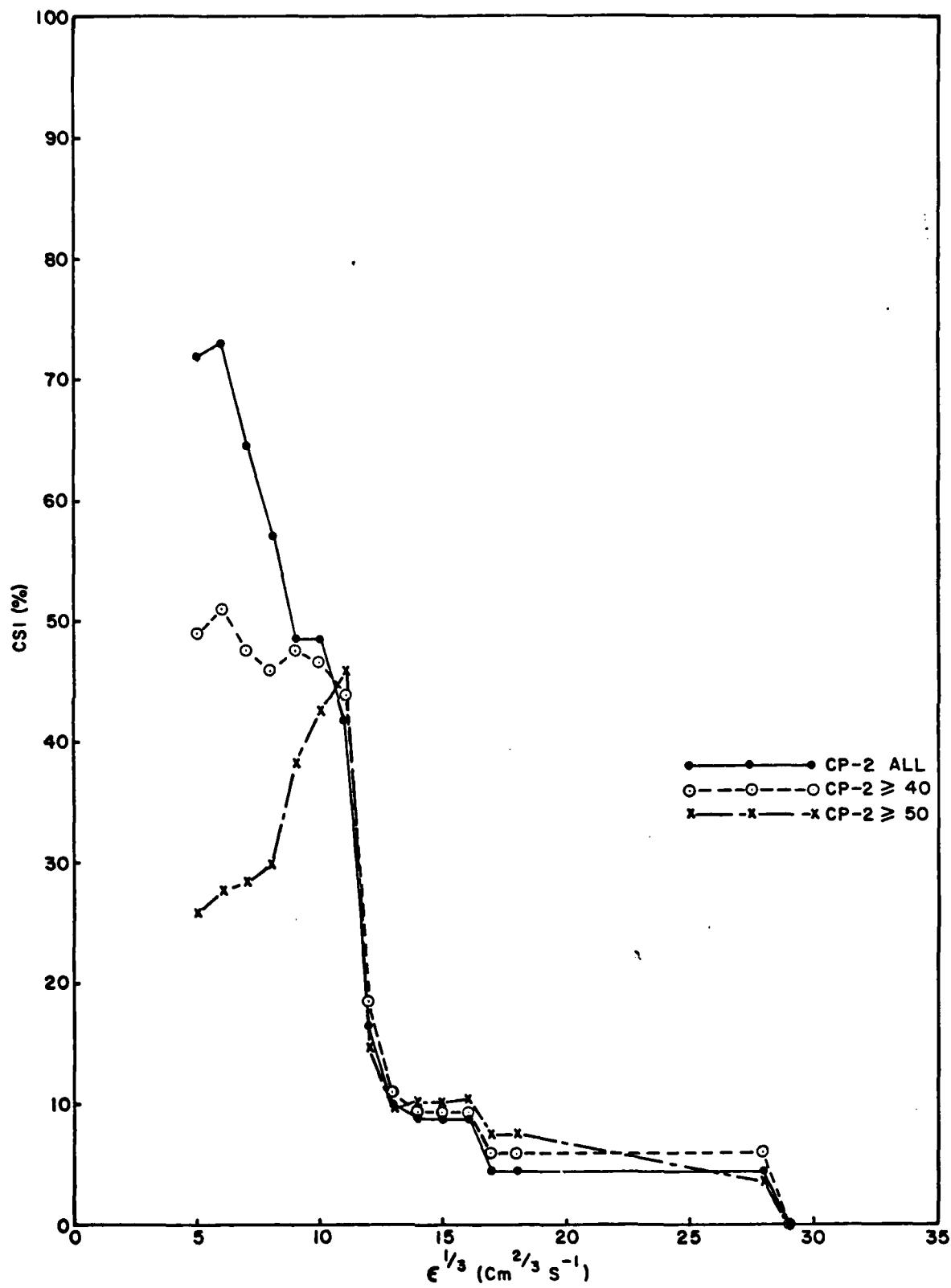
Figure 26a   Critical success index

81
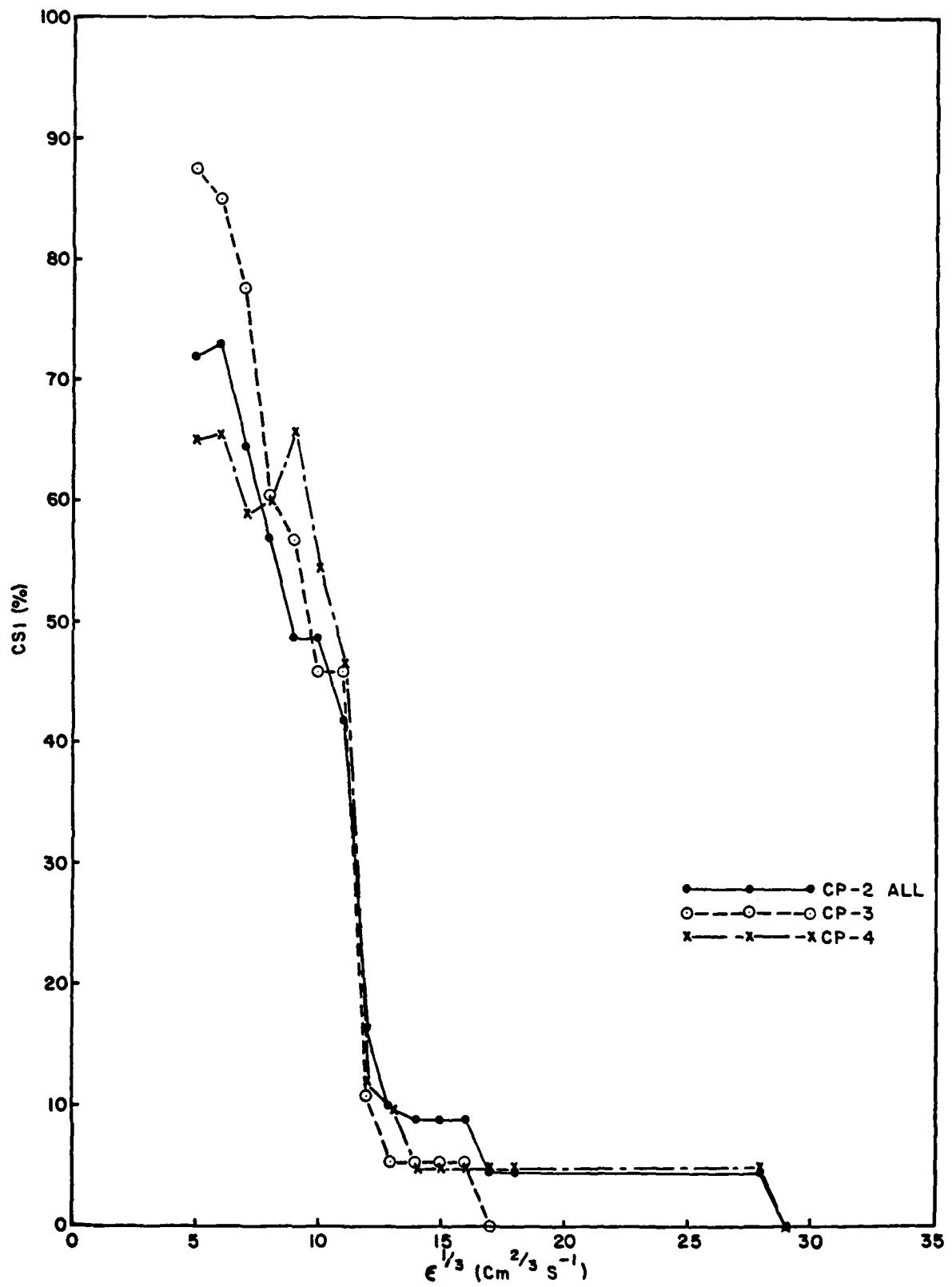
Figure 26b   Critical success index

82
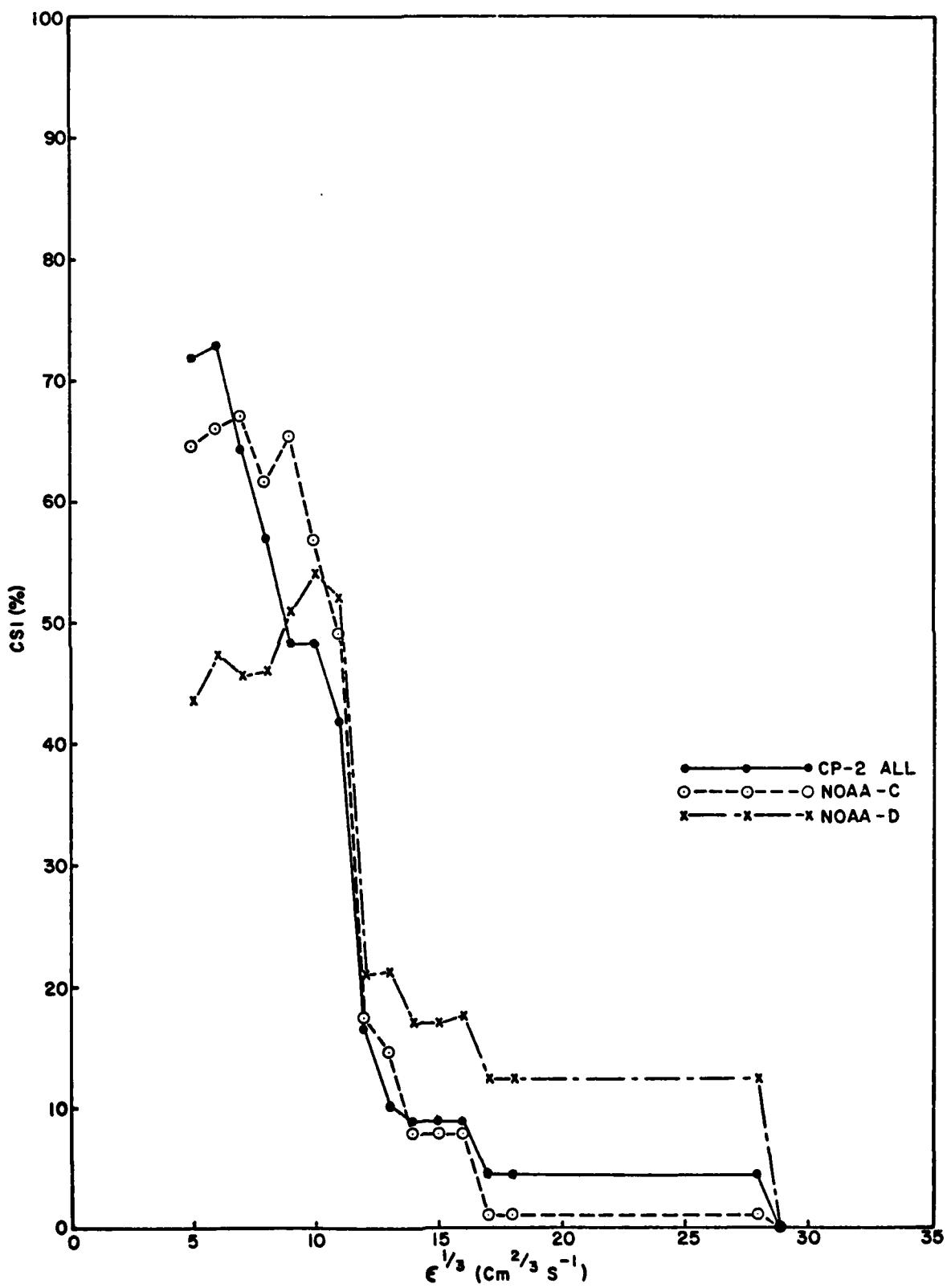
Figure 26c   Critical success index

83

hypotheses (CSI value) as the turbulence threshold is increased but an increase in CSI as the radius of influence is increased.

The results for reflectivity data alone show that the CSI is a maximum at the lowest $\varepsilon^{1/3}$ value (5 $cm^{2/3}$ s^{-1}) when all reflectivity levels are used but is a maximum at $\varepsilon^{1/3} \sim 10$ $cm^{2/3}$ s^{-1} when only the higher reflectivity values are employed. The use of the higher reflectivity values alone does not improve the performance of the algorithm relative to the results obtained using all the data.

The use of Doppler data appears to improve the hazard detection results (CSI values) in the $8 \leq \varepsilon^{1/3} \leq 12$ $cm^{2/3}$ s^{-1} range relative to the results obtained using reflectivity data alone. At lower thresholds, the C-band Doppler data and the reflectivity data alone produce comparable results (Figure 3).

The results obtained for a 6-km radius of influence and a $\varepsilon^{1/3} \geq 5$ $cm^{2/3}$ s^{-1} threshold are excellent as illustrated in Table 1. The curves in Figures 1 through 3 suggest even better results for larger radii of influence. The mid-level flow field depicted in Figure 15b indicates that a distance as large as 10 km may be required to embrace regions of blocked flow upwind of a strong updraft especially as the region develops and few tracers are available to provide radar detection.

The radius of influence analysis was not extended to distances beyond 6 km for several reasons. The intent of the analysis was to show that the cell approach to hazard detection was viable and a radius of influence did exist. The intent of the analysis was satisfied by the results. The selection of an optimum radius of influence depends upon the environment through which penetrations are to be attempted. The values may be different for flights through the debris downwind of a cell from flights through the regions of new growth. The former regions should be less turbulent and are therefore of more interest to air traffic control. Measurements should be made under the conditions for which the system should operate before an optimum set of parameters can be established. More than two sets of observations are required to establish the optimum set of parameters.

5.4 Relationship Between $\epsilon^{1/3}$ and Volume Cell Parameters

The aircraft penetrations flown on 22 July were used to compare the observed turbulence levels with the significant volume cell parameters. The highest level $(\epsilon^{1/3})$ patch within the specified radii of influence are listed for each cell observed within that radius of the aircraft track in Appendix A. Figure 27 presents the observed relationships between volume cell average reflectivity and $\epsilon^{1/3}$; Figure 28 presents the observed relationship between the averaged magnitude of the tangential shear and $\epsilon^{1/3}$. No correlation is evident in either figure. If anything, the highest observed $\epsilon^{1/3}$ value was associated with the lowest observed tangential shear values.

A lack of correlation between derived gust velocities and colocated reflectivity, reflectivity gradient, Doppler spread, or Doppler velocity shear values was reported by Lee (1977). He associated the radar observations and turbulence encounters over distances less than 2 km. A similar lack of correlation is reported here where the associations are to local maxima in the reflectivity or shear fields at distances up to 6 km.

The results obtained to date indicate that cell age is more important than reflectivity or tangential shear in establishing a correlation between $\epsilon^{1/3}$ and the cell parameters. The several cases of severe turbulence depicted in Figure 13c and 13d all occur outside regions of high reflectivity but are associated with regions that later produced significant cells and clusters.

Significant regions of turbulence are most active just before or at the time of first detection. They cannot be detected, processed, and used to forecast hazard location 10 to 20 minutes in the future because they did not exist for a long enough time to be tracked before the region becomes hazardous. No radar based system of observations will solve this basic hazard detection problem. Only forecasts of probable locations of new cell (or cluster) development can provide a solution to the hazard detection problem. The regular organization of new cluster development (Figure 14) indicates that the larger-than-cloud scale organization controls the development of new cells and that an early recognition of the pattern of new cell development could be useful in providing forecasts.
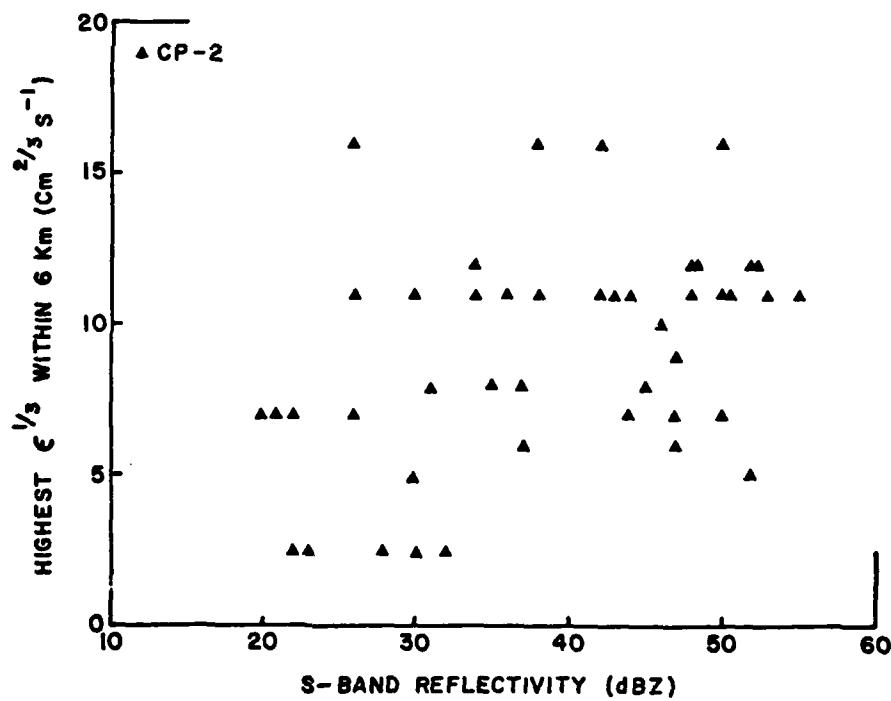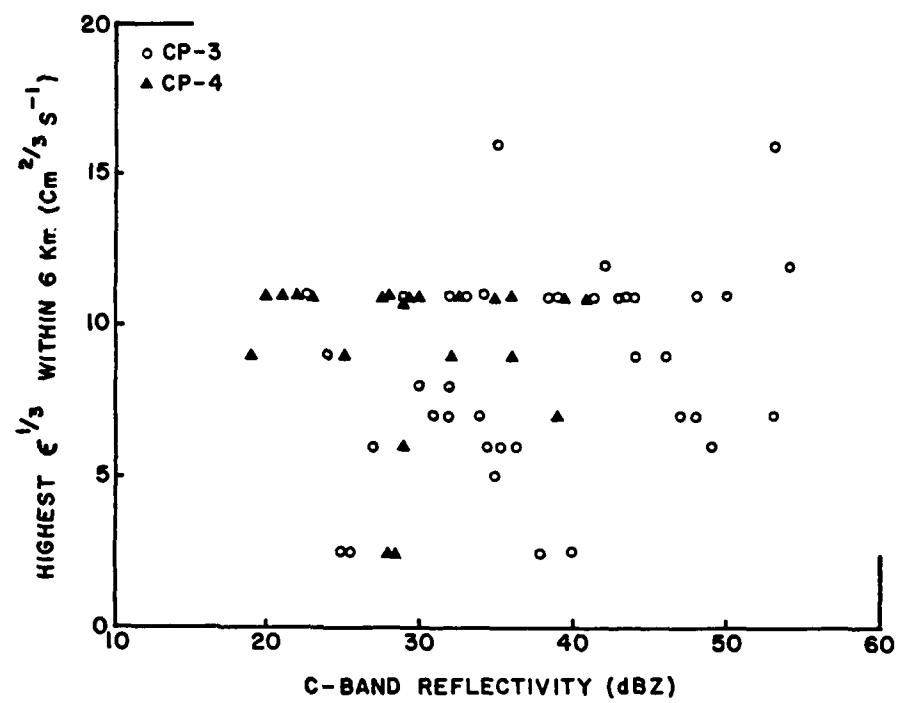
Figure 27   Observed relationship between eddy dissipation rate and
volume cell reflectivity, 22 July 1976
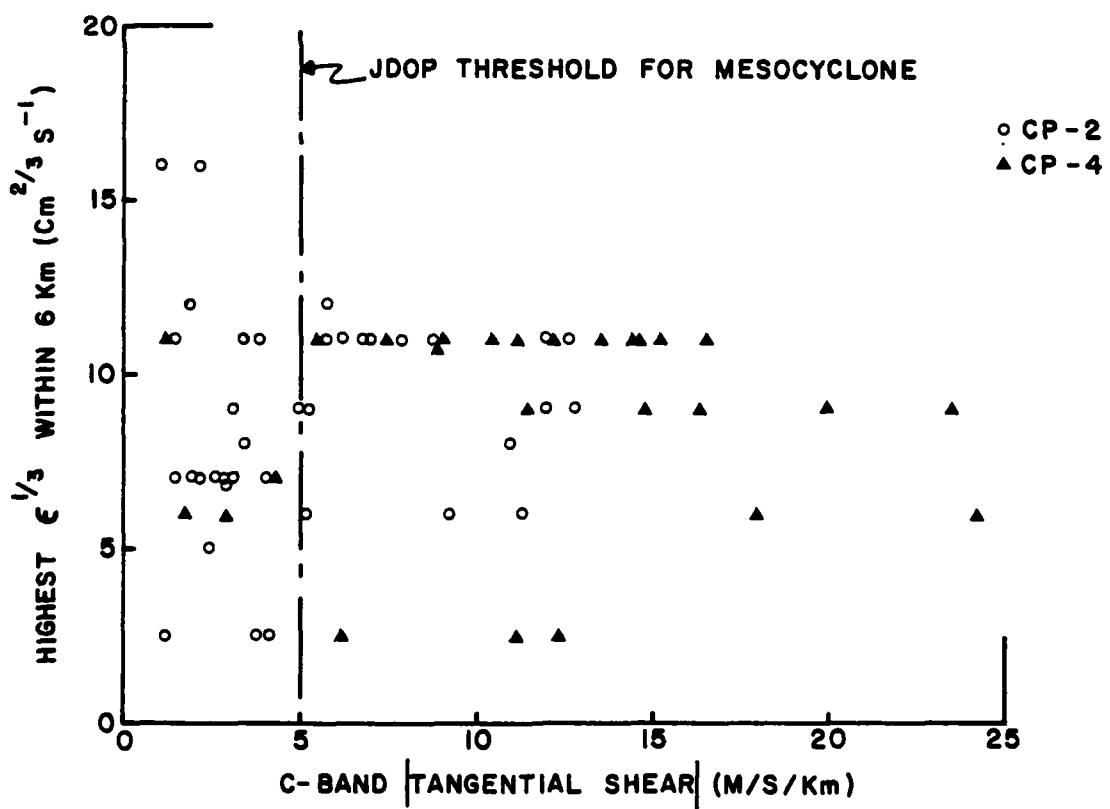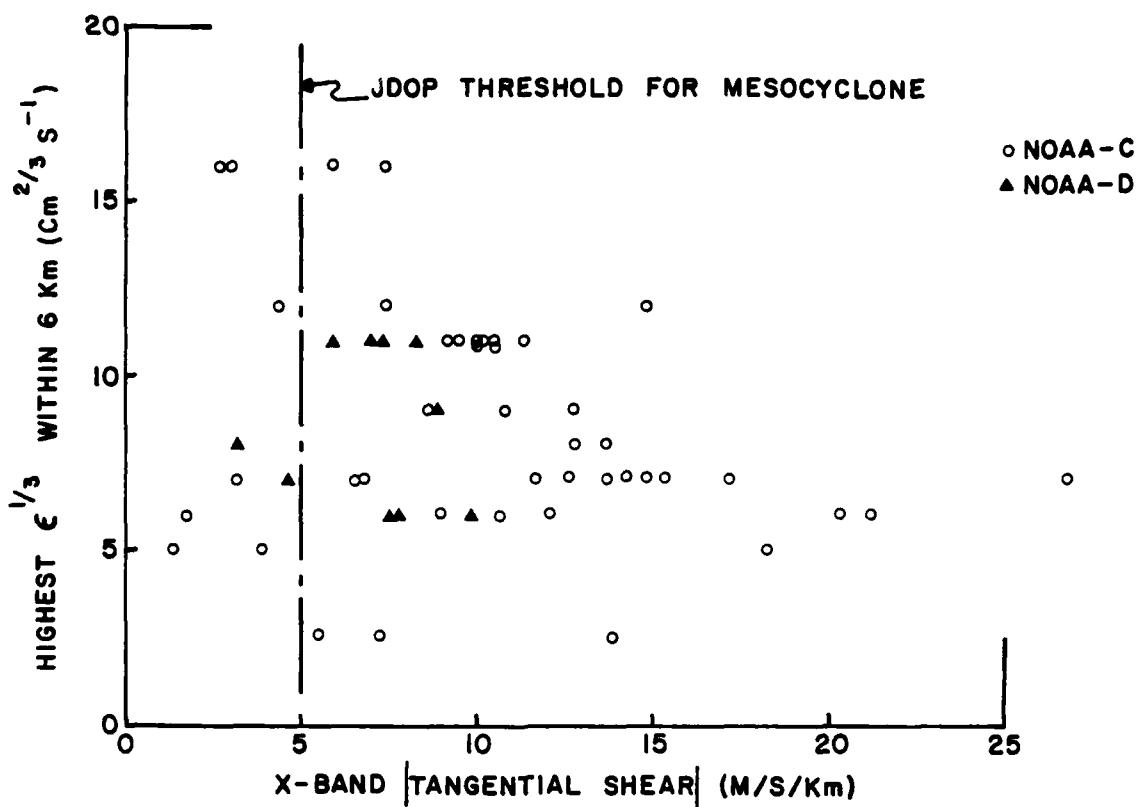
Figure 28   Observed relationship between eddy dissipation rate and
volume cell tangential shear, 22 July 1976

87

6. CONCLUSIONS AND RECOMMENDATIONS

This report documents the development and testing of a viable aircraft hazard detection scheme which operates as well employing conventional radar data as it does employing Doppler radar data. The detection scheme was evaluated using aircraft penetrations into the most turbulent regions of hail storms. These regions are of interest when verifying that turbulence can be detected but are not optimum for evaluating the detection technique under realistic operating conditions. If, in the latter case, higher false alarm rates can be expected, more development will be necessary to utilize more effectively the available information before the hazard detection procedure can be incorporated into an air traffic control environment.

Continued algorithm refinement is necessary and should be pursued. The horizontal flow field maps (Figure 15) showed that single Doppler radars can be successfully employed to locate the cores of the strongest (non-entraining) updrafts. Cluster age was also an important indicator of severity. It is an indicator which will be important in separating cells or clusters formed in the debris region downwind of an active cluster from the active and potentially hazardous growth regions. The progressive cluster development pattern can be used to separate automatically new growth and debris regions.

Continued flight testing should proceed hand-in-hand with the continued algorithm development. Of particular importance is the development of a real-time significant cell, cluster, and potential hazard display capability. The real-time display provides the only means to evaluate successfully the hazard detection scheme. Aircraft must be vectored into apparently hazard-free areas to evaluate the probability of detection and into apparently hazardous areas to evaluate the probability of a false alarm. Only with positive flight control will enough data be amassed to optimize threshold criteria, the radius of influence, and algorithm improvements yet to be made.

A major conclusion of the work reported here is that the severity of the turbulence was inversely related to the age of the cluster; the younger the cluster, the more turbulent. Unfortunately, a detection scheme based only on observations requires several observations to establish the existence and motion of a cluster. The danger is highest

before the hazard can be detected. A short range forecast of the probable locations of new cell development is required to complete the development of the hazard detection scheme.

The recommended program to develop the automatic hazard detection system for use by the FAA is:

1) refine the cell and cluster detection algorithms to reduce the effect of the statistical uncertainties in the estimation of velocity perturbations;

2) refine the cell significance algorithms using cell age, location in the development pattern, apparent vertical transport of horizontal momentum and similar parameters to provide an indication of the intensity of the turbulence;

3) develop a graphical display of the cell, cluster, and contour data that can be provided both to meteorologists for the development of short range forecasts and to controllers for use in vectoring test aircraft into regions expected to be hazardous or free of hazard to evaluate the algorithms;

4) develop a real time version of the program for use in the continued evaluation of the algorithms;

5) using the real time system and the controller displays, conduct flight tests to evaluate the refined velocity perturbation detection and turbulence intensity estimation algorithms;

6) analyze the new cell and cluster development patterns to isolate the propagating disturbances that trigger the convection;

7) automate the display of the propagating disturbances to provide forecasters and controllers with the tools necessary for the short range forecast of hazardous areas;

8) evaluate the short range hazardous region forecast procedures in several different climate regions; and

9)   based on the short range hazard forecast evaluations,
      automate the successful features to provide timely
      forecasts to the controllers.

The recommended program includes tasks that can be readily defined
at the present time (1 through 4 and 6), tasks to be completed when
refined algorithms are available (5 and 8), and tasks whose definition
depends on the results of future work (7 and 9).

7. REFERENCES

AWST (1978): "Thrust Loss Cited in Southern Accident", Aviation Week and Space Technology, August 21, 1978, 55-58.

Barclay, P.A. (1968): "An Operational System for the Avoidance by Aircraft of Severe Convective Turbulence", Proc. 13th Radar Meteorol. Conf., Amer. Meteorol. Soc., Boston, 438-441.

Barclay, P.A. (1974): "Aircraft Turbulence Encounters During Commercial Operations in the Vicinity of Thunderstorms", Preprint 6th Conf. on Aerospace and Aeronautical Meteorol., Amer. Meteorol. Soc., Boston, 357-360.

Brown, R.A. and L.R. Lemon (1976): "Single Doppler Radar Vortex Recognition: Part 2 - Tornadic Vortex Signature", Preprints 17th Radar Meteorol. Conf., Amer. Meteorol. Soc., Boston, 104-109.

Browning, K.A. and G.B. Foote (1976): "Airflow and Hail Growth in Supercell Storms and Some Implications for Hail Suppression", Quart. J. Roy. Met. Soc., 102, 499-533.

Brunstein, A.I. (1971): "Study of Lesson to be Learned from Accidents Attributed to Turbulence", NTSB-AAS-71-1, National Transportation Safety Board.

Burgess, D.W. (1976): "Single Doppler Radar Vortex Recognition: Part I - Mesocyclone Signatures", Preprints 17th Radar Meteorol. Conf., Amer. Meteorol. Soc., Boston, 97-103.

Burnham, J. and J.T. Lee (1969): "Thunderstorm Turbulence and Its Relationship to Weather Radar Echoes", J. Aircraft, 6, 438-445.

Crane, R.K. (1976): "Radar Detection of Thunderstorm Hazards for Air Traffic Control, Vol. I, Storm Cell Detection", Rept. ATC-67, Vol. 1, MIT Lincoln Laboratory, Lexington, Mass.

Crane, R.K. (1977): "Parameterization of Weather Radar Data for Use in the Prediction of Storm Motion and Development", AFGL-TR-77-0216, Air Force Geophysics Laboratory, Hanscom AFB, Mass.

Crane, R.K. (1978): "Development of Techniques for Short-Range Precipitation Forecasts", AFGL-TR-78-0005, Air Force Geophysics Laboratory, Hanscom AFB, Mass.

Crane, R.K. (1979a): "Automatic Cell Detection and Tracking", IEEE Trans. Geoscience Elect., GE-17, 250-262.

Crane, R.K. (1979b): "Automatic Weather Radar Echo Assessment and Tracking", AFGL-TR-79-0248, Air Force Geophysics Laboratory, Hanscom AFB, Mass.

Crane, R.K. and K.R. Hardy (1981): "The HIPLEX Program in Colby-Goodland Kansas: 1976-1980", ERT Doc. P-1552-F, Environmental Research & Technology, Inc., Concord, Mass.

Donaldson, R.J., Jr. (1970): "Vortex Signature Recognition by a Doppler Radar", J. Appl. Meteorol., 9, 661-670.

Ehernberger, L.J. (1974): "High Altitude Turbulence Encountered by the Supersonic YF-12A Airplane", Preprints 6th Conf. Aerospace and Aeronaut. Meteorol., Amer. Meteorol. Soc., Boston, 305-312.

FAA (1978): "Thunderstorms", Advisory Circular 00-24A, Federal Aviation Administration, U.S. Dept. of Transportation, Washington, D.C.

Foote, G.B., A.J. Heymsfield, D.J. Musil, C.G. Wade, T.J. Kelley and H.W. Frank (1978): "The Colorado Hail Storm of 22 July 1976: IV Storm Model and Implications", Preprints 18th Conf. Radar Meteorol., Amer. Meteorol. Soc., Boston, 232-237.

Fujita, T.T. (1978): "Manual of Downburst Identification for Project Nimrod", SMRP Research Paper No. 156, Department of the Geophysical Sciences, The University of Chicago.

Gustafson, G.B. (1980): "Software Routines for the Automatic Processing of Weather Radar Data", ERT Doc. P-1552-IP-5, Environmental Research & Technology, Inc., Concord, Mass.

Harris, F.I., J.C. Frankhauser and J.R. Miller (1978): "A Complex Convective Storm System Studied by Multiple Doppler Radar Analysis" Preprints 18th Conf. Radar Meteorol., Amer. Meteorol. Soc., Boston, 252-259.

Heymsfield, A.J., D.J. Musil and B.G. Foote (1978): "The Colorado Hail Storm of 22 July 1976: III Characteristics of the Updraft Region", Preprints 18th Conf. Radar Meteorol., Amer. Meteorol. Soc., Boston, 226-231.

Heymsfield, A.J., A.R. Jameson and H.W. Frank (1980): "Hail Growth Mechanisms in a Colorado Storm: Part II: Hail Formation Processes", J. Atmosph. Sci., 37, 1779-1807.

Jameson, A.R. and A.J. Heymsfield (1980): "Hail Growth Mechanisms in a Colorado Storm: Part I: Dual-Wavelength Radar Observations", J. Atmosph. Sci., 37, 1763-1778.

JDOP (1979): "Final Report on the Joint Doppler Operational Project (JDOP) 1976-1978", ERL-NSSL-86, National Severe Storms Laboratory, Norman, Oklahoma.

Kelly, T.J., H.W. Frank, G.B. Foote and C.G. Wade (1978): "The Colorado Hail Storm of 22 July 1976: II Internal Circulation", Preprints 18th Conf. Radar Meteorol., Amer. Meteorol. Soc., Boston, 219-225.

Lee, J.T. (1974): "Thunderstorm Turbulence Concurrent Doppler Radar and Aircraft Observations 1973", Preprints 6th Conf. on Aerospace and Aeronautics Meteorology, Amer. Meteorol. Soc., Boston, 295-298.

Lee, J.T. (1977): "Application of Doppler Weather Radar to Turbulence Measurements which Affect Aircraft", Rept. NSSL-1, National Severe Storms Laboratory, Norman, Oklahoma.

MacCready, P.B., Jr. (1964): "Standardization of Gustiness Values from Aircraft", J. Appl. Meteorol., 3, 439-449.

Marwitz, J.D. (1972): "The Structure and Motion of Severe Hailstorms, Part II: Multicell Storms", J. Appl. Meteorol., 11, 180-188.

Monin, A.S. and A.J. Yaglom (1975): Statistical Fluid Mechanics, Vol. 2, English ed. edited by J.L. Lumley, 874 pp., MIT Press, Cambridge, Mass.

Pratt, K.G. and W.G. Walker (1954): "A Revised Gust-Load Formula and a Re-evaluation of V-G Data Taken on Civil Transport Airplanes from 1933 to 1950", Rept. 1206, National Advisory Committee of Aeronautics, 1-4.

Renick, J.H. (1971): "Radar Reflectivity Profiles in Individual Cells in a Persistent Multicellular Alberta Hailstorm", Preprints 7th Conf. Severe Local Storms, Amer. Meteorol. Soc., Boston, 63-70.

Sand, W.R. and R.A. Schleusener (1974): "Development of an Armored T-28 Aircraft for Probing Hailstorms", Bull. Amer. Meteorol. Soc., 55, 1115-1122.

Sand, W.R., D.J. Musil and T.G. Kyle (1974): "Observations of Turbulence and Icing inside Thunderstorms", Preprints 6th Conf. Aerospace and Aeronaut. Meteoro., Amer. Meteorol. Soc., Boston, 299-304.

Sand, W.R., J.L. Halvorson and T.G. Kyle (1976): "Turbulence Measurements Inside Thunderstorms Used to Determine Diffusion Characteristics for Cloud Seeding", 2nd WMO Scientific Conf. on Weather Modification, Boulder, World Meteorological Organization, Geneve, 539-545.

Wade, C.G. and G.B. Foote (1978): "The Colorado Hailstorm of 22 July 1976: 1. General Features, Radar Structure and Evolution", Preprints 18th Conf. Radar Meteorol., Amer. Meteorol. Soc., Boston, 212-218.

Wilson, J., R. Carbone, H. Baynton and R. Serafin (1980): "Operational Application of Meteorological Doppler Radar", Bull. Amer. Meteorol. Soc., 61, 1154-1168.

Zbrozek, J.K. (1961): "Aircraft and Atmospheric Turbulence", Tech. Note AERO 2790, Roy. Air. Estab.

ACKNOWLEDGMENTS

APPENDIX A

VOLUME CELL DATA AND AIRCRAFT TURBULENCE
ENCOUNTERS FOR THE 22 JULY 1976 CASE STUDY

CELL DATA, 22 JULY 1976, #1

Penetra. Number	Cluster	Cell No	REFLECTIVITY (dBZ)										MAG. TANGENTIAL SHEAR (m/s/km)								TURBULENCE (1/3 ≥ 5 cm$^{2/3}$ s^{-1})					
			CP-2 Ref	No	CP-3 Ref	No	CP-4 Ref	No	WPL-C Ref	No	WPL-D Ref	No	CP-3 TS	No	CP-4 TS	No	WPL-C TS	No	WPL-D TS	No	0-2 km Peak	No	2-4 km Peak	No	4-6 km Peak	No
1	A	1		-		1	36	1	24	4	34	1			3.0	1	10.6	4	9.9	1			6	1	6	1
	-	2	47	7			35	1	22	4	37	1			1.8	1	20.3	8	7.8	1					6	1
	C	3	22	3	25	1			20	1			1.2	1			5.5	1								No
	A	4	31	1	30	1			25	2	32	1	3.5	1			12.8	2	3.3	1			6	2	8	1
	-	5	35	1	32	2	20	1	22	3			11.0	2	5.1	1	13.7	3							8	3
	-	6	26	2	33	3							6.9	3							8		8		11	2
	-	7	42	2			27	2	28	1					12.2	2	9.1	1							11	2
	V	8	44	3			36	4							10.5	4						1			11	2
	a	9	55	6	48	4	41	2	27	3	35	3	3.9	4	9.1	2	10.5	3	7.0	3			11	3	8	1
	V	10	53	6	43	5	23	2	31	4	39	2	3.4	5	14.7	2	10.3	4	8.3	2			11	2	11	2
	a	11	30	6	34	3	35	2					1.5	3	11.2	2									11	2
	V	12	43	1	43	1	29	2	32	1	31	2	8.8	1	16.6	2	11.4	1	5.9	2		No	11	1	11	1
	-	13			29	2	29	2	23	1			5.7	2	24.3	2	9.5	1					11	2	11	1
	-	14			35	2	29	1	26	2	29	1	9.3	2	7.5	1	12.1	2	7.6	1				No	6	1
	-	15																							11	2
		-0-																								
2	V	8	34	1	39	1	28	1	26	3	35	3	7.9	1	15.3	1	10.1	3	8.9	3			11	2	9	2
	a	9	47	4	46	3	32	3	31	2	39	1	5.0	3	14.8	3	10.8	2	7.3	1					9	2
	V	10	50	3	44	2	39	1	30	1			6.9	2	1.3	1	10.0	1				2	11	2	9	3
	a	11			41	2	30	4							12.2	4					9	2				No
	E	12	48	1	44	3	33	2	32	2			6.2	2	8.9	1	10.6	2							9	2
	-	13			39	1	36	2	24	1			3.1	3	20.0	2	8.8	1					9	1		
	E	14					22	2					12.2	1	13.6	2									11	3
	-	15					27	1							18.0	2									6	1
	V	16	50	2	50	2	30	1	30	1			5.0	2	16.4	1	12.8	1			9	2	6	No	11	2
	A	17	28	1			28	1							11.1	1										No
	C	18	32	1	38	3	28	1	31	2	37	1	3.8	3	6.2	1	7.2	2	4.7	1			9	No		No
	C	19	44	3	47	1	39	1	33	1			1.5	1	4.4	1	3.2	1							7	1
	-	20					19	1							11.5	1							9	1		
	-	21			32	2	21	2					12.6	2	14.5	1							9	2	11	2

A-2

CELL DATA, 22 JULY 1976, #2

Penetra. Number	Cluster	Cell No	REFLECTIVITY (dBZ) CP-2 Ref	No	CP-3 Ref	No	CP-4 Ref	No	WPL-C Ref	No	WPL-D Ref	No	MAG, TANGENTIAL SHEAR (m/s/km) CP-3 TS	No	CP-4 TS	No	WPL-C TS	No	WPL-D TS	No	TURBULENCE (1/3 ≥ 5 cm$^{2/3}$ s^{-1}) 0-2 km Peak	No	2-4 km Peak	No	4-6 km Peak	No
2	σ	22			35	1							3.1	1								No		No	7	1
		23			24	1	25	2					12.8	1	23.6	2					9	No	6	1	9	1
	σ	24			23	1							12.0	1								1	11	2		
	σ	25							27	1							6.8	1							7	1
		26	21	1																					7	1
		-0-																							6	1
3	σ	14	38	2																	7		No		11	2
	σ	27	36	2																			11	1		3
	σ	28	38	2																			16	3	7	1
		29	26	2																			16	2	12	1
	τ	30	30	2																		1			(4.9)	1
		-0-																								
4	σ	14	52	3	48	3			29	2			2.6	3			14.9	2			12	3	8	1	8	2
	σ	27	49	1					34	2							6.8	2					12	4	12	3
	σ	28	37	2	36	1			31	1			11.4	1			11.7	1							10	1
	σ	31	49	2					27	2							13.9	2							12	3
		32	46	1	40	1			29	1			5.2	1			21.2	2					8			No
		33	33	1	53	1			34	1			2.0	1			13.8	1								
	σ	34	30	1	49	1			28	1			2.9	1			17.2	1								
		-0-																								
5	σ	14	50	3					29	2							14.9	2			7	1	6	1	5	1
	σ	27	47	2					34	2							6.8	2					5	1	7	1
	σ	28	45	3					31	1							11.7	1							8	2
	σ	31	37	3					27	2							13.9	2						No	6	2
		35	23	1					29	1							21.2	2								No
		36							34	1							13.8	1			5	2*				
		37							28	1							17.2	1			6	2				
	τ	38							33	1							15.4	1							5	1
		39							29	1							26.8	1							7	2
	τ	40																							7	1

*Defected Next Pass

NO DATA (WPL-D, CP-4 shear, WPL-D shear columns)

A-3

CELL DATA, 22 JULY 1976, #3

Penetra. Number	Cluster	Cell No	REFLECTIVITY (dBZ) CP-2 Ref	CP-2 No	CP-3 Ref	CP-3 No	CP-4 Ref	CP-4 No	WPL-C Ref	WPL-C No	WPL-D Ref	WPL-D No	MAG. TANGENTIAL SHEAR (m/s/km) CP-3 TS	CP-3 No	CP-4 TS	CP-4 No	WPL-C TS	WPL-C No	WPL-D TS	WPL-D No	TURBULENCE (1/3 ≥ 5 cm$^{2/3}$ s^{-1}) 0-2 km Peak	0-2 km No	2-4 km Peak	2-4 km No	4-6 km Peak	4-6 km No
5		41			25	1							4.1	1												No
		42							31	1							12.6	1					7	1	6	2
		43					NO DATA		28	1	NO DATA						9.0	1							6	1
		44			33	1			27	1			2.5	1			18.3	1						No	5	1
		45							24	1							1.8	1							6	2
		46							23	1							14.3	1					5	1	7	2
		-0-																								
6	o	14	52	1	54	1			35	1			1.9	1			1.4	1					6	3	5	1
	o	27	52	4	53	1			32	1			1.1	1			4.4	1					12	3	12	2
	o	28	50	4					36	1							7.4	1					5	2	16	3
	o	38			42	1			33	1							3.9	1				No	10	1		
		47			35	1			29	1			5.8	1			7.4	1			6	2	10	1	12	2
		48			31	1							2.2	1							16	3			12	1
		49											2.0	1							(7)	1				
	o	50							28	1							3.0	1					16	3	16	3
		51							33	1							2.7	1					12	3	12	1
		52							33	1							14.8	1							12	2
		-0-																								
7		48	42	2					30	1							5.9	1			(16)	3	7	1	7	1
		53	26	1																		No		No		
		54	22	1																		No	7			
		55	20	1																				2		1
		-0-																								

A-4

APPENDIX B

AIRCRAFT PENETRATION SUMMARY REPORTS PROVIDED
BY DR. P.L. SMITH, JR.,
SOUTH DAKOTA SCHOOL OF MINES & TECHNOLOGY

MEMORANDUM FOR THE RECORD

FROM: P. L. Smith, Jr. *Pls*

SUBJECT: Notes Based on Perusal of T-28 Data Plots for 22 June 1976
          (Flight 167)

    All numerical values given are approximate values read from the
computer-generated plots. Detailed listings should be consulted if more
precise values are desired.

1a & 1b <u>Penetration 1 (16:02:04 to 16:09:27)</u>

    Altitude range: 6.1 to 6.5 km

    Temperature range: -10C to -16.5C

    Updraft characteristics:

        Maximum updraft speed about 14 m sec^{-1} near 16:05:36.

        Width* of main updraft about 5 km.

        Gradient of θ_e across main updraft 8K (partly related to
        altitude change?).

        Maximum downdraft speed about 10 m sec^{-1} (two locations).

        Width* of main downdrafts 3 - 4 km.

    Hydrometeor characteristics:

        Cloud liquid water concentration up to about 0.9 g m^{-3} except
        for suspicious looking peaks between 1603 and 1604. Little
        cloud liquid water in the main updraft (perhaps because of
        depletion by the hail?). Cloud LWC values up to about 0.7 g m^{-3}
        appear in some downdraft regions.

        Hail present in substantial concentrations in the main updraft
        at 1605-1606 as well in the downdraft region around 1607. Hail
        recorded continuously for more than 40 km (1604-1611+). Hail

---

* Extent of the draft region along the flight path, which is probably
  smaller than its true width.

mass concentrations of more than 10 g m^{-3} are suspicious*, as are reflectivity factors up to 73-74 dBz. Hail concentrations exceeding 1 g m^{-3} show up <u>outside</u> the cloud (16:09:27 - 16:11+); pilot comments should be checked to see whether there is any corresponding annotation.

Turbulence: Maximum values about 10 cm$^{2/3}$ sec^{-1}, occuring at edges of main updraft.

Acceleration: Less than 0.5 g either direction. Maximum values occur in downdrafts.

C1 & C2 In-Cloud Period Between 16:13:30 and 16:25:00 or Later

This period which had a peak updraft exceeding 20 m sec^{-1} and cloud liquid water concentrations up to 1.5 g m^{-3} was not logged as a penetration. During this period, there are several places where the reverse flow temperature (RFT) probe trace and the Johnson-Williams (JW) liquid water concentration trace look suspisciously similar. See for example 16:14:25-16:15:40 or 16:18:00-16:18:30 or 16:19:25-16:20:00 or 16:21:55-16:23:00 or 16:24:10-16:25:05. There is little suggestion of similar behavior during Penetration 1. An acceleration peak of +0.7 g occurred at a "hole in an updraft" just after 16:19:45.

3a & 3b Penetration 2 (16:25:41-16:39:29)

Altitude range: 5.2 to 6.7 km

Temperature range: -4C to -17C

Updraft characteristics:

Maximum updraft speed about 16 m sec^{-1} (several places; probably underestimated due to effects of aircraft icing).

Width of main updraft about 8 km; actually about 30 km of essentially sustained upward motion from 16:27:45 to 16:32:45. During the 5 min crossing of the large (30 km) updraft area, the aircraft gained about 1.35 km in altitude. The peak updraft speed was only about 15 m sec^{-1}, but the average for

---

* But note that the hail concentrations plotted are for 1-sec samples; they should be averaged over several seconds to get representative values.

the entire 30 km was 4.5 m sec^{-1}. Cloud liquid water
concentrations were so large and extensive that the aircraft
picked up enough ice to require descending below the melting
level to thaw out.

Maximum downdraft speed about 22 m sec^{-1} near 16:34:05
(probably overestimated).

Width of main downdraft areas about 3 km (indications of
broader downdrafts after 1637 believed due to degradation
of aircraft performance because of structural icing).

Hydrometeor characteristics:

Cloud liquid water concentrations reached about 2 g m^{-3}; values
of 0.8 g m^{-3} or more were indicated across the full 30 km width
of the major updraft area, and indications of cloud LWC above
zero were maintained for more than 60 km. Cloud liquid water
concentrations of more than 1 g m^{-3} appear in downdrafts in
several places.

Hail concentrations up to about 9.6 g m^{-3}, mostly in updraft
regions. Width of main hail zone about 13 km (2:10); inter-
mittent hail encounters over more than 40 km (16:26:45-16:33:45).
Significant amounts of hail coexist with more than 1 g m^{-3} of
cloud liquid in the major updraft area. Reflectivity factors
up to 68 dBz are more plausible.

Turbulence: Major jolt of 28 $cm^{2/3}$ sec^{-1} at 16:27:40; two other
peaks in excess of 15. The major jolt occurred at a sharp -14 m sec^{-1}
to $+10$ m sec^{-1} downdraft/updraft boundary; the secondary peaks were
in updraft regions.

Acceleration: Peaks in both directions of nearly 1 g indicated
around 1628; several peaks of more than ± 0.5 g.

The correspondence between the RFT and JW traces is again remarkable;
see for example, 16:31:00-16:35:00 or later. The temperature excursions
at 16:33-16:34 are especially implausible and the strong correlation between
the RFT and JW traces during that period is highly suspect.

The period after about 16:37 was the descent to allow for deicing
the aircraft. During this period, the plot shows downdrafts which on
occasion exceed 15 m sec^{-1}. Our updraft formula is supposed to correct
for aircraft-induced effects, and thus there should be essentially no up

or downdraft in this region of the plot. This suggests that there may
be some difficulty with the calculation. One factor is doubtless that
the amount of ice accumulated degraded the aircraft performance so that
with the indicated airspeed and manifold pressure at normal level flight
conditions, the T-28 would actually be sinking; our computations would
treat the sink rate as a downdraft. In support of this argument, the
departures from zero indicated vertical air motion diminished markedly
within a couple of minutes after the aircraft descended below the OC level.
It is also worth noting that the K-probe was carried on this flight, adding
to the effects of icing on aircraft performance.

4a & 4b   Penetration 3 (16:48:20-16:56:51)

Altitude range: 5.0 to 5.6 km

Temperature range; -3C to -8C

Updraft characteristics:

Maximum updraft speed about 16 m sec^{-1} at 16:50:20.

Width of main updraft about 4 km.

Maximum downdraft speed about 8 m sec^{-1}.

Hydrometeor charcteristics:

Cloud liquid water concentrations up to 1.7 g m^{-3}; peak value
observed on the edge of a downdraft region.

No hail recorded on this penetration. Pilot comments that
aircraft was in and out of cloud, and that no hail was
encountered.

Turbulence: Exceeded 15 cm$^{2/3}$ sec^{-1} at 16:50:40 in a downdraft
region. Another indicated peak at about 16:49:10 is suspicious
because its appearance and magnitude (near 40) suggest an error
of some kind.

Acceleration: Maximum +0.6 g near 16:50:45 at downdraft/updraft
boundary.

The temperature probe still shows evidence of following the JW LWC trace (see 16:49:45 and later).

PLS:pal
cc: D. J. Musil
     J. R. Miller, Jr.
     G. N. Johnson
     J. H. Killinger
     R. A. Sarma
     T. C. Jameson
     J. L. Halvorson
     C. A. Knight
     A. J. Heymsfield
     R. K. Crane

MEMORANDUM FOR THE RECORD

FROM: P. L. Smith, Jr. *PLS*

SUBJECT: Notes Based on Perusal of T-28 Data Plot and Related Data
          for 22 July 1976 (Flight 183)

Most numerical values given are approximate values read from the
computer-generated plots. Detailed listings should be consulted if
more precise values are desired.

1 Penetration 1 (16:30:31 to 16:34:43)

    Altitude range: 6.1 to 6.7 km

    Temperature range: -10.5C to -15.5C

    Updraft characteristics:

        Maximum updraft speed 21 m sec^{-1} near 16:32:55.

        Width* of updraft about 6 km.

        Range of θ_e across updraft about 10 K.

        Maximum downdraft speed 6 m sec^{-1} at 16:33:14.

        Width* of main downdraft about 4 km.

    Hydrometeor characteristics:

        Cloud liquid water concentrations up to 2.7 g m^{-3} in updraft.

        Foil impactor data show significant numbers of particles larger
        than 3 mm from about 16:32:23 to 16:33:31 (approximately 7 km,
        mostly in updraft). Counts start about 15 seconds later and
        continue about 45 seconds longer than hail spectrometer counts,
        suggesting the possibility of a time shift in the foil analysis
        (although differences in sampling volumes and size ranges are
        other possible explanations.)

---

*Extent of the draft region along the flight path, which is probably smaller
than its true width.

Maximum recorded particle size nearly 1.5 cm
around 16:32:45 (in updraft) and again near
16:33:21 (in downdraft).

Maximum number concentration (D > 3 mm) 10-20/m^3
in updraft from about 16:32:30 to 16:33:10.

Maximum indicated mass concentration[†] more than
3 g/m^3 from roughly 16:32:40 to 16:32:50.

Hail spectrometer active from 16:32:10 to 16:32:43
(approximately 3 km, mostly on the weak side of the
updraft).

Maximum hail mass concentration 0.7 g/m^3 at
16:32:33 in updraft with about 0.3 g/m^3 cloud
LWC.

Maximum observed hailstone size about 1.0 cm
(Category No. 6; two places).

Maximum number concentration 7/m^3, also at 16:32:33.

Possible indications of hail depletion of cloud
water in updraft around 16:32:10-16:32:35.

Reflectivity factors to about 50 dBz.

Turbulence: Maximum intensity 11 cm$^{2/3}$ sec^{-1} in the updraft.

Acceleration: Peaks about $\pm$0.5 g in and on edges of the updraft;
a recorded -0.7 g was not plotted.

There is some indication that the reverse flow temperature (RFT) trace
follows the Johnson-Williams liquid water concentration (LWC) trace from
about 16:32:20 onwards.

2 Penetration 2 (16:38:56 to 16:45:48)

Altitude range: 6.2 to 6.9 km

[†]Foil-derived mass concentrations quoted are 12-sec averages for particles
larger than 3 mm; contribution of 1-3 mm particles on this flight is always
less than 0.26 g/m^3.

Temperature range: -12.5C to -18.5C

Updraft characteristics:

Maximum updraft speed of 33 m sec^{-1} at 16:40:40.

Width of main updraft about 4 km.

Range of θ_e across main updraft about 5 K.

Maximum downdraft speed 17 m sec^{-1} at 16:41:30.

Width of main downdraft about 5 km.

Hydrometeor characteristics:

Cloud liquid water concentrations up to 2.3 g m^{-3} predominantly in main updraft; LWC values to 0.4 g m^{-3} in some downdraft regions.

Foil data show significant numbers of particles larger than 3 mm from about 16:40:12 to 16:41:44 (approximately 9 km across main updraft and downdraft).

Maximum recorded particle size about 0.8 cm near peak of main updraft around 16:40:38.

Maximum number concentration (D > 3 mm) about 16/m^3 in main downdraft near 16:41:20.

Maximum indicated mass concentration about 0.5 g/m^3 in main updraft near 16:40:30 and again in main downdraft around 16:41:20.

Hail spectrometer active between 16:40:28 and 16:41:39 (about 7 km), with a few sporadic counts elsewhere. Width of main hail zone about 5 km, on edge of main updraft and primarily in main downdraft.

Maximum hail mass concentration 1.9 g/m^3 at 16:41:20 in main downdraft.

Maximum observed hailstone size nominally 1.25 cm (Category 8; two places).

Maximum number concentration $32/m^3$ at 16:41:21.

Suggestion of hail depletion of cloud liquid water in region of main updraft after 16:40:45.

Reflectivity factors to 55 dBz are plausible.

Turbulence: Maximum intensity 11 $cm^{2/3}$ sec^{-1} in main updraft.

Acceleration: Peak +0.8 g at 16:40:35 in main updraft.

There is only slight indication that the RFT trace follows the LWC trace on this pass.

3 Penetration 3 (16:49:25 to 16:53:43)

Altitude range: 6.1 to 6.7 km

Temperature range: -11C to -17C

Updraft characteristics:

Maximum updraft speed 12 m sec^{-1} at 16:51:22 (not in main updraft).

Width of main updraft about 5 km.

Maximum downdraft speed 7 m sec^{-1} around 16:51; 10 m sec^{-1} downdraft 20 seconds (2 km) before cloud entry.

Downdraft widths of the order of 2-3 km; no major downdraft encountered during in-cloud period.

Hydrometeor characteristics:

Cloud liquid water concentrations to 2.4 g m^{-3} mostly in updrafts, but values to near 1 g m^{-3} occur in downdraft areas as well.

Foil impactor data not reduced; few particles indicated.

No hail encountered on this penetration.

Turbulence: Maximum intensity 16 $cm^{2/3}$ sec^{-1} at 16:51:07 on
edge of downdraft.

Acceleration: Peak about -0.5 g at 16:52:35 in main
updraft region; recorded peaks of +0.8, -0.7 g were
not plotted.

From 16:50:30 the RFT trace tends to follow the JW LWC trace again,
making the temperature data suspect.

4   Penetration 4 (16:55:34 to 17:01:59)

Altitude range: 6.4 to 7.1 km

Temperature range: -13.5C to -21C

Updraft characteristics:

Maximum updraft speed 25 m sec^{-1} at 16:57:10.

Width of main updraft about 5 km.

Range of θ_e across main updraft about 7 K.

Maximum downdraft speed 13 m sec^{-1} at 16:58:12.

Width of main downdraft about 4 (7?) km.

Hydrometeor characteristics:

Cloud liquid water concentrations to 2 g m^{-3}, essentially
all in main updraft.

Foil data show significant numbers of particles larger than
3 mm from about 16:57:30 to 16:59:02 (approximatley 9 km,
predominantly in main downdraft region); counts start about
12 sec later than hail spectrometer counts.

Maximum particle size recorded about 1.1 cm in
downdraft near 16:57:40 and 16:58:04.

Maximum number concentration (D > 3 mm) 20-23/m^3
in main downdraft area from about 16:57:50 to 16:58:25.

Maximum indicated mass concentration about 1.8 g/m^3 in main downdraft near 16:58:00.

Hail spectrometer active between 16:57:18 and 16:58:54 (approximately 9 km, almost entirely in main downdraft region), with a few counts elsewhere. Width of main hail zone about 7.5 km.

Maximum hail mass concentration more than 10 g/m^3 at 16:57:41 in downdraft; value of W essentially remains above 1 g/m^3 from 16:57:28 to 16:58:11.

Maximum observed hailstone size nominally 4.4 cm (Category No. 14), also at 16:57:41.

Maximum number concentration 25/m^3 at 16:57:55 in downdraft.

Large hail mass concentrations and reflectivity factors up to 72 dBz are suspicious.**

Turbulence: Maximum intensity 12 $cm^{2/3}$ sec^{-1} at edge of main updraft.

Acceleration: Peaks about ±0.5 g in and at edge of main updraft; peak of +0.9 g was not plotted.

Little indication of correlation between RFT and JW LWC traces.

5   Penetration 5 (17:04:43 to 17:10:02)

Altitude range: 5.8 to 6.1 km

Temperature range: -9C to -15.5c

**But note that the concentrations plotted are for 1-sec samples; they should be averaged over several seconds to get representative values.

Updraft characteristics:

Maximum updraft speed 8 m sec^{-1} near 17:09.

Updraft areas no more than 2 km wide; no major updraft encountered.

Maximum downdraft speed 11 m sec^{-1} near 17:07.

Widths of main downdraft areas 3-4 km.

Hydrometeor characteristics:

Very little cloud liquid water. Maximum cloud LWC 0.6 g m^{-3}; some smaller values in downdraft areas.

Foil data show significant numbers of particles larger than 3 mm from about 17:06:43 to 17:09:03 (approximately 14 km in predominantly downdraft area); counts start about 10 sec later and continue about 10 sec longer than hail spectrometer counts, suggesting the possibility of a time shift in the foil analysis.

Maximum particle size recorded about 1.0 cm near 17:08:13.

Maximum number concentration ($D > 3$ mm) 10-14/m^3 from about 17:08:07 to 17:08:51.

Maximum indicated mass concentration about 1.3 g/m^3 from 17:08:35 to 17:08:47 (with a secondary max 0.9-1.0 g/m^3 around 17:08:03-17:08:15).

All these maxima occurred in downdrafts.

Hail spectrometer active from 17:06:34 to 17:08:52 (approximately 14 km, essentially all in downdrafts).

Maximum hail mass concentration about 5 g/m^3 at 17:08:14; value of W remained above 1 g/m^3 from 17:08:10 to 17:08:34.

Maximum observed hailstone size nominally 3.4 cm
(Category No. 13) at 17:08:03 and 17:08:10.

Maximum number concentration $27/m^3$ at 17:08:15.

Reflectivity factors to 67 dBz.

Turbulence: Maximum value 8 $cm^{2/3}$ sec^{-1} in downdraft.

Acceleration: Peak +0.5 g in downdraft.

(Note to Bob Crane: Slight baseline shift occured on the plotter
at about 17:08:10.)

6   Penetration 6 (17:13:41 to 17:22:12)

Altitude range: 5.6 to 6.4 km

Temperature range: -9C to -15C

Updraft characteristics:

Maximum updraft speed 21 m sec^{-1} at 17:14:45.

Width of main updraft about 5 km.

Maximum downdraft speed 20 m sec^{-1} at 17:15:30.

Width of main downdraft 2 (or 4?) km.

Hydrometeor characteristics:

Cloud liquid water concentrations up to 2.3 g m^{-3} in
updrafts; values up to more than 1 g m^{-3} in downdrafts.
Cloud LWC above zero for more than 2 min (12 km).

Foil impactor jammed early in penetration, apparently
because of ice accumulated during previous penetrations;
data not reduced.

Hail spectrometer intermittently active from 17:14:27
to 17:22:04 (about 45 km), mainly in downdraft areas.
Substantial amounts of hail found only in major down-
draft areas between 17:15:03 and 17:16:24; main hail
zones about 2 km wide. Sporadic indications of small
hail elsewhere.

Maximum hail mass concentration 2.5 g/m^3 at
17:16:02 on edge of downdraft.

Maximum observed hailstone size about 2.0 cm
(Category No. 11) also at 17:16:02.

Maximum number concentration $27/m^3$ at same
location.

Hail and nearly 1 g m^{-3} of cloud liquid water
appear together in a <u>downdraft</u> region after
17:16.

Reflectivity factors to 55 dBz are plausible.

Turbulence: Maximum intensity 16 $cm^{2/3}$ sec^{-1} at peak downdraft
at 17:15:30.

Acceleration: Peaks +0.9, -0.7 g in downdraft around 17:15:30;
a -0.8 g peak was recorded but not plotted.

The RFT trace conspicuously follows the JW LWC trace after 17:14:10.

PLS:pal
cc: D. J. Musil
    G. N. Johnson
    J. H. Killinger
    H. D. Orville
    T. C. Jameson
    J. L. Halvorson
    C. A. Knight
    G. B. Foote
    A. J. Heymsfield
    R. K. Crane ✓
    J. R. Miller, Jr.

APPENDIX C

STATISTICAL HAZARD DETECTION SUMMARIES
BY RADAR AND RADIUS OF INFLUENCE

Radar: CP-2, All   Radius: 2 km $Y_o = 27$

$\epsilon^{1/3}$	W	X	Y	POD	CSI	7 dBZ W' No.	7 dBZ W' %	POD'	CSI'	20 dBZ W" No.	20 dBZ W" %	POD"	CSI"	FAR
5	135	33	19	24.4	14.7	110	81.5	30.0	18.3	89	65.9	37.1	22.9	29.6
6	121	31	19	25.6	16.2	99	81.8	31.3	20.0	79	65.3	39.2	25.3	29.6
7	87	20	16	23.0	17.0	71	81.6	28.2	20.5	61	70.1	32.8	23.5	40.7
8	70	16	11	22.9	13.6	58	82.9	27.6	15.9	48	68.6	33.3	18.6	59.3
9	45	11	7	24.4	11.5	39	86.7	28.2	12.7	32	71.1	34.4	14.6	74.1
10	33	9	6	27.3	11.8	29	87.9	31.0	12.8	23	69.7	39.1	14.6	77.8
11	24	7	5	29.2	11.4	22	91.7	31.8	11.9	17	70.8	41.2	13.5	81.5
12	13	5	4	38.5	11.4	12	92.3	41.7	11.8	7	53.8	71.4	13.8	85.2
13	7	3	3	42.9	9.7	7	100	42.9	9.7	4	57.1	75.0	10.7	88.9
14	6	2	2	33.3	6.5	6	100	33.3	6.5	3	50.0	66.7	7.1	92.6
15	6	2	2	33.3	6.5	6	100	33.3	6.5	3	50.0	66.7	7.1	92.6
16	5	2	2	40.0	6.7	5	100	40.0	6.7	3	60.0	66.7	7.1	92.6
17	2	2	2	100	7.4	2	100	100	7.4	2	100	100	7.4	92.6
18	2	2	2	100	7.4	2	100	100	7.4	2	100	100	7.4	92.6
19														
28	1	1	2	100	7.4	1	100	100	7.4	1	100	100	7.4	92.6
29	0	0	0											

$$POD = (X/W) \cdot 100$$

$$FAR = (Y_o - Y/Y_o) \cdot 100$$

$$CSI = (Y/Y_o + W - X) \cdot 100$$

Radar: CP-2, All   Radius: 4 km $Y_o = 58$

$\varepsilon^{1/3}$	W	X	Y	POD	CSI	7 dBZ W' No.	7 dBZ W' %	POD'	CSI'	20 dBZ W" No.	20 dBZ W" %	POD"	CSI"	FAR
5	135	86	50	63.7	46.7	113	83.7	76.1	58.8	110	81.5	78.2	61.0	13.8
6	121	80	49	66.1	49.5	102	84.3	78.4	61.2	99	81.8	80.8	63.6	15.5
7	87	60	38	69.9	44.7	73	83.9	82.2	53.5	72	82.8	83.3	54.3	34.5
8	70	49	32	70.0	40.5	59	84.3	83.1	47.1	58	82.9	84.5	47.8	44.8
9	45	30	26	66.7	35.6	39	86.7	76.9	38.8	38	84.4	78.9	39.4	55.2
10	33	23	23	69.7	33.8	29	87.9	79.3	35.9	28	84.8	82.1	36.5	60.3
11	24	17	20	70.8	30.8	22	91.7	77.3	31.7	21	87.5	81.0	32.3	65.5
12	13	8	9	61.5	14.3	12	92.3	66.7	14.5	11	84.6	72.7	14.8	84.5
13	7	4	6	57.1	9.8	7	100	57.1	9.8	6	85.7	66.7	10.0	89.7
14	6	3	5	50.0	8.2	6	100	50.0	8.2	5	83.3	60.0	8.3	91.4
15	6	3	5	50.0	8.2	6	100	50.0	8.2	5	83.3	60.0	8.3	91.4
16	5	3	5	60.0	8.3	5	100	60.0	8.3	5	100	60.0	8.3	94.8
17	2	2	3	100	5.2	2	100	100	5.2	2	100	100	5.2	94.8
18	2	2	3	100	5.2	2	100	100	5.2	2	100	100	5.2	94.8
28	1	1	3	100	5.2	1	100	100	5.2	1	100	100	5.2	94.8
29	0	0	0		0									

Radar: CP-2, All   Radius: 6 km $Y_o = 89$

$\epsilon^{1/3}$	W	X	Y	POD	CSI	7 dBZ W' No.	7 dBZ W' %	POD'	CSI'	20 dBZ W" No.	20 dBZ W" %	POD"	CSI"	FAR
5	135	110	82	81.5	71.9	118	87.4	93.2	84.5	117	86.7	94.0	85.4	7.9
6	121	102	79	84.3	73.1	107	88.4	95.3	84.0	106	87.6	96.2	84.9	11.2
7	87	75	65	85.2	64.4	77	88.5	97.4	71.4	76	87.4	98.7	72.2	27.0
8	70	61	56	87.1	57.1	63	90.0	96.8	61.5	62	88.6	98.4	62.2	37.1
9	45	39	46	86.7	48.4	40	88.9	97.5	51.1	39	86.7	100	51.7	48.3
10	33	29	45	87.9	48.4	30	90.9	96.7	50.0	29	87.9	100	50.6	49.4
11	24	22	38	91.7	41.8	23	95.8	95.7	42.2	22	91.7	100	42.7	57.3
12	13	11	15	84.6	16.5	13	100	92.3	16.7	12	92.3	91.7	16.9	83.1
13	7	6	9	85.7	10.0	7	100	85.7	10.0	6	85.7	100	10.1	89.9
14	6	5	8	83.3	8.9	6	100	83.3	8.9	5	83.3	100	9.0	91.0
15	6	5	8	83.3	8.9	6	100	83.3	8.9	5	83.3	100	9.0	91.0
16	5	5	8	100	9.0	5	100	100	9.0	5	100	100	9.0	91.0
17	2	2	4	100	4.5	2	100	100	4.5	2	100	100	4.5	95.5
18	2	2	4	100	4.5	2	100	100	4.5	2	100	100	4.5	95.5
28	1	1	4	100	4.5	1	100	100	4.5	1	100	100	4.5	95.5
29	0	0	0											

Radar: CP-2, ≥ 40 dBZ   Radius: 2 km $Y_o = 14$

$\epsilon^{1/3}$	W	X	Y	POD	CSI	7 dBZ W' No.	7 dBZ W' %	POD'	CSI'	20 dBZ W'' No.	20 dBZ W'' %	POD''	CSI''	FAR
5	135	23	11	17.0	8.7	110	81.5	20.9	10.9	89	65.9	25.8	13.8	21.4
6	121	21	11	17.4	9.6	99	81.8	21.2	12.0	79	65.3	26.6	15.3	21.4
7	87	14	9	16.1	10.3	71	81.6	19.7	12.7	61	70.1	23.0	14.8	35.7
8	70	12	7	17.1	9.7	58	82.9	20.7	11.7	48	68.6	25.0	14.0	50.0
9	45	9	6	20.0	12.0	39	86.7	23.1	13.6	32	71.1	28.1	16.2	57.1
10	33	7	5	21.2	12.5	29	87.9	24.1	13.9	23	69.7	30.4	16.7	64.3
11	24	6	5	25.0	15.6	22	91.7	27.3	16.7	17	70.8	35.3	20.0	64.3
12	13	4	4	30.8	17.4	12	92.3	33.3	18.2	7	53.8	57.1	23.5	71.4
13	7	3	3	42.9	16.7	7	100	42.9	16.7	4	57.1	75.0	20.0	78.6
14	6	2	2	33.3	11.1	6	100	33.3	11.1	3	50.0	66.7	13.3	85.7
15	6	2	2	33.3	11.1	6	100	33.3	11.1	3	50.0	66.7	13.3	85.7
16	5	2	2	40.0	11.8	5	100	40.0	11.8	3	60.0	66.7	13.3	85.7
17	2	2	2	100	14.3	2	100	100	14.3	2	100	100	14.3	85.7
18	2	2	2	100	14.3	2	100	100	14.3	2	100	100	14.3	85.7
19	0		0											
28	1	1	1	100	14.3	1	100	100	7.1	1	100	100	7.1	85.7
29	0	0	0											

C-5

Radar: CP-2, $\geq$ 40 dBZ   Radius: 4 km $Y_o = 34$

$\epsilon^{1/3}$	W	X	Y	POD	CSI	7 dBZ W' No.	%	POD'	CSI'	20 dBZ W" No.	%	POD"	CSI"	FAR
5	135	57	32	42.2	28.6	113	83.7	50.4	35.6	110	81.5	51.8	36.8	5.9
6	121	53	31	43.8	30.4	102	84.3	52.0	37.3	99	81.8	53.5	38.8	8.8
7	87	41	22	47.1	27.5	73	83.9	56.2	33.3	72	82.8	56.9	33.8	35.3
8	70	36	20	51.4	29.4	59	84.3	61.0	35.1	58	82.9	62.1	35.7	41.2
9	45	24	18	53.3	32.7	39	86.7	61.5	36.7	38	84.4	63.2	37.5	47.1
10	33	18	16	54.4	32.7	29	87.9	62.1	35.6	28	84.8	64.3	36.4	52.9
11	24	13	14	54.2	31.1	22	91.7	59.1	32.6	21	87.5	61.9	33.3	58.8
12	13	6	6	46.2	14.6	12	92.3	50.0	15.0	11	84.6	54.5	15.4	82.4
13	7	3	3	42.9	7.9	7	100	42.9	7.9	6	85.7	50.0	8.1	91.2
14	6	2	2	33.3	5.3	6	100	33.3	5.3	5	83.3	40.0	5.4	94.1
15	6	2	2	33.3	5.3	6	100	33.3	5.3	5	83.3	40.0	5.4	94.1
16	5	2	2	40.0	5.4	5	100	40.0	5.4	5	100	40.0	5.4	94.1
17	2	2	2	100	5.9	2	100	100	5.9	2	100	100	5.9	94.1
18	2	2	2	100	5.9	2	100	100	5.9	2	100	100	5.9	94.1
28	1	1	2	100	5.9	1	100	100	5.9	1	100	100	5.9	94.1
29	0	0	0											

Radar: CP-2, $\geq$ 40 dBZ   Radius: 6 km $Y_o = 52$

$\epsilon^{1/3}$	W	X	Y	POD	CSI	7 dBZ				20 dBZ				FAR
						W'		POD'	CSI'	W''		POD''	CSI''	
						No.	%			No.	%			
5	135	81	52	60.0	49.1	118	87.4	68.6	58.4	117	86.7	69.2	59.1	0.0
6	121	75	50	62.0	51.0	107	88.4	70.1	59.5	106	87.6	70.8	60.2	3.8
7	87	57	39	65.5	47.6	77	88.5	74.0	54.2	76	87.4	75.0	54.9	25.0
8	70	48	34	68.6	45.9	63	90.0	76.2	50.7	62	88.6	77.4	51.5	34.6
9	45	34	30	75.6	47.6	40	88.9	85.0	51.7	30	86.7	87.2	52.6	42.3
10	33	25	28	75.8	46.7	30	90.0	83.3	49.1	29	87.9	86.2	50.0	46.2
11	24	19	25	79.2	43.9	23	95.8	82.6	44.6	22	91.7	86.4	45.5	51.9
12	13	11	10	84.6	18.5	13	100	92.3	19.2	12	92.3	91.7	18.9	80.8
13	7	5	6	71.4	11.1	7	100	71.4	11.1	6	85.7	83.3	11.3	88.5
14	6	4	5	66.7	9.3	6	100	66.7	9.3	5	83.3	80.0	9.4	90.4
15	6	4	5	66.7	9.3	6	100	66.7	9.3	5	83.3	80.0	9.4	90.4
16	5	4	5	80.0	9.4	5	100	80.0	9.4	5	100	80.0	9.4	90.4
17	2	2	3	100	5.8	2	100	100	5.8	2	100	100	5.8	94.2
18	2	2	3	100	5.8	2	100	100	5.8	2	100	100	5.8	94.2
28	1	1	3	100	5.8	1	100	100	5.8	1	100	100	5.8	94.2
29	0	0	0											

Radar: CP-2, $\geq$ 50 dBZ   Radius: 2 km $Y_o = 9$

| $\varepsilon^{1/3}$ | W | X | Y | POD | CSI | 7 dBZ | | | | 20 dBZ | | | | FAR |
| | | | | | | W' | | POD' | CSI' | W" | | POD" | CSI" | |
						No.	%			No.	%			
5	135	17	8	12.6	6.3	110	81.5	15.5	7.8	89	65.9	19.1	9.9	11.1
6	121	17	8	14.0	7.1	99	81.8	17.2	8.8	79	65.3	21.5	11.3	11.1
7	87	10	6	11.5	7.0	71	81.6	14.1	8.6	61	70.1	16.4	10.0	33.3
8	70	8	4	11.4	5.6	58	82.9	13.8	6.8	48	68.6	16.7	8.5	55.6
9	45	6	3	13.3	6.3	39	86.7	15.4	7.1	32	71.1	18.8	8.6	66.7
10	33	5	2	15.2	5.4	29	87.9	17.2	6.1	23	69.7	21.7	7.4	77.8
11	24	4	2	16.7	6.9	22	91.7	18.2	7.4	17	70.8	23.5	9.1	77.8
12	13	3	2	23.1	10.5	12	92.3	25.0	11.1	7	53.8	42.9	15.4	77.8
13	7	2	1	28.6	7.1	7	100	28.6	7.1	4	57.1	50.0	9.1	88.9
14	6	2	1	33.3	7.7	6	100	33.3	7.7	3	50.0	66.7	10.0	88.9
15	6	2	1	33.3	7.7	6	100	33.3	7.7	3	50.0	66.7	10.0	88.9
16	5	2	1	40.0	8.3	5	100	40.0	8.3	3	60.0	66.7	10.0	88.9
17	2	2	1	100	11.1	2	100	100	11.1	2	100	100	10.0	88.9
18	2	2	1	100	11.1	2	100	100	11.1	2	100	100	11.1	88.9
28	1	1	1	100	11.1	1	100	100	11.1	1	100	100	11.0	88.9
29	0	0	0											

Radar: CP-2, $\geq$ 50 dBZ   Radius: 4 km $Y_o = 18$

$\epsilon^{1/3}$	W	X	Y	POD	CSI	7 dBZ W' No.	7 dBZ W' %	POD'	CSI'	20 dBZ W'' No.	20 dBZ W'' %	POD''	CSI''	FAR
5	135	44	18	32.6	16.5	113	83.7	38.9	20.7	110	81.5	40.0	21.4	0.0
6	121	42	18	34.7	18.6	102	84.3	41.2	23.1	99	81.8	42.4	24.0	0.0
7	87	31	13	35.6	17.6	73	83.9	42.5	21.7	72	82.8	43.1	22.0	27.8
8	70	27	12	38.6	19.7	59	84.3	45.8	24.0	58	82.9	56.6	24.5	33.3
9	45	20	12	44.4	27.9	39	86.7	51.3	32.4	38	84.4	52.6	33.3	33.3
10	33	16	11	48.5	31.4	29	87.9	55.2	35.5	28	84.8	57.1	36.7	38.9
11	24	9	9	37.5	27.3	22	91.7	40.9	29.0	21	87.5	42.9	30.0	50.0
12	13	4	3	30.8	11.1	12	92.3	33.3	11.5	11	84.6	36.4	12.0	83.3
13	7	2	1	28.6	4.3	7	100	28.6	4.3	6	85.7	33.3	4.5	94.4
14	6	2	1	33.3	4.5	6	100	33.3	4.5	5	83.3	40.0	4.8	94.4
15	6	2	1	33.3	4.5	6	100	33.3	4.5	5	83.3	40.0	4.8	94.4
16	5	2	1	40.0	4.8	5	100	40.0	4.5	5	100	40.0	4.8	94.4
17	2	2	1	100	5.6	2	100	100	5.6	2	100	100	5.6	94.4
18	2	2	1	100	5.6	2	100	100	5.6	2	100	100	5.6	94.4
28	1	1	1	100	5.6	1	100	100	5.6	1	100	100	5.6	94.4
29	0	0	0											

Radar: CP-2, $\geq$ 50 dBZ   Radius: 6 km $Y_o = 27$

$\varepsilon^{1/3}$	W	X	Y	POD	CSI	7 dBZ		POD'	CSI'	20 dBZ		POD"	CSI"	FAR
						W' No.	%			W" No.	%			
5	135	58	27	43.0	26.0	118	87.4	49.2	31.0	117	86.7	49.6	31.4	0.0
6	121	54	26	44.6	27.7	107	88.4	50.5	32.5	106	87.6	50.9	32.9	3.7
7	87	40	21	46.0	28.4	77	88.5	51.9	32.8	76	87.4	52.6	33.3	22.2
8	70	33	19	47.1	29.7	63	90.0	52.4	33.3	62	88.6	53.2	33.9	29.6
9	45	25	18	55.6	38.3	40	88.9	62.5	42.9	39	86.7	64.1	43.9	33.3
10	33	20	17	60.6	42.5	30	90.9	66.7	45.9	29	87.9	69.0	47.2	37.0
11	24	14	17	58.3	45.9	23	95.8	60.9	47.2	22	91.7	63.6	48.7	37.0
12	13	6	5	46.2	14.7	12	92.3	50.0	15.2	11	84.6	54.5	15.6	81.5
13	7	3	3	42.9	9.7	7	100	42.9	9.7	6	85.7	50.0	10.0	88.9
14	6	3	3	50.0	10.0	6	100	50.0	10.0	5	83.3	60.0	10.3	88.9
15	6	3	3	50.0	10.0	6	100	50.0	10.0	5	83.3	60.0	10.3	88.9
16	5	3	3	60.0	10.3	5	100	60.0	10.3	5	100	60.0	10.3	88.9
17	2	2	2	100	7.4	2	100	100	7.4	2	100	100	7.4	92.6
18	2	2	2	100	7.4	2	100	100	7.4	2	100	100	7.4	92.6
28	1	1	1	100	3.7	1	100	100	3.7	1	100	100	3.7	92.6
29	0	0	0											

Radar: CP-3, Doppler   Radius: 2 km $Y_o = 15$

$\epsilon^{1/3}$	W	X	Y	POD	CSI	7 dBZ W' No.	%	POD'	CSI'	20 dBZ W" No.	%	POD"	CSI"	FAR
5	35	16	10	45.7	29.4					30	86.7	53.3	34.5	33.3
6	31	14	9	45.2	28.1					26	83.9	53.8	33.3	40.0
7	22	10	7	45.5	25.9					22	100	45.5	25.9	53.3
8	16	10	6	62.5	28.6					16	100	62.5	28.6	60.0
9	12	8	5	66.7	26.3					12	100	66.7	26.3	66.7
10	8	4	2	50.0	10.5					8	100	50.0	10.5	86.7
11	6	3	2	50.0	11.1					6	100	50.0	11.1	86.7
12	3	2	1	66.7	6.3					3	100	66.7	6.3	93.3
13	1	1	1	100	6.7					1	100	100	6.7	93.3
14	1	1	1	100	6.7					1	100	100	6.7	93.3
15	1	1	1	100	6.7					1	100	100	6.7	93.3
16	1	1	1	100	6.7					1	100	100	6.7	93.3
17	0	0	0											
18														
28														
29														

Radar: CP-3, Doppler   Radius: 4 km $Y_o = 28$

$\epsilon^{1/3}$	W	X	Y	POD	CSI	7 dBZ W' No.	7 dBZ W' %	POD'	CSI'	20 dBZ W" No.	20 dBZ W" %	POD"	CSI"	FAR
5	35	27	24	77.1	66.7									14.3
6	31	24	23	77.4	65.7									17.9
7	22	17	18	77.3	54.5									35.7
8	16	15	15	93.8	51.7									46.4
9	12	12	14	100	50.0									50.0
10	8	8	11	100	39.3									60.7
11	6	6	10	100	35.7									64.3
12	3	3	2	100	7.1									92.9
13	1	1	1	100	3.6									96.4
14	1	1	1	100	3.6									96.4
15	1	1	1	100	3.6									96.4
16	1	1	1	100	3.6									96.4
17														
18														
28														
29														

Radar: CP-3, Doppler   Radius: 6 km $Y_o = 37$

$\epsilon^{1/3}$	W	X	Y	POD	CSI	7 dBZ W' No.	7 dBZ W' %	POD'	CSI'	20 dBZ W'' No.	20 dBZ W'' %	POD''	CSI''	FAR
5	35	32	35	91.4	87.5									5.4
6	31	28	34	90.3	85.0									8.1
7	22	19	31	86.4	77.5									16.2
8	16	15	23	93.8	60.5									37.8
9	12	12	21	100	56.8									43.2
10	8	8	17	100	45.9									54.1
11	6	6	17	100	45.9									54.1
12	3	3	4	100	10.8									89.2
13	1	1	2	100	5.4									94.6
14	1	1	2	100	5.4									94.6
15	1	1	2	100	5.4									94.6
16	1	1	2	100	5.4									94.6
17														
18														
28														
29														

Radar: CP-4, Doppler Radius: 2 km Y_o = 25

$\varepsilon^{1/3}$	W	X	Y	POD	CSI	7 dBZ W' No.	7 dBZ W' %	POD'	CSI'	20 dBZ W" No.	20 dBZ W" %	POD"	CSI"	FAR
5	88	25	19	28.4	21.6	67	76.1	37.3	28.4	52	59.1	48.1	36.5	24.0
6	82	24	19	29.3	22.9	62	75.6	38.7	30.2	48	58.5	50.0	38.8	24.0
7	57	18	16	31.6	25.0	42	73.7	42.9	32.7	36	63.2	50.0	37.2	36.0
8	47	16	12	34.0	21.4	36	76.6	44.4	26.7	30	63.8	53.3	30.8	52.0
9	29	11	10	37.9	23.3	23	79.3	47.8	27.0	20	69.0	55.0	29.4	60.0
10	20	5	4	25.0	10.0	16	80.0	31.2	11.1	13	65.0	38.5	12.1	84.0
11	14	4	3	28.6	8.6	12	85.7	33.3	9.1	10	71.4	40.0	8.3	88.0
12	5	3	2	60.0	7.4	4	80.0	75.0	7.7	3	60.0	100	8.0	92.0
13	4	3	2	75.0	7.7	4	100	75.0	7.7	3	75.0	100	8.0	92.0
14	3	2	2	66.7	7.7	3	100	66.7	7.7	2	66.7	100	8.0	92.0
15	3	2	2	66.7	7.7	3	100	66.7	7.7	2	66.7	100	8.0	92.0
16	2	2	2	100	8.0	2	100	100	8.0	2	100	100	8.0	92.0
17	2	2	2	100	8.0	2	100	100	8.0	2	100	100	8.0	92.0
18	2	2	2	100	8.0	2	100	100	8.0	2	100	100	8.0	92.0
28	1	1	2	100	8.0	1	100	100	8.0	1	100	100	8.0	92.0
29	0	0	0											

C-14

Radar: CP-4, Doppler   Radius: 4 km $Y_o = 52$

ϵ 1/3	W	X	Y	POD	CSI	7 dBZ W' No.	7 dBZ W' %	POD'	CSI'	20 dBZ W" No.	20 dBZ W" %	POD"	CSI"	FAR
5	88	45	44	51.1	46.3	68	77.3	66.2	58.7	67	76.1	67.2	59.5	15.4
6	82	43	44	52.4	48.4	63	76.8	68.3	61.1	62	75.6	69.4	62.0	15.4
7	57	33	36	57.9	47.4	43	75.4	76.7	58.1	42	73.7	78.6	59.0	30.8
8	47	29	36	61.7	51.4	36	76.6	80.6	61.0	35	74.5	82.9	62.1	30.8
9	29	20	35	69.0	57.4	23	79.3	87.0	63.6	22	75.9	90.9	64.8	32.7
10	20	13	25	65.0	42.4	16	80.0	81.2	45.5	15	75.0	86.7	46.3	51.9
11	14	11	19	78.6	34.5	12	85.7	91.7	35.8	11	78.6	100	36.5	63.5
12	5	3	5	60.0	9.3	4	80.0	75.0	9.4	3	60.0	100	9.6	90.4
13	4	3	5	75.0	9.4	4	100	75.0	9.4	3	75.0	100	9.6	90.4
14	3	2	3	66.7	5.7	3	100	66.7	5.7	2	66.7	100	5.8	94.2
15	3	2	3	66.7	5.7	3	100	66.7	5.7	2	66.7	100	5.8	94.2
16	2	2	3	100	5.8	2	100	100	5.8	2	100	100	5.8	94.2
17	2	2	3	100	5.8	2	100	100	5.8	2	100	100	5.8	94.2
18	2	2	3	100	5.8	2	100	100	5.8	2	100	100	5.8	94.2
28	1	1	3	100	5.8	1	100	100	5.8	1	100	100	5.8	94.2
29	0	0	0											

Radar: CP-4, Doppler   Radius: 6 km $Y_o = 82$

$\epsilon^{1/3}$	W	X	Y	POD	CSI	7 dBZ W' No.	W' %	POD'	CSI'	20 dBZ W'' No.	W'' %	POD''	CSI''	FAR
5	88	55	75	62.5	65.2	73	83.0	75.3	75.0	72	81.8	76.4	75.8	8.5
6	82	51	74	62.2	65.5	68	82.9	75.0	74.7	67	81.7	76.1	75.5	9.8
7	57	37	60	64.9	58.8	47	82.5	78.7	65.2	46	80.7	80.4	65.9	26.8
8	47	31	59	66.0	60.2	40	85.1	77.5	64.8	39	83.0	79.5	65.6	28.0
9	29	21	59	72.4	65.6	24	82.8	87.5	69.4	23	79.3	91.3	70.2	28.0
10	20	14	48	70.0	54.5	17	85.0	82.4	56.5	16	80.0	87.5	57.1	41.5
11	14	12	39	85.7	46.4	13	92.9	92.3	47.0	12	85.7	100	47.6	52.4
12	5	4	10	80.0	12.0	4	80.0	100	12.2	4	80.0	100	12.2	87.8
13	4	3	8	75.0	9.6	4	100	75.0	9.6	3	75.0	100	9.8	90.2
14	3	2	4	66.7	4.8	3	100	66.7	4.8	2	66.7	100	4.9	95.1
15	3	2	4	66.7	4.8	3	100	66.7	4.8	2	66.7	100	4.9	95.1
16	2	2	4	100	4.9	2	100	100	4.9	2	100	100	4.9	95.1
17	2	2	4	100	4.9	2	100	100	4.9	2	100	100	4.9	95.1
18	2	2	4	100	4.9	2	100	100	4.9	2	100	100	4.9	95.1
28	1	1	4	100	4.9	1	100	100	4.9	1	100	100	4.9	95.1
29	0	0	0											

Radar: NOAA-C, Doppler   Radius: 2 km $Y_o = 30$

1/3 ε	W	X	Y	POD	CSI	7 dBZ W' No.	%	POD'	CSI'	20 dBZ W'' No.	%	POD''	CSI''	FAR
5	119	35	25	29.4	21.9	94	79.0	37.2	28.1	77	64.7	45.5	34.7	16.7
6	106	33	24	31.1	23.3	84	79.2	39.3	29.6	68	64.2	48.5	36.9	20.0
7	74	24	21	32.4	26.3	58	78.4	41.4	32.8	51	68.9	47.1	36.8	30.0
8	60	20	14	33.3	20.0	48	80.0	41.7	24.1	41	68.3	48.8	27.5	53.3
9	39	13	12	33.3	21.4	33	84.6	39.4	24.0	28	71.8	46.4	26.7	60.0
10	27	7	8	25.9	16.0	23	85.2	30.4	17.4	19	70.4	36.8	19.0	73.3
11	19	5	5	26.3	11.4	17	89.5	29.4	11.9	14	73.7	35.7	12.8	83.3
12	10	1	1	10.0	2.6	9	90.0	11.1	2.6	6	60.0	16.7	2.9	96.7
13	6	1	1	16.7	2.9	6	100	16.7	2.9	5	83.3	20.0	2.9	96.7
14	5	0	0	0	0					4	80.0			100
15	5									4	80.0			
16	4													
17	2													
18	2													
28	1													
29	0													

Radar: NOAA-C, Doppler   Radius: 4 km $Y_o = 62$

$\epsilon^{1/3}$	W	X	Y	POD	CSI	7 dBZ W' No.	7 dBZ W' %	POD'	CSI'	20 dBZ W" No.	20 dBZ W" %	POD"	CSI"	FAR
5	119	58	55	48.7	44.7	97	81.5	59.8	54.5	94	79.0	61.7	56.1	11.3
6	106	55	52	51.9	46.0	87	82.1	63.2	55.3	84	79.2	65.5	57.1	16.1
7	74	42	47	56.8	50.0	60	81.1	70.0	58.8	59	79.7	71.2	59.5	24.2
8	60	35	40	58.3	46.0	49	81.7	71.4	52.6	48	80.0	72.9	53.3	35.5
9	39	26	39	66.7	52.0	33	84.6	78.8	56.5	32	82.1	81.2	57.4	37.1
10	27	18	30	66.7	42.3	23	85.2	78.3	44.8	22	81.5	81.8	45.5	51.6
11	19	13	23	68.4	33.8	17	89.5	76.5	34.8	16	84.2	81.2	35.4	62.9
12	10	5	5	50.0	7.5	9	90.0	55.6	7.6	8	80.0	62.5	7.7	91.9
13	6	2	3	33.3	4.5	6	100	33.3	4.5	5	83.3	40.0	4.6	95.2
14	5	1	1	20.0	1.5	5	100	20.0	1.5	4	80.0	25.0	1.5	98.4
15	5	1	1	20.0	1.5	5	100	20.0	1.5	4	80.0	25.0	1.5	98.4
16	4	1	1	25.0	1.5	4	100	25.0	1.5	4	100	25.0	1.5	98.4
17	2				0									
18	2													
28	1													
29	0													

C-18

Radar: NOAA-C, Doppler   Radius: 6 km $Y_o = 102$

$\epsilon^{1/3}$	W	X	Y	POD	CSI	7 dBZ W' No.	W' %	POD'	CSI'	20 dBZ W'' No.	W'' %	POD''	CSI''	FAR
5	119	74	95	62.2	64.6	112	94.1	66.1	67.9	111	93.3	66.7	68.3	6.9
6	106	69	92	65.1	66.2	92	86.8	75.0	73.6	91	85.8	75.8	74.2	9.8
7	74	51	84	68.9	67.2	64	86.5	79.7	73.0	63	85.1	81.0	73.7	17.6
8	60	42	74	70.0	61.7	53	88.3	79.2	65.5	52	86.7	80.8	66.1	27.5
9	39	31	72	79.5	65.5	34	87.2	91.2	68.6	33	84.6	93.9	69.2	29.4
10	27	22	61	81.5	57.0	24	88.9	91.7	68.7	23	85.2	95.7	59.2	40.2
11	19	17	51	89.5	49.0	18	94.7	94.4	49.5	17	89.5	100	50.0	50.0
12	10	9	18	90.0	17.5	9	90.0	100	17.6	9	90.0	100	17.6	82.4
13	6	5	15	83.3	14.6	6	100	83.3	14.6	5	83.3	100	14.7	85.3
14	5	4	8	80.0	7.8	5	100	80.0	7.8	4	80.0	100	7.8	92.2
15	5	4	8	80.0	7.8	5	100	80.0	7.8	4	80.0	100	7.8	92.2
16	4	4	8	100	7.8	4	100	100	7.8	4	100	100	7.8	92.2
17	2	2	1	100	1.0	2	100	100	9.3	2	100	100	9.8	99.0
18	2	2	1	100	1.0	2	100	100	9.8	2	100	100	9.8	99.0
28	1	1	1	100	1.0	1	100	100	9.8	1	100	100	9.8	99.0
29	0	0	0											

Radar: NOAA-D, Doppler   Radius: 2 km $Y_o = 12$

$\epsilon^{1/3}$	W	X	Y	POD	CSI	7 dBZ W' No.	7 dBZ W' %	POD'	CSI'	20 dBZ W'' No.	20 dBZ W'' %	POD''	CSI''	FAR
5	100	15	8	15.0	8.2	75	75.0	20.0	11.1	60	60.0	25.0	14.0	33.3
6	92	14	8	15.2	8.9	70	76.1	20.0	11.8	56	60.9	25.0	14.8	33.3
7	64	10	6	15.6	9.1	48	75.0	20.8	12.0	41	64.1	24.4	14.0	50.0
8	53	9	6	17.0	10.7	41	77.4	22.0	13.6	34	64.2	26.5	16.2	50.0
9	33	5	4	15.2	10.0	27	81.8	18.5	11.8	22	66.7	22.7	13.8	66.7
10	22	5	4	22.7	13.8	18	81.8	27.8	16.0	14	63.6	35.7	12.9	66.7
11	16	4	4	25.0	16.7	14	87.5	28.6	18.2	11	68.8	36.4	13.8	66.7
12	7	2	2	28.6	11.8	6	85.7	33.3	12.5	4	57.1	50.0	14.3	83.3
13	5	2	2	40.0	13.3	5	100	40.0	13.3	4	80.0	50.0	14.3	83.3
14	4	2	2	50.0	14.3	4	100	50.0	14.3	3	75.0	66.7	15.4	83.3
15	4	2	2	50.0	14.3	4	100	50.0	14.3	3	75.0	66.7	15.4	83.3
16	3	2	2	66.7	15.4	3	100	66.7	15.4	3	66.7	66.7	15.4	83.3
17	2	2	2	100	16.7	2	100	100	16.7	2	100	100	16.7	83.3
18	2	2	2	100	16.7	2	100	100	16.7	2	100	100	16.7	83.3
28	1	1	2	100	16.7	1	100	100	16.7	1	100	100	16.7	83.3
29	0	0	0											

Radar: NOAA-D, Doppler   Radius: 4 km $Y_o = 24$

$\epsilon^{1/3}$	W	X	Y	POD	CSI	7 dBZ W' No.	%	POD'	CSI'	20 dBZ W" No.	%	POD"	CSI"	FAR
5	100	27	23	27.0	23.7	78	78.0	34.6	30.7	75	75.0	36.0	31.9	4.2
6	92	26	23	28.3	25.6	73	79.3	35.6	32.4	70	76.1	37.1	33.8	4.2
7	64	20	19	31.1	27.9	50	78.1	40.0	35.2	49	76.6	40.8	35.8	20.8
8	53	19	18	35.8	31.0	42	79.2	45.2	38.3	41	77.4	46.3	39.1	25.0
9	33	13	17	39.4	38.6	27	81.8	48.1	44.7	26	78.8	50.0	45.9	29.2
10	22	10	15	45.5	41.7	18	81.8	55.6	46.9	17	77.3	58.8	48.4	37.5
11	16	9	14	56.3	45.2	14	87.5	64.3	48.3	13	81.2	69.2	50.0	41.7
12	7	2	4	28.6	13.8	6	85.7	33.3	14.3	5	71.4	40.0	14.8	83.3
13	5	2	4	40.0	14.8	5	100	40.0	14.8	4	80.0	50.0	15.4	83.3
14	4	2	3	50.0	11.5	4	100	50.0	11.5	3	75.0	66.7	12.0	87.5
15	4	2	3	50.0	11.5	4	100	50.0	11.5	3	75.0	66.7	12.0	87.5
16	3	2	3	66.7	12.0	3	100	66.7	12.0	3	100	66.7	12.0	87.5
17	2	2	3	100	12.5	2	100	100	12.5	2	100	100	12.5	87.5
18	2	2	3	100	12.5	2	100	100	12.5	2	100	100	12.5	87.5
28	1	1	3	100	12.5	1	100	100	12.5	1	100	100	12.5	87.5
29	0	0	0											

Radar: NOAA-D, Doppler   Radius: 6 km $Y_o = 40$

$\epsilon^{1/3}$	W	X	Y	POD	CSI	7 dBZ W' No.	7 dBZ W' %	POD'	CSI'	20 dBZ W'' No.	20 dBZ W'' %	POD''	CSI''	FAR
5	100	51	39	51.0	43.8	83	83.0	61.4	54.2	82	82.0	62.2	54.9	2.5
6	92	50	39	54.3	47.6	78	84.8	64.1	57.4	77	83.7	64.9	58.2	2.5
7	64	34	32	53.1	45.7	54	84.4	63.0	53.3	53	82.8	64.2	54.2	20.0
8	53	28	30	52.8	46.2	46	86.8	60.0	51.7	45	84.9	62.2	52.6	25.0
9	33	18	28	54.5	50.9	28	84.8	64.3	56.0	27	81.8	66.7	57.1	30.0
10	22	14	26	63.6	54.2	19	86.4	73.7	57.8	18	81.8	77.8	59.1	35.0
11	16	12	23	75.0	52.3	15	93.8	80.0	53.5	14	87.5	85.7	54.8	42.5
12	7	4	9	57.1	20.9	6	85.7	66.7	21.4	5	71.4	80.0	22.0	77.5
13	5	3	9	60.0	21.4	5	100	60.0	21.4	4	80.0	75.0	22.0	77.5
14	4	3	7	75.0	17.1	4	100	75.0	17.1	3	75.0	100	17.5	82.5
15	4	3	7	75.0	17.1	4	100	75.0	17.1	3	75.0	100	17.5	82.5
16	3	3	7	100	17.5	3	100	100	17.5	3	100	100	17.5	82.5
17	2	2	5	100	12.5	2	100	100	12.5	2	100	100	12.5	87.5
18	2	2	5	100	12.5	2	100	100	12.5	2	100	100	12.5	87.5
28	1	1	5	100	12.5	1	100	100	12.5	1	100	100	12.5	87.5
29	0	0	0											

END

DATE
FILMED

9-81

DTIC